Dissertation zur Erlangung des Doktorgrades
der Fakultät für Chemie und Pharmazie
der Ludwig-Maximilians-Universität München

Molecular basis of RNA polymerase III transcription repression by Maf1

&

Structure of human mitochondrial RNA polymerase

Eva Rieke Ringel
aus
Essen

2011

Dissertation zur Erlangung des Doktorgrades
der Fakultät für Chemie und Pharmazie
der Ludwig-Maximilians-Universität München

Molecular basis of RNA polymerase III transcription repression by Maf1

&

Structure of human mitochondrial RNA polymerase

Eva Rieke Ringel
aus
Essen

2011

Erklärung

Diese Dissertation wurde im Sinne von § 13 Abs. 3 bzw. 4 der Promotionsordnung vom 29. Januar 1998 (in der Fassung der sechsten Änderungssatzung vom 16. August 2010) von Herrn Prof. Dr. Patrick Cramer betreut.

Ehrenwörtliche Versicherung

Diese Dissertation wurde selbständig, ohne unerlaubte Hilfe erarbeitet.

München, ...

.....
Eva Rieke Ringel

Dissertation eingereicht am	26.05.2011
1. Gutachter	Prof. Dr. Patrick Cramer
2. Gutachter	Prof. Dr. Dietmar Martin
Mündliche Prüfung am	26.07.2011

Acknowledgements

Life-science is like teamsports. If you want to play in a high league, you need to have good players and, even more importantly, a strong and diehard team effort. Without good passes from your teammates you would never score a goal and without the right tactics, training input and motivation from your coach, there would be nothing to win. I am very grateful that I was part of such a successful and inspiring squad, the Cramer lab team.

I want to thank Patrick, the coach, not only for letting me be part of this team but also for his leadership. You gave me at the right time a lot of freedom to decide over my daily labwork and provided helpful feedback and project plans, when it was required. You trusted in me and my capabilities, like representing the Pol III team on a conference in the US. You also motivated me to start the risky, challenging but also extremely exciting "mito Pol" project, and in the end it worked out and was worse it!

Special thanks go to Dmitry, who initiated the mitoRNAP match! I learned so much about single subunit polymerases from you! Only your enthusiasm about these tiny initial crystals, and your staying power, enabled the success of this project. Thanks for sharing many ideas for experiments with me and explaining in long emails good biochemistry. And yes, the next time you visit the Genecenter, there will be a cold Bavarian beer in the fridge again.

I would also like to thank my teammates in the Maf1/Pol III match, Anselm Kusser and Alessandro Vannini! Your passes with plenty of Pol III purifications and cryo EM reconstructions were wonderful and "this time it worked". I am very glad that our Pol III team succeeded not only in science but also beyond (and that I got your famous tiramisu recipe, Ale and your delicious restaurant tip, Anselm).

Many teammates in the lab did not only help with advices, supports and discussions, but also contributed to the fruitful atmosphere at work. Thank you: Alan, for so much help at the synchrotron, with data processing, and discussions about crystallography. You are a famous teacher! Christian, for discussions about life beyond science and for teaching me, a convinced child of the Ruhrpott, the beauty of your home. Claudia (Blattner), for mastering our PhD times side by side, for sharing uncountable lunch times and for always barely listening and speaking about all these enjoyments, doubts and thoughts in this time. Claudia (Buchen), for keeping the lab running and being always a great help for finding everything. Dirk, for providing a lot of expertise in crystallography and ideas to process the data and build the models even a bit better. Elisabeth, for helping me with the RNA-extension assays and sharing the great experience in the lab. Elmar, for many useful ideas in the daily lab work, for your contagious enthusiasm at the bench, and for spending many hours in the lab speaking about everything under the sun. Jasmin, for sharing her expertise with the bead-based transcription assays and of course for your "krass" famous Persian meals. Jenne, for discussing with me about soccer and all the other important things in life and of course for sharing your exceptional theories about the Pol I architecture. Laurent, for his open-minded interest and challenging questions. Martin, for his advices and help to establish his transcription assay in the Pol III system. Stefan (Benkert) for fermenting hugh amounts of Pol III. Tobias, for helping with Äkta-systems also late in the evening, for listening to the latest successes and failures of experiments, and of course for sharing many delicious coffees.

Also I would like to thank my students Lukas and Alexander.You were more than only substitutes of the team, but really offered great help in the lab. I learned a lot from teaching you and appreciate your interest in my projects.

Additionally, many thanks go to Hans-Joerg and Maxi from the IMPRS of the MPI Martinsried. I will profit from your continuous work to offer students good trainings, suitable workshops, and interesting talk schedules – a real trainingscamp, so to say.

Auch meinen Eltern, meinem Bruder und meinen Großeltern möchte ich danken. Danke, dass ihr mir die Freiheit geschaffen habt, zu tun, was ich möchte und mir die Unterstützung gegeben habt, die ich dafür brauche!
Danke Robin, für Dein Verständnis und Deine Hilfe und dass Du mich immer daran erinnerst, was wirklich wichtig ist!

Summary

Topic I
Molecular basis of RNA polymerase III transcription repression by Maf1

RNA polymerase III (RNAP III) is a conserved 17-subunit enzyme that transcribes genes encoding short untranslated RNAs such as transfer RNAs (tRNAs) and 5S ribosomal RNA (rRNA). These genes are essential and involved in fundamental processes like protein biogenesis; hence RNAP III activity needs to be tightly regulated. RNAP III is repressed upon stress and this is regulated by Maf1, a protein conserved from yeast to humans. Many stress pathways were shown to converge on Maf1 and result in its phosphorylation, followed by its nuclear import and eventual repression of RNAP III activity. However, the molecular mechanisms of this repression activity were not known at the beginning of these studies.

This work establishes the mechanism of RNAP III specific transcription repression by Maf1. The crystal structure of Maf1 was solved. It has a globular fold with surface accessible NLS sequences, which sheds new light on already published results and explains how stress-induced phopshorylation leads to import of Maf1 into the nucleus. Additionally, cryo EM studies and competition assays show that Maf1 binds RNAP III at its clamp domain and thereby induces structural rearrangements of RNAP III, which inhibits the interaction with Brf1, a subunit of the transcription initiation factor TFIIIB. This specifically impairs recruitment of RNAP III to its promoters and implies that Maf1 is a repressor of transcription initiation. Competition and transcription assays show that Maf1 also binds RNAP III that is engaged in transcription, leaving RNAP III activity intact but preventing re-initiation.

Topic II
Structure of human mitochondrial RNA polymerase

The nuclear-encoded human mitochondrial RNAP (mitoRNAP) transcribes the mitochondrial genome, which encodes rRNA, tRNAs and mRNAs. MitoRNAP is a single subunit (ss) polymerase, related to T7 bacteriophage and chloroplast polymerases. All share a conserved C-terminal core, whereas the N-terminal parts of mitoRNAP do not show any homology to other ss RNAPs. Unlike phage RNAPs, which are self-sufficient, human mitoRNAP needs two essential transcription factors for initiation, TFAM and TFB2M. Both of these factors are likely to control the major steps of transcription initiation, promoter binding and melting. Thus human mitoRNAP has evolved a different mechanism for transcription initiation and exhibits a unique transcription system. Structural studies thus far concentrated on the nuclear enzymes or phage RNAPs, whereas the structure of mitochondrial RNA polymerase remained unknown. The structural organization of human mitoRNAP and the molecular mechanisms of promoter recognition, binding and melting were subject of interest in these studies.

In this work the crystal structure of human mitoRNAP was solved at 2.4 Å resolution and reveals a T7-like C-terminal catalytic domain, a N-terminal domain that remotely resembles the T7 promoter-binding domain (PBD), a novel pentatricopeptide repeat (PPR) domain, and a flexible N-terminal extension.
MitoRNAP specific adaptions in the N-terminus include the sequestering of one of the key promoter binding elements in T7 RNAP, the AT-rich recognition loop, by the PPR domain. This sequestration and repositioning of the N-terminal domain explain the need for the additional initiation factor TFAM. The highly conserved active site within the C-terminal core was observed to bind a sulphate ion, a well known phosphate mimic, and thereby suggests conserved substrate binding and selection mechanisms between ss RNAPs. However, conformational changes of the active site were observed due to a movement of the adjacent fingers subdomain. The structure reveals a clenching of the active site by a repositioned fingers subdomain and an alternative position of the intercalating β-hairpin. This explains why the conserved transcription factor TFB2M is required for promoter melting and initiation. A model of the mitochondrial initiation complex was build to further explore the initiation mechanism, and to rationalize the available biochemical and genetic data.

The structure of mitoRNAP shows how this enzyme uses mechanisms for transcription initiation that differ from those used by phage and cellular RNAPs, and which may have enabled regulation of mitochondrial gene transcription and adaptation of mitochondrial function to changes in the environment.

Publications

Part of this work has been published or is in the process of being published.

Vannini,A.*, Ringel,R.*, Kusser,A.G.*, Berninghausen,O., Kassavetis,G.A., and Cramer,P. (2010). **Molecular basis of RNA polymerase III transcription repression by Maf1.** Cell *143*, 59-70.

* equally contributed

Author contributions:
A.V. prepared RNAP III complexes, A.V. and A.G.K. determined EM structures, R.R. prepared and crystallized Maf1, R.R. and A.V. determined the Maf1 X-ray structure, R.R. and A.V. conducted functional assays, G.A.K. advised on RNAP III preparation, A.V., R.R., A.G.K., and P.C. wrote the manuscript, and P.C. designed and supervised research.

Author contributions in additional results (parts of this thesis):
R.R. prepared all used proteins and complexes (RNAP III, $Brf1_N$/TBP_C/$Brf1_C$, Maf1) and perfomed all described assays and experiments; Anja Schüller pepared C34 protein; Anselm Kusser performed cryo EM data processing.

Ringel,R., Sologub,M., Morozov,Y.I., Litonin,D., Cramer,P., and Temiakov,D. (2011). **Structure of the human mitochondrial RNAP**. *Nature (accepted)*

Author contributions:
M.S. and D.L. cloned mitoRNAP variants; M.S., D.L., D.T., and Y.I.M. carried out mitoRNAP purification and biochemical assays; R.R. and D.T. prepared the crystals, R.R. carried out structure determination and modelling. P.C. and D.T. designed and supervised the project and prepared the manuscript.

Contents

I

■ ■ ■

General Introduction

1 Transcription by DNA-dependent RNA polymerases

Transcription is the process of reading DNA into RNA, which for mRNA can be translated by ribosomes into proteins, or used for regulation of cellular processes by non-coding RNAs. Transcription is fundamental to all living organisms and is carried out by DNA-dependent RNA polymerases (RNAPs).

1.1 Transcription by multisubunit RNAPs

Gene expression across the three kingdoms of life is predominantly performed by multisubunit RNAPs. Whereas bacteria and archaea have one multisubunit RNAP, which transcribe the entire gene repertoire in the cell, eukaryotes have three multisubunit RNAPs, which transcribe mainly the nuclear genome (Cramer, 2002; Kwapisz et al., 2008). RNAP I is responsible for the synthesis of ribosomal RNA, RNAP II for pre-messenger RNA and RNAP III for small RNAs including transfer RNAs synthesis. Two additional closely related RNAPs, RNAP IV and V, were found in plants and are involved in RNA-dependent DNA methylation and heterochromatin formation (Dalmay et al., 2000; Herr et al., 2005; Pontier et al., 2005).

Multisubunit RNAPs differ in their subunit composition (Table 1) and enzyme surfaces are specialized for interactions with initiation or elongation factors. High resolution data from multisubunit RNAPs from all three kingdoms of life show a conserved catalytic core formed by Rpb1 and Rpb2 or their corresponding subunits (Cramer et al., 2001; Hirata et al., 2008; Zhang et al., 1999) whereas subunits specific to RNAP I and III are homologous to transcription factors from the RNAP II system (Table 1 (Carter and Drouin, 2010; Geiger et al., 2010; Kassavetis et al., 2010; Kuhn et al., 2007)).

Table 1. Subunit composition of RNAPs

	Eukaryotes			Archaea	Bacteria
	RNAP I	RNAP II	RNAP III		
core	A190	Rpb1	C160	A' + A"	β'
	A135	Rpb2	C128	B (B' + B")	β
	AC40	Rpb3	AC40	D	α
	Rpb5	Rpb5	Rpb5	H	-
	Rpb6	Rpb6	Rpb6	K	ω
	Rpb8	Rpb8	Rpb8	-	-
	A12.2	Rpb9	C11	-	-
	Rpb10	Rpb10	Rpb10	N	-
	AC19	Rpb11	AC19	L	α
	Rpb12	Rpb12	Rpb12	P	-
Rbp4/7-like	A14	Rpb4	C17	F	-
	A43	Rbp7	C25	E´	-
TFIIF-like	A49 (N-ter.)	-	C37	-	-
	A34.5	-	C53	-	-
TFIIE-like	-	-	C82	-	-
	A49 (C-ter.)	-	C34	-	-
	-	-	C31	-	-
no. SU	14	12	17	11 (12)	5

1.2 Transcription by single subunit RNAPs

Single subunit (ss) RNAPs can be found in bacteriophages and eukaryotic cell organelles, such as T7 phage (Sousa et al., 1993; Steitz, 2009) and mitochondria (Gaspari et al., 2004b), respectively. Notably, mitochondrial RNAP (mitoRNAP) is responsible for transcribing the mitochondrial genome, which encodes several subunits of key enzymes involved in oxidative phosphorylation, the major source of energy production during respiration (Sologub et al., 2009). Therefore an understanding of the molecular mechanisms underlying transcription and transcription regulation in mitochondria is critical.

No structure of a mitoRNAP has yet been published. Sequence similarities within structural elements of the T7 RNAP and the mitoRNAP catalytic C-terminus strongly suggest that they have a conserved structure (Cermakian et al., 1997; Jeruzalmi and Steitz, 1998). In contrast the N-terminus of mitoRNAPs does not show any sequence homology to T7 RNAP and is predicted to feature a new class of protein fold containing two PPR motifs, whose function remains unknown (Small and Peeters, 2000; Tiranti et al., 1997).

T7 RNAP is one of the best understood RNAPs, since several structures were solved over the last 17 years in different functional states using different scaffolds to mimick the initiation state, the transition state from initiation to elongation, four different elongation states showing structural changes during a single nucleotide addition cycle, and an inhibited state, where T7 RNAP is bound to T7 Lysozyme (Cheetham et al., 1999; Jeruzalmi and Steitz, 1998; Sousa et al., 1993; Tahirov et al., 2002; Durniak et al., 2008; Temiakov et al., 2004; Yin and Steitz, 2002; Yin and Steitz, 2004). Single subunit RNAPs are probably very ancient RNAPs and therefore do not show homologies to the multisubunit RNAPs of the nucleus (Sousa, 1996). Only the mechanism of transcription, the nucleotide addition cycle, is comparable between these enzymes (Sousa, 1996; Temiakov et al., 2000).

1.3 A common transcription cycle

Each cycle of transcription by RNAPs involves three phases: promoter binding and duplex opening during initiation, processive synthesis of RNA during elongation, and release of the transcript and dissociation of RNAP during termination.

Initiation starts by binding of the RNAP to a specific promoter DNA sequence upstream of the transcription start site (TSS) and formation of a transcription bubble by melting the duplex DNA at the TSS. RNA synthesis has to start *de novo* using the downstream DNA as a template and a single ribonucleotide as a primer, whereupon RNAP stays bound to the promoter during initial formation of first DNA-RNA hybrids (Brieba and Sousa, 2001).
In the elongation phase, single nucleotide addition takes place by binding of the substrate NTP in a pre-insertion mode, followed by NTP insertion into the NTP-binding site (N-site) and a phosphoryl-transfer reaction to extend the RNA transcript and release pyrophosphate (PP_i). Subsequently, the RNA 3´-end sits in the N-site and translocation is required to shift the 3´-end of the elongated primer-template to the priming site (P-site) thereby vacating the N-site for the next round of nucleotide addition (Steitz and Yin, 2004; Yin and Steitz, 2004).

Termination finally stops transcription at the correct site and is linked to RNA transcript release, allowing the RNAP to be released from the template and to reengage in another round of transcription (Birse et al., 1997; Dye and Proudfoot, 2001; Evers and Grummt, 1995; Landrieux et al., 2006).

These mechanistic features are shared between multisubunit and ss RNAPs, hence parts of the core enzyme from both types of RNAP show similarities (Cramer et al., 2008). These include the conserved configuration of the nucleic acid scaffold of the ternary complexes, similar lengths of the DNA/RNA heteroduplexes and conserved residues in the active site, and closing of the catalytic site by movement of a particular functional element (the O-helix in T7-like RNAPs and the trigger loop in multisubunit RNAPs) (Steitz, 2004; Temiakov et al., 2004).

2 Transcription initation and regulation

Transcription initiation has to be tighly regulated to allow promoter-specific transcription by the cognate RNAP (Schramm and Hernandez, 2002). Additionally, gene expression is not static but dynamically altered in response to the changing cellular environment. In higher eukaryotes regulation of transcription is needed for development and cellular differentiation. So each differentiation stage shows altered expression profiles (Levine and Tjian, 2003). Also cell-type-specific expression programs have to be co-ordinated (Goodrich and Tjian, 2010). Additionally, cells have to adapt according to environmental signals and stresses, subsequentially changing their expression profiles (Fraser and Germain, 2009; White and Sharrocks, 2010). Large differences beween multisubunit and ss RNAPs are apparent during transcription initiation and regulation.

2.1 Transcription initiation and regulation of multisubunit RNAPs

Multisubunit RNAPs depend on accessory factors for the transcription of genes. They act with their cognate RNAP as activators, adaptors, inhibitors, terminators, or anti-terminators (Tjian, 1996).

General transcription factors enable the general mechanism of transcription

The general transcription factors (GTFs) serve to help with promoter recognition, recruitment of the RNAP, and with subsequent activation of the RNAP by promoting transcriptional initiation and elongation (Chedin et al., 1998a; Geiduschek and Kassavetis, 2001). Since each RNAP differs in its subunit composition and has to transcribe specific sets of genes, each RNAP uses a large number and own set of GTFs.
The structure and function of some transcription factors are conserved across the three kingdoms of life, whereas other factors that are non-homologous by sequence show an intringuing level of structural and functional similarity, suggestive of convergent evolution (Werner and Grohmann, 2011). For example, TATA binding protein (TBP) is present in archeal and eukaryotic organisms but absent from prokaryotes, whereas the elongation factor Spt5/NusG is conserved in all three kingdoms of life (Khoo et al., 1994; Martinez-Rucobo et al., 2011). Additionally, TFIIB, a factor essential for RNAP II transcription initiation has homologs in archaea and in the RNAP III system as TFB and

TFIIIB respectively, yet features of this protein strongly resemble the unrelated sigma factors used by prokaryotic RNAP.

The general mechanism of transcription initiation starts with core promoter recognition and building of a pre-initation complex (PIC). However, due to the different subunit composition of each of the RNAPs, their usage of GTFs, and the varying promoter structures of their transcribed genes, the PIC compositions are highly variable.
In the well characterized RNAP II system, the general transcription factors TFIIA, TFIIB, TFIID, TFIIE, TFIIF and TFIIH, the major coactivator, termed Mediator, and RNAP II build the general transcription machinery (Carey et al., 2009). The PIC of RNAP II is constituted by the GTFs TFIIB, TFIID, TFIIE, TFIIF and TFIIH (Kostrewa et al., 2009). The structure of RNAP II-TFIIB was solved recently and when combined with chemical probing experiments to locate TFIIE, -F and -H, allowed the first modelling of an eukaryotic PIC (Chen et al., 2007; Kim et al., 2000; Kostrewa et al., 2009). In the model of Kostrewa et al. TFIIH, which opens dsDNA, binds near the jaws and cleft close to downstream DNA (Kim et al., 2000); TFIIE binds to the clamp and is probably involved in non-template DNA binding and open complex stabilization (Chen et al., 2007), and TFIIF binds to the opposite side of the cleft.

RNAP III is much larger than RNAP II and has consequently integrated some of its required transcription factors into the enzyme (Table 1). RNAP III can transcribe three distinct types of class III genes, which vary in their promoter control elements, and uses varying transcription factor compositions at each type of gene. For type III promoters RNAP III needs just the TFIIIB complex, which is composed of TBP, Brf1 and BdpI, to form a minimal functional initiation complex (Kassavetis et al., 1990). On type II promoters the transcription factor TFIIIC and on type I promoters TFIIIC and TFIIIA, are needed to recruit TFIIIB and subsequentially RNAP III to build a functional PIC (Dieci et al., 2007). This illustrates nicely how different promoters rely on different DNA-protein and protein-protein interactions to ultimately recruit the same RNAP. Despite knowing which factors were present at each class III promoter, no structure or model of a RNAP III PIC was published at the beginning of this study, although a crystal structure of the Brf1-TBP-DNA complex (Juo et al., 2003) and a low resolution cryo EM reconstruction of RNAP III (Fernandez-Tornero et al., 2007) were available.

Transcriptional activity of RNAPs can be affected by nucleosomes, which associate with the coding regions of many RNAP II and III transcribed genes. The susceptibility of class III genes to nucleosomal repression is extremely template-dependent. Whereas tRNA genes and U6 genes are significantly resistant to chromatin-mediated repression, others are highly susceptible (Paule and White, 2000). *In vitro* studies have shown that TFIIIC weakens the interaction of nucleosomes with the transcribed region of these resistant genes (Burnol et al., 1993).

Cofactors link transcription to extracellular signals

In addition to the general transcription machineries, cofactors also play an important role in transducing different regulatory signals and influencing transcription according to the cellular condition. In the case of RNAP III, cofactors like the growth suppressors RB (retinoblastoma) and p53 in metazoa or Dr1 and Maf1 in human and yeast serve to integrate the transcriptional response to extracellular signals (Paule and White, 2000; White and Sharrocks, 2010). Coordination of these processes is crucial and is achieved by signalling pathways.

Maf1 is an inhibitor of RNAP III transcription and various signalling pathways converge on Maf1 to regulate RNAP III-dependent transcription. Growth factors and oncogenic mutations lead to inhibition of Maf1 and thereby promote RNAP III-dependent transcription, whereas nutrient limitation and DNA damage result in Maf1 activation and following RNAP III transcription repression (White, 2008; Willis et al., 2004; Johnson et al., 2007). Well studied signalling pathways, which converge on Maf1, are the target of rapamycin complex (TORC) pathway and the Ras/cAMP pathway (Moir et al., 2006; Wei et al., 2009).
TOR is an evolutionary conserved PI3K-related kinase with a large impact on the protein synthesis machinery and growth, including the stimulation of tRNA and 5S rRNA gene transcription (Mayer and Grummt, 2006; Woiwode et al., 2008). TORC1 is one of two complexes containing the TOR kinase and is sensitive to the antibiotic rapamycin. Rapamycin is often used to induce the transcriptional effects of nutrient limitation (Rohde et al., 2001). Growth factors like insulin activate the pathway by extracellular signal-regulated kinases (ERK) –mediated and ERK-independent steps, leading to activation of the small GTPase Rheb, which in turn can activate TORC1. Nutrient limitations can be detected in the cell by the AMP/ATP ratio. These lead to activation of the AMP kinase, which can phosphorylate and inhibit TORC1 (White and Sharrocks, 2010). The Sch9 kinase is a direct target of TORC1 (Urban et al., 2007) and found in yeast to target Maf1 at a subset of protein kinase A (PKA) sites, thereby leading to location of Maf1 in the cytoplasm (Lee et al., 2009). TORC1 itself was shown to inactivate Maf1 in the nucleolus (Wei et al., 2009). Additionally, the phosphatase PP2A acts downstream of TORC1 and dephosphorylates Maf1 (Oficjalska-Pham et al., 2006). This shows that the TORC pathways controls many steps of Maf1 activity and enables a coordinated RNAP III transcription activity in response to the cellular environment.

Another well characterized pathway, which influences Maf1 activity, is the Ras/cAMP pathway. Ras is a small GTPase that gets activated in cells upon growth factor or hormone binding to cell receptors and can in turn activate several pathways like the mitogen activated protein kinase (MAPK) pathway (Zhong et al., 2004). This pathway can influence all three eukaryotic RNAPs by phosphorylation of the transcription factor Elk1 and thereby activation of TBP transcription (Johnson et al., 2007). In yeast one of many effectors of activated Ras is adenylate cyclase, which causes cAMP accumulation. cAMP binds to the regulatory subunits of PKA and thereby activates PKA (Chiaradonna et al., 2008). PKA itself was shown to phosphorylate and inactivate Maf1 both in the cytoplasm and the nucleus and thereby represents an additional signal mediator mechanism for RNAP III transcription (Moir et al., 2006).

Although much is known about the signal pathways that influence RNAP III transcription repression by Maf1, few molecular details are known. Uncovering these details promises great insights into basic regulatory interactions and mechanisms in the RNAP III system.

2.2 Transcription initiation and regulation of single subunit RNAPs

Transcription regulation of ss RNAPs is diverse. Whereas T7 RNAPs do not need any accessory factor for initiation (Chamberlin et al., 1983), mitoRNAPs can only recognize its promoters in a self-sufficient manner like T7 RNAPs, but need the transcription factor Mtf1 (in yeast) or TFAM and TFB2M (in human) for efficient initiation (Cheetham et al., 1999; Litonin et al., 2010).

The basal transcription machinery in mitochondria

The basal transcription machinery in mammalian mitochondria consists of TFAM, TFB2M and mitoRNAP. These three proteins are sufficient to reconstitute transcription from promoter-containing DNA *in vitro* (Litonin et al., 2010).
TFAM, a protein consisting of two HMG-boxes, can specifically recognize and unspecifically bind and unwind DNA and is suggested to enable transcription initiation (Dairaghi et al., 1995b). TFAM binds and bends DNA 15-40 bps upstream of the TSS (Dairaghi et al., 1995b) and genetic and biochmemical data suggest that the C-terminus of TFAM interacts with TFB2M and thereby recruits the initiation complex (Falkenberg et al., 2007; McCulloch and Shadel, 2003; Sologub et al., 2009). However, the high abundance of TFAM in human mitochondria supports a rather unspecific mechanism (Cotney et al., 2007). TFAM generally functions in maintenance of the mitochondrial genome, but its function in transcription is not conserved in yeast, where it lacks a C-terminal region required for transcription in human mitochondria (Antoshechkin et al., 1997; Dairaghi et al., 1995a; Shadel and Clayton, 1996).
In contrast, the function of TFB2M, a member of a large family of dimethyltransferases, is preserved in mitochondria of many eukaryotes (Antoshechkin and Bogenhagen, 1995; Cotney et al., 2007; Falkenberg et al., 2002; Jang and Jaehning, 1991). In mammals, TFB2M assists mitoRNAP in DNA melting and reaches the active site of mitoRNAP to make direct interactions with promoter DNA at the first bp of the RNA/DNA hybrid (Sologub et al., 2009). A similar role was shown for the yeast TFB2M analog Mtf1 (Savkina et al., 2010). Consistent, mitoRNAP can transcribe single-stranded and bubble templates, but not double stranded promoters, explaining the factor-dependency for ds DNA melting.

The fact that TFB2M was found to act as a transient component of the catalytic site of the mitochondrial initiation complex and helps binding of the priming nucleotide, which is a unique feature compared to cellular and T7 RNAPs (Sologub et al., 2009). The promoter release of mitoRNAP is thought to require the dissociation of TFB2M or Mtf1 (Mangus et al., 1994; Sologub et al., 2009). In this respect, mitoRNAPs resemble the structurally unrelated multisubunit RNAPs.

In summary, mitochondrial transcription shares a number of features with phage, bacterial, and eukaryotic transcription and forms a unique system among well studied bacteriophage and multisubunit RNAPs (Table 2).

Table 2. Transcription initiation of single- and multisubunit RNAPs

	Single subunit RNAPs		Multisubunit RNAPs	
	T7 RNAP	mito RNAP	Bacterial RNAP	Eukaryotic RNAP
promoter recognition	core	core	holo	holo
promoter melting	core	core +TFB2M/TFAM	holo	holo
NTP interactions	core	TFB2M	core	core
promoter clearance	refolding of Nt-domain	release of TFB2M	release of σ-subunit	release of TFIIB/ TFIIIB/ core factor

Additional regulatory mechanisms are needed in mitochondria, since mtDNA forms a higher structure called nucleoid, which corresponds to the nucleosomes of nuclear DNA. These nucleoids contain 2–10 mtDNA molecules and affect the accessibility of mtDNA. TFAM was found to bind to nucleoids (Legros et al., 2004) and it is suggested that different amounts of bound TFAM influence the promoter usage in human mitochondria (Shutt et al., 2011). In yeast mitochondria nucleoids comprise many different proteins in addition to the TFAM ortholog Abf2p. Therefore nucleoids play a role in transcription regulation by changing their protein composition in response to metabolic signals to adjust mtDNA expression (Kucej et al., 2008).

Extracellular signals affect mitochondrial transcription

Like in multisubunit RNAPs, a number of regulatory cofactors play an important role for the activity of mitoRNAPs (Woo and Shadel, 2011). Since mitochondria generate energy through oxidative catabolism and provide substrates for the synthesis of fatty acids and multiple amino acids, their activity has to be tightly linked to cellular nutrient availability. This signal-dependent regulation takes place by transcriptional control in the nucleus as well as in mitochondria (Scheffler, 2001; Woo and Shadel, 2011).

In mitochondria some cofactors directly interact with the RNAP. The N-terminal non-conserved part of yeast mitoRNAPs is suggested to couple factors like Nam1, a protein involved in RNA processing and translation (Rodeheffer et al., 2001). Importantly, the loss of the N-terminal part of mitoRNAP is characterized in yeasts by an increased instability and eventual loss of the mitochondrial genome, which indicates functional N-terminal domains that couple additional activities to the transcription process in mitochondria (Wang and Shadel, 1999). However, a recent publication revealed that also a larger deletion (first 270 AA) in yeast mitoRNAP has no effect on transcription activity *in vitro* (Paratkar et al., 2011). In human cells, a nuclear active splicing variant of the mitoRNAP was found, which has its N-terminal 262 AA deleted (Kravchenko et al., 2005; Wang and Shadel, 1999).

Mitochondrial transcription is also regulated at the level of termination to enable different steady-state levels of promoter-proximal and distal transcripts. The mTERF (mitochondrial transcription termination factor) protein can modulate mitochondrial transcription in humans and *D.melanogaster* (Linder et al., 2005). A DNA-binding protein (mDBP) was identified in mitochondria of *P. lividus* and found to arrest elongating RNAP (Loguercio et al., 1999). These termination factors bind at the 3'-end of blocks of genes transcribed on opposite strands (Fernandez-Silva et al., 2001).

The exact sequence of events in initiation and regulation of mitochondrial gene expression, the molecular transcription mechanism by mitoRNAPs and the structural background for these unique mechanisms in promoter binding and melting still remain unknown.

3 Evolution of DNA-dependent RNA polymerases

The molecular basis of complexity in higher organisms cannot be simply explained with an enlarged number of genes (just 30,000 protein-coding genes in humans compared to 20,000 in *C. elegans*) but rather with an increased complexity in gene expression regulation (Levine and Tjian, 2003). The yeast genome encodes about 300 transcription factors (Wyrick and Young, 2002), *C. elegans* about 1,000 transcription factors (Ruvkun and Hobert, 1998), and humans about 3,000 transcription factors (Lander et al., 2001). These varying degrees of relationships in gene expression regulation are also reflected in the structures and mechanisms of multisubunit and ss RNAPs.

RNAPs show similar mechanistic features and therefore conservations in some parts of the enzyme core (Cramer et al., 2008). Since five structurally discrete and evolutionary unrelated folds of RNAP active sites exist, polymerization of ribonucleotides has probably been invented several times during evolution, pointing to a convergent evolution of these RNAP classes (Werner and Grohmann, 2011). It is possible that both the multisubunit RNAPs in the three kingdoms of life and the ss RNAPs from phages and subcellular organelles each have a unique and separate ancestory (Cermakian et al., 1997; Werner and Grohmann, 2011).

3.1 Evolution of multisubunit RNAPs

All multisubunit RNAPs have a common structural framework and show conserved molecular mechanisms like the usage of three key aspartic residues in the active site. This could be explained according to the ´RNA-world hypothesis´ by their evolution from one ancestral ribonucleic acid polymerase, which is thought to have existed very early in evolution (Steitz and Steitz, 1993). The contemporary multisubunit RNAPs may have derived from a common ancestral ribozyme that contained a non-catalytic homodimeric RNA-binding protein (Iyer et al., 2003). It is suggested that evolution of multisubunit RNAPs emerged by duplication and diversification of this homodimeric RNA-binding protein followed by its acquisition of a polymerase activity, and subsequently losing its RNA compounds and acting as a platform to evolve more complex multisubunit RNAPs (Iyer et al., 2003). Subunit complexity of multisubunit RNAPs increased from bacteria to archaea and eukaryotes by recruitment and incorporation of existing transcription factors, like TFS (Carter and Drouin, 2010), which illustrates the divergent evolution from the last common ancestor within this class of multisubunit RNAPs. This can be also seen in the subunit composition of multisubunit RNAPs, where some homologous proteins are permanently incorporated into RNAPs in one system but just reversibly incorporated in another RNAP (Table 1) and the associated use of RNAP-specific subsets of GTFs.

By recruitment of existing transcription factors, multisubunit RNAPs expanded. This allowed better regulation and explains diversification and specialization into RNAP I, II and III. Comparing the eukaryotic subunits A49/A34.5 of RNAP I and C53/C37 of RNAP III, they show homology to TFIIF of the RNAP II system (Geiger et al., 2010; Kassavetis et al., 2010; Werner and Grohmann, 2011) and the C-terminus of A49 as well as regions of C34 and C82 structurally resemble TFIIE (Geiger et al., 2010), also of the RNAP II system. Consequentially, RNAP-specific cofactors, like Maf1 in the RNAP III system, evolved in a later step of evolution as it can be seen in sequence comparisons and phylogenetic trees (Pluta et al., 2001). Therefore understanding the molecular mechanisms of those specific cofactors not only offers insights into the activity of one special regulatory protein but also into RNAP-specific mechanisms.

3.2 Evolution of single subunit RNAPs

The evolution of ss RNAPs is also an enigma. As described, strong sequence similarities of bacteriophage T7 with mitoRNAP and other ss RNAPs were found widespread within eukaryotic genomes (Cermakian et al., 1996). Sequence alignments as well as structure-function analysis of highly conserved amino acids point to a common ancestral sequence (Cermakian et al., 1997; Delarue et al., 1990; Sousa, 1996). Since ss RNAPs do not share homologies to multisubunit RNAPs but rather expose a handshape-like structure, which is comparable with the Klenow fragment of *E.coli* DNA polymerase I (DNAP) it is suggested that ss RNAPs and DNAP I-like enzymes arosed by divergent evolution (Cermakian et al., 1996; Sousa, 1996). Nevertheless, the timing of the appereance of an ancestral ss RNAP gene is unknown, or even if this ancestor occurred in a cellular or virus-like genome (Cermakian et al., 1996).
Additional implications can be derived from analysis of ss DNAPs. These proteins can be devided into six families, namely A, B, C, D, X, Y, which can also be grouped based on their structures into proteins containing either classic (Klenow fragment like) or β-nucleotidyltransferase-like palm domains (Baley et al., 2006).

It is almost certain that the ancestor of the mitochondrion was an α-proteobacterium, which was incorporated by endosymbiosis into an unknown host (Gray et al., 2004) and that the complete mitochondrial transcription machinery composed of the mitoRNAP, the replicative primase-helicase Twinkle, and the DNAPγ, shows ancestry with T7 bacteriophages. Possibly, the mitoRNAP was acquired as part of the endosymbiont genome rather than directly from an accompying phage-like entity, since phage-like genes were found in bacterial genomes (Shutt and Gray, 2006). The broad phylogenetic distribution suggests an appearance of mitoRNAP early in evolution and that at some point during early evolution the unique ss mitoRNAP replaced the multisubunit bacteria-like RNAP that was originally brought into the eukaryotic cell by the proto-mitochondrial genome (Shutt and Gray, 2006). So the mitoRNAP evolved from interaction of three distinct entities, namely the host cell, a bacterium and a phage.

Therefore mitoRNAPs use a unique transcription system and investigation of its molecular transcription and regulation mechanisms establishes ties between the evolutionary diversification of RNAPs and is a highly important area of research.

II

■ ■ ■

Molecular basis of RNA polymerase III transcription repression by Maf1

1 Introduction

1.1 RNA Polymerase III

1.1.1 RNA Polymerase III structure

RNAP III, with its 17 subunits and nearly 700 kDa mass, is the most complex nuclear RNAP (Schramm and Hernandez, 2002). No X-ray crystal structure is available so far (Cramer et al., 2008). Five subunits, Rpb5, 6, 8, 10, and 12, are common to RNAP I, II and III. Subunits AC40 and AC19 are common to RNAP I and III, and homologous to RNAP II subunits Rpb3 and Rpb11, respectively. The two largest RNAP III subunits C160 and C128 are homologous to RNAP II subunits Rpb1 and Rpb2, respectively, and encompass the active center of the enzyme. Subunits C17 and C25 form a heterodimeric subcomplex, whose structure is solved, and shows homology to the RNAP II subcomplex Rpb4/7 (Ferri et al., 2000; Jasiak et al., 2006; Sadhale and Woychik, 1994). Subunit C11 shares homology with RNAP II subunit Rpb9. The RNAP III-specific subunits C82, C53, C37, C34 and C31 form two subcomplexes. The C53/37 subcomplex shows limited homology to the RNAP II initiation factor TFIIF and is involved in promoter opening, elongation, correct termination and re-initiation (Carter and Drouin, 2010; Cramer et al., 2008; Kassavetis et al., 2010; Landrieux et al., 2006). The structure of its RNAP I homologue A49/34.5 was solved recently and indeed shows homology to TFIIF (Geiger et al., 2010). The C-terminal region of A49 forms a tandem winged helix (tWH) domain and is predicted in TFIIE. The subcomplex C82/34/31 is involved in promoter recognition and initiation. C34 interacts with TFIIIB, the initiation factor that recruits RNAP III to promoters (Thuillier et al., 1995; Wang and Roeder, 1997; Werner et al., 1993) and plays a subsequent role in open complex formation (Brun et al., 1997). NMR structures of two WH domains of C34 were solved (PDB codes 2dk5 and 2dk8). Also the structure of the human homologue of C82, hC62, was solved recently, and shows in two of its four extended WH domains homology to TFE/ eukaryotic TFIIEα (Lefevre et al., 2011). So regions of C34 and C82 structurally resemble TFIIE (Geiger et al., 2010).

1.1.2 The function and regulation of RNAP III

RNAP III transcribes genes encoding short, untranslated RNAs such as tRNAs, 5S rRNA, the spliceosomal U6 snRNA, the signal recognition particle 7SL RNA, and short regulatory RNAs. RNAP III genes are essential in all cells and involved in fundamental processes such as ribosome and protein biogenesis, RNA processing, and protein transport. RNAP III transcription is tightly co-regulated with RNAP I activity, accounting together for up to 80% of nuclear gene transcription in growing cells (Grummt, 2003; Paule and White, 2000; Willis et al., 2004). Therefore RNAP III has to be tightly regulated.

In humans deregulation of RNAP I and III transcription is a hallmark of many cancer cells and therefore became an important research target over the last years. Namely, overexpression of RNAP III products is oncogenic (Marshall, 2008) and RNAP III transcription machineries are targeted by several oncogene products like Erk and c-Myc and by tumor suppressors like RB and p53 in metazoan (White, 2005). This indicates a critical role of RNAP III in tumorigenesis. Maf1, as a negative regulator of RNAP III transcription repression, is thereby a potential tumor suppressor (White, 2008).

1.2 The Maf1 protein

1.2.1 Maf1 is a mediator of signalling pathways

Because of the central role of RNAP III transcripts in basal cellular processes, the level of RNAP III transcription is a critical determinant of cell growth. In yeast, the ability to rapidly shut off synthesis of tRNAs and rRNAs during environmental stress conditions ensures cell survival (Warner, 1999).

Stress conditions lead to RNAP III repression by Maf1, a phosphoprotein that is phylogenetically conserved from yeast to human (Pluta et al., 2001; Upadhya et al., 2002). Maf1 is an essential and specific regulator of transcriptional repression in the RNAP III system and provides a critical link between diverse stress signaling pathways and the RNAP III transcriptional machinery. Signaling pathways activated in response to rapamycin-induced nutrient limitation (TOR pathway), DNA-damage (MMS treatment), and secretory pathway defects (Tunicamycin treatment) all need Maf1 in order to affect RNAP III transcriptional repression (Upadhya et al., 2002). Also conditions of carbon source starvation, endoplasmatic reticulum stress (DTT treatment) and oxidative stress (peroxide treatment) require Maf1 to cause RNAP III transcription repression (Boguta et al., 1997; Upadhya et al., 2002). Additionally, not only stress signals but also the switch between fermentation and respiration in yeast induces Maf1 activity (Willis et al., 2004). Under respiratory conditions, Maf1 is activated by dephosphorylation (1.2.3), and transition to a glucose media induces Maf1 deactivation again, thereby leading to a Maf1-dependent cell activity. An example effect is the induction of tRNA-synthesis rate on glucose media. It was shown several times, that the inactivation of Maf1 (maf1Δ), results in higher tRNA-levels due to deregulated RNAP III activity (Pluta et al., 2001; Upadhya et al., 2002) and posited that the temperature-sensitive growth phenotype can be explained by the toxic effect of accumulated tRNAs (Ciesla and Boguta, 2008).
Importantly, in human cells Maf1 overexpression inhibits oncogenic transformation, likely due to Maf1´s ability to restrain RNAP III-dependent transcription (Johnson et al., 2007).

1.2.2 Maf1 architecture and interaction properties

Maf1 is phylogenetically highly conserved and lacks homology to any known motifs. Its size ranges from 45 kDa (*S. cerevisiae.*) to 26 kDa (human, *S.pombe*) and sequence alignments reveal among different species four conserved regions, the A-, B- and C-box and a C-terminal acidic tail with varying length (Pluta et al., 2001).

Two nuclear localization sequences (NLS) have been found to affect Maf1 localization in yeast and sit at position K205-K208 (Nt-NLS) and R328-R332 (Ct-NLS) (Moir et al., 2006). Human NLS sequences can be predicted at the same positions. Recent studies have identified several phosphorylation sites in yeast and human Maf1, and most of these phospho-serines occur in the region between the A- and B-boxes. The six yeast phosphorylation sites (S90, S101, S177/178, S209/210) are targeted by PKA and/or Sch9 kinases (Lee et al., 2009; Moir et al., 2006). Human phosphorylation sites (S60, S68, S75) were detected by phospho-proteomic analysis, and their biological relevance has been determined recently (Michels et al., 2010).

First hints for functional aminoacids and regions were determined by point mutation analysis. Measurements of *in vivo* point mutation effects like growth on glycerol, tRNA gene-mediated (tgm) silencing, antisupression, cellular localization, binding to RNAP III, phosphorylation

state of Maf1 and repression of RNAP III transcription activity after rapamycin treatment revealed various essential aminoacids for Maf1 activity (Moir et al., 2006; Roberts et al., 2006; Towpik et al., 2008). Such residues are part of predicted folded regions, of signal sequences like the N-terminal and C-terminal NLS-sequences or of a conserved so-called PDxDFS-motif.

To investigate Maf1 activity, physical interactions were analyzed. Pull-down experiments confirmed a direct binding of Maf1 to the N-terminal 235 residues of RPC160, the largest subunit of RNAP III. Also other subunits of RNAP III, namely C128, C82, AC40, C34, AC19, C17, and ABC14.5, co-immunoprecipitated from yeast lysate (Oficjalska-Pham et al., 2006; Pluta et al., 2001). Brf1, a subunit of the transcription factor TFIIIB, interacts weakly but specifically with Maf1, in contrast to to the TFIIIB subunits TBP and Bdp1 or TFIIIC, which do not interact (Desai et al., 2005).

1.2.3 Regulation of Maf1-mediated Polymerase III transcription repression

In growing yeast, Maf1 is phosphorylated and localized mainly in the cytoplasm. Stress conditions lead to rapid Maf1 dephosphorylation and import into the nucleus (Oficjalska-Pham et al., 2006; Roberts et al., 2006). Here, Maf1 is signal-dependently phosphorylated by PKA and/ or Sch9 and dephosphorylated by protein phosphatase 2A (PP2A) (Moir et al., 2006; Oficjalska-Pham et al., 2006; Lee et al., 2009).

Nuclear import of yeast Maf1 is directed by the two independent NLS sequences. This nuclear import is impared by phosphorylation of the six phospho-serine sites (Lee et al., 2009; Moir et al., 2006).
Once in the nucleus another regulatory mechanism has to take place, since Maf1 mutants, which are constitutively nuclear, remain regulated by the rapamycin-sensitive kinase TORC1 (Moir et al., 2006; Wei et al., 2009). Recent data show that rapamycin treatment leads to localization of Maf1 from the nucleus into the nucleolus, where 5s rRNA is located (Wei et al., 2009). TORC1 acts as an essential second control step of Maf1 activity in the nucleus. Under normal conditions TORC1 is active, phosphorylates and thereby inactivates Maf1, which could still be in the nucleolus but gets subsequentially excluded. Rapamycin treatment leads to inactivation of TORC1 and thereby active, dephosphorylated Maf1. This demonstrates a new control mechanism (Wei et al., 2009). Dephosphorylated Maf1 binds to RNAP III, blocking its interaction with TFIIIB, thus preventing recruitment of RNAP III to promoters (Desai et al., 2005; Moir et al., 2006; Roberts et al., 2006).

Maf1 also inhibits TFIIIB assembly at RNAP III promoters by binding Brf1, a subunit of TFIIIB that resembles TFIIB in its N-terminal half but also contains a RNAP III-specific C-terminal domain (Desai et al., 2005). Maf1 leads to reduced genome-wide occupancy of RNAP III genes by Brf1 and RNAP III (Oficjalska-Pham et al., 2006; Roberts et al., 2006).

Similar results have been obtained in human cells, where also additional factors (e.g. p53, RB and c-Myc) regulate RNAP III activity. Equally, human Maf1 acts as a RNAP III transcription repressor *in vivo* and *in vitro* (Goodfellow et al., 2008; Reina et al., 2006). After stress signals, transcription from promoter types 1, 2 and 3 are downregulated in human cells and phosphorylation-dependent association of Maf1 with RNAP III and Brf1 could be detected (Reina et al., 2006), as well as an additional weak interaction with Brf2 (Rollins et al., 2007). Human Maf1 activity is also regulated in a signal-dependent manner by its phosphorylation or dephosphorylation state.

Thus Maf1 is established as a conserved global repressor of RNAP III transcription (Reina et al., 2006). Recently, the effect of human Maf1 on facilitated recycled transcription of RNAP III was investigated *in vitro*. It was shown that RNAP III multiple-round transcription but not single-round transcription is inhibited by Maf1 (Cabart et al., 2008).

Inactivation of Maf1 is connected to its re-phosphorylation, which takes place in a signal-dependent manner in the nucleus. Concomitantly, Msn5 carries Maf1 back to the cytoplasm. Notably, despite the constitutive presence of Maf1 in msn5Δ strains, its regulation is not affected, which can be explained by the essential TORC1-dependent regulation inside the nucleus. This indicates a direct and indirect phosphorylation-dependent inactivation of Maf1, decreasing Maf1-mediated repression and stimulating Msn5-mediated nuclear export, respectively (Towpik et al., 2008).

1.3 Aims and scope

Signal-dependent regulation of cells is necessary to control the consumption of metabolic energy, to enable normal cell growth and development and to avoid oncogenic dysregulation (Marshall, 2008; White, 2005). Repression of RNAP III transcription, which together with RNAP I accounts up to 80% of nuclear gene transcription (Grummt, 2003; Paule and White, 2000; Willis et al., 2004), and whose products are oncogenic (Marshall, 2008), is robust and coordinated in all organisms studied to date (White and Sharrocks, 2010). Whereas in higher eukaryotes tumor suppressors like RB and p53 are well characterized as direct repressors of RNAP I and III transcription (White, 2005), less is known about the highly conserved key regulator of RNAP III transcription, Maf1. Functional data emphasize the role of Maf1 in yeast and human as a mediator of several signal pathways and as a direct repressor of RNAP III transcription (Goodfellow et al., 2008; Upadhya et al., 2002).

Understanding the molecular mechanisms of Maf1 as a transcription regulator will offer insights into the activity of an essential RNAP III regulator protein, which integrates many signal pathways and is highly conserved in eukaryotes, thereby explaining a globally used regulation mechanism (Goodfellow et al., 2008; Pluta et al., 2001). This will also help to elucidate the mechanism of transcription by RNAP III in general. Additionally, as Maf1 exhibits exclusive specificity for the RNAP III system in yeast, understanding transcription regulation by Maf1 also promises insights into basic regulatory interactions and mechanisms specific for the RNAP III system.

Furthermore, Maf1 is a potential tumor suppressor (Johnson et al., 2007; Marshall, 2008) and understanding its activity and the complex activation and regulation mechanisms could assist future research approaches in this direction. Potentially, it could be investigated if Maf1/RNAP III could be usefully targeted for therapeutic benefits.

The aim of this study was to elucidate the molecular mechanism of the Maf1 mediated repression mechanism for RNAP III. Several strategies were chosen to achieve this goal.

A crystal structure of Maf1 was the initial priority in this study, potentially explaining Maf1 activation, which is dependent on phosphorylation and dephosphorylation. A structure gives insights into the regulatory mechanism of the cellular Maf1 distribution and serves as a basis for structure based interaction analysis with RNAP III and other regulatory proteins, thereby giving the first molecular details for Maf1 activity as a RNAP III transcription repressor.

Following a successful structure determination, the interaction of Maf1 with RNAP III can be investigated. *In vitro* binding studies with different Maf1 variants and mutants can elucidate binding surfaces and conserved essential residues. Also *in vivo* complementation assays can be used to analyze and understand the Maf1 structure.

Thirdly, the activity of Maf1 as a repressor of RNAP III transcription can be explored by functional assays. Therefore transcription assays as well as competitive binding assays with components of the RNAP III minimal PIC were performed.

Finally, cryo EM reconstructions of Maf1 bound to RNAP III were attempted, and the crystal structure of Maf1 used for docking into any potential difference densities.

2 Materials and Methods

2.1 Materials

2.1.1 Bacterial strains

Table 2. *E. coli* strains.

Strain	Genotype	Source
XL-1 Blue	*rec1A*; *endA1*; *gyrA96* ; *thi-1* ; *hsdR17*; *supE44* ; *relA1* ; *lac*[F´*proAB lacI* qZD*M15* Tn*10*(Tetr)]	Stratagene
BL21-CodonPlus (DE3)RIL	B; F−; *ompT*; *hsdS*(rB− mB−); *dcm*+; Tetr; *gal* _(DE3); *endA*; Hte [*argU*, *ileY*, *leuW*, Camr]	Stratagene
BL21-(DE3)pLysS	F- *ompT hsdS*B (rB-mB-) *gal dcm* (DE3) pLysS (CamR)	Invitrogen

2.1.2 Yeast strains

Table 3. List of *S. cerevisiae* strains used or generated within this study.

Strain	Genotype	Source
wt	BY4741; *MATa*; *his3*D1; *leu2*D0; *met15*D0; *ura3*D0	Euroscarf Y00000
wt	BY4742; *MAT*_ ; *his3*D1; *leu2*D0; *lys2*D0; *ura3*D0	Euroscarf Y10000
maf1 Δ	BY4741; Mat a; his3D1; leu2D0; met15D0; ura3D0; YDR005c::kanMX4	Euroscarf Y03945
maf1 Δ/ *sc*Maf1 fl	BY4741; Mat a; his3D1; leu2D0; met15D0; ura3D0; YDR005c::kanMX4 pRS316-*sc*Maf1 1-395	this work
maf1 Δ/ *hs*Maf1 fl	BY4741; Mat a; his3D1; leu2D0; met15D0; ura3D0; YDR005c::kanMX4 pRS316-*hs*Maf1 1-256	this work
maf1 Δ/ *sc*Maf1 1-345	BY4741; Mat a; his3D1; leu2D0; met15D0; ura3D0; YDR005c::kanMX4 pRS316-*sc*Maf1 1-345	this work
maf1 Δ/ *sc*Maf1 fl Δ36-52	BY4741; Mat a; his3D1; leu2D0; met15D0; ura3D0; YDR005c::kanMX4 pRS316-*sc*Maf1 1-395 Δ36-52	this work
maf1 Δ/ *sc*Maf1 fl Δ36-224	BY4741; Mat a; his3D1; leu2D0; met15D0; ura3D0; YDR005c::kanMX4 pRS316-*sc*Maf1 1-395 Δ36-224	this work
maf1 Δ/ *sc*Maf1 1-345 Δ36-224	BY4741; Mat a; his3D1; leu2D0; met15D0; ura3D0; YDR005c::kanMX4 pRS316-*sc*Maf1 1-345 Δ36-224	this work
maf1 Δ/ *sc*Maf1 fl D40A	BY4741; Mat a; his3D1; leu2D0; met15D0; ura3D0; YDR005c::kanMX4 pRS316-*sc*Maf1 1-395 D40A	this work
maf1 Δ/ *sc*Maf1 fl E272A	BY4741; Mat a; his3D1; leu2D0; met15D0; ura3D0; YDR005c::kanMX4 pRS316-*sc*Maf1 1-395 E272A	this work
maf1 Δ/ *sc*Maf1 fl K233A	BY4741; Mat a; his3D1; leu2D0; met15D0; ura3D0; YDR005c::kanMX4 pRS316-*sc*Maf1 1-395 K233A	this work

maf1 Δ/ *sc*Maf1 fl R232H	BY4741; Mat a; his3D1; leu2D0; met15D0; ura3D0; YDR005c::kanMX4 pRS316-*sc*Maf1 1-395 R232H	this work
maf1 Δ/ *sc*Maf1 fl G316E	BY4741; Mat a; his3D1; leu2D0; met15D0; ura3D0; YDR005c::kanMX4 pRS316-*sc*Maf1 1-395 G316E	this work
maf1 Δ/ *sc*Maf1 fl S263R	BY4741; Mat a; his3D1; leu2D0; met15D0; ura3D0; YDR005c::kanMX4 pRS316-*sc*Maf1 1-395 S263R	this work
maf1 Δ/ *sc*Maf1 fl D250A	BY4741; Mat a; his3D1; leu2D0; met15D0; ura3D0; YDR005c::kanMX4 pRS316-*sc*Maf1 1-395 D250A	this work
maf1 Δ/ *sc*Maf1 fl D248A	BY4741; Mat a; his3D1; leu2D0; met15D0; ura3D0; YDR005c::kanMX4 pRS316-*sc*Maf1 1-395 D248A	this work
maf1 Δ/ *sc*Maf1 fl D248A/D250A	BY4741; Mat a; his3D1; leu2D0; met15D0; ura3D0; YDR005c::kanMX4 pRS316-*sc*Maf1 1-395 D248A/D250A	this work
maf1 Δ/ *sc*Maf1 fl K329A/K331A	BY4741; Mat a; his3D1; leu2D0; met15D0; ura3D0; YDR005c::kanMX4 pRS316-*sc*Maf1 1-395 K329A/K331A	this work
maf1 Δ/ *sc*Maf1 fl D40N/R232H	BY4741; Mat a; his3D1; leu2D0; met15D0; ura3D0; YDR005c::kanMX4 pRS316-*sc*Maf1 1-395 D40N/R232H	this work

2.1.3 Plasmids and primers

Table 4. List of vectors used in this study.

Vector	Inserts/ Description	Type	Tag	Restr. sites	Primer
RR008	saccharomyces cerevisiae Maf1 1-395 (=fulllenght)	pET28b(+)	Nt His	NotI, NdeI	scMaf1 1 for NdeI scMaf1 395 rev
RR009	human Maf1 1-256 (=fulllenght)	pET28b(+)	Nt His	NotI, NdeI	hMaf1 ABC NdeI for hMaf1 f.l. NotI Stop rev
RR010	human Maf1 1-205 Δ36-82 (=X-tal construct)	pET28b(+)	Nt His	NotI, NdeI	hMaf1 ABC NdeI for hMaf11-205 NotI Stop rev hMaf1 D36-82 for hMaf1 D36-82 rev
RR011	sc Maf1 1-345 Δ36-224 (=X-tal assigned to yeast); insert ordered at mr gene with optimized sequence	pET28b(+)	Nt His	NotI, NdeI	scMaf1 1 for opt. NdeI scMaf1 345 rev opt NotI Stop
RR012	human Maf1 1-256 (=fulllenght)	pET21b(+)	_	NotI, NdeI	hMaf1 ABC NdeI for hMaf1 f.l. NotI Stop rev
RR013	human Maf1 82-213 (= "BC-box")	pET21b(+)	_	NotI, NdeI	hMaf1 BC NdeI for hMaf1 BC NotI rev
RR014	human Maf1 82-213 (= "BC-box")	pET28b(+)	Nt His	NotI, NdeI	hMaf1 BC NdeI for hMaf1 BC NotI rev
RR015	human Maf1 1-213 (="ABC-box")	pET28b(+)	Nt His	NotI, NdeI	hMaf1 ABC NdeI for hMaf1 BC NotI rev
RR016	human Maf1 1-213 (="ABC-box")	pET21b(+)	_	NotI, NdeI	hMaf1 ABC NdeI for hMaf1 BC NotI rev
RR017	human Maf1 1-81 (="A-box")	pET28b(+)	Nt His	NotI, NdeI	hMaf1 ABC NdeI for hMaf1 1-81 NotI Stop rev
RR018	human Maf1 1-81 (="A-box")	pET21b(+)	_	NotI, NdeI	hMaf1 ABC NdeI for hMaf1 1-81 NotI Stop rev
RR019	human Maf1 1-205 (="ABC-box - complete acidic tail")	pET28b(+)	Nt His	NotI, NdeI	hMaf1 ABC NdeI for hMaf1 1-205 NotI Stop rev

RR020	human Maf1 82-205 (="BC-box - complete acidic tail")	pET28b(+)	Nt His	NotI, NdeI	hMaf1 BC NdeI for hMaf1 1-205 NotI Stop rev
RR021	human Maf1 1-205 (="ABC-box - complete acidic tail")	pET21b(+)	_	NotI, NdeI	hMaf1 ABC NdeI for hMaf1 1-205 NotI Stop rev
RR022	human Maf1 52-213 (="mobile insertion + BC-box")	pET21b(+)	_	NotI, NdeI	hMaf1 52 NdeI for hMaf1 BC NotI rev
RR023	human Maf1 52-213 (="mobile insertion + BC-box")	pET28b(+)	Nt His	NotI, NdeI	hMaf1 52 NdeI for hMaf1 BC NotI rev
RR024	human Maf1 1-213 Δ63-78 (= -part of mobile insertion and -part of acidic tail)	pET28b(+)	Nt His	NotI, NdeI	hMaf1 ABC NdeI for hMaf1 BC NotI rev hMaf1 D63-78 for hMaf1 D63-78 rev
RR025	human Maf1 1-213 Δ 63-82 (= -part of mobile insertion and -part of acidic tail)	pET28b(+)	Nt His	NotI, NdeI	hMaf1 ABC NdeI for hMaf1 BC NotI rev hMaf1 D63-82 for hMaf1 D63-82 rev
RR026	human Maf1 1-256 Δ 63-82 (= -part of mobile insertion and fulllenght)	pET28b(+)	Nt His	NotI, NdeI	hMaf1 ABC NdeI for hMaf1 f.l. NotI Stop rev hMaf1 D63-82 for hMaf1 D63-82 rev
RR027	human Maf1 1-256 Δ 55-78 (= -part of mobile insertion and fulllenght)	pET21b(+)	_	NotI, NdeI	hMaf1 ABC NdeI for hMaf1 f.l. NotI Stop rev hMaf1 D55-78 for hMaf1 D55-78 rev
RR028	human Maf1 1-205 Δ55-78 (= -part of mobile insertion and -complete acidic tail)	pET21b(+)	_	NotI, NdeI	hMaf1 ABC NdeI for hMaf1 1-205 NotI Stop rev hMaf1 D55-78 for hMaf1 D55-78 rev
RR029	human Maf1 1-205 Δ55-82 (= -part of mobile insertion and -complete acidic tail)	pET21b(+)	_	NotI, NdeI	hMaf1 ABC NdeI for hMaf1 1-205 NotI Stop rev hMaf1 D55-82 for hMaf1 D55-82 rev
RR030	human Maf1 52-256 (="+ mobile insertion + BC-box + acidic tail")	pET21b(+)	_	NotI, NdeI	hMaf1 52 NdeI for hMaf1 f.l. NotI Stop rev
RR031	human Maf1 52-205 (="+ mobile insertion + BC-box - complete acidic tail")	pET21b(+)	_	NotI, NdeI	hMaf1 52 NdeI for hMaf1 1-205 NotI Stop rev
RR032	human Maf1 1-205 Δ63-82 (= -part of mobile insertion and -complete acidic tail)	pET21b(+)	_	NotI, NdeI	hMaf1 ABC NdeI for hMaf1 1-205 NotI Stop rev hMaf1 D63-82 for hMaf1 D63-82 rev
RR033	human Maf1 1-205 Δ63-78 (= -part of mobile insertion and -complete acidic tail)	pET21b(+)	_	NotI, NdeI	hMaf1 ABC NdeI for hMaf1 1-205 NotI Stop rev hMaf1 D63-78 for hMaf1 D63-78 rev
RR034	human Maf1 1-256 Δ55-82 (= -part of mobile insertion and fulllenght)	pET21b(+)	_	NotI, NdeI	hMaf1 ABC NdeI for hMaf1 f.l. NotI Stop rev hMaf1 D55-82 for hMaf1 D55-82 rev
RR035	human Maf1 1-205 Δ63-78 (= -part of mobile insertion and -complete acidic tail)	pET28b(+)	nt His	NotI, NdeI	hMaf1 ABC NdeI for hMaf1 1-205 NotI Stop rev hMaf1 D63-78 for hMaf1 D63-78 rev
RR036	human Maf1 82-256 (="- mobile insertion + BC-box + acidic tail")	pET21b(+)	_	NotI, NdeI	hMaf1 BC NdeI for hMaf1 f.l. NotI Stop rev
RR037	human Maf1 82-256 (="- mobile insertion + BC-box + acidic tail")	pET28b(+)	nt His	NotI, NdeI	hMaf1 BC NdeI for hMaf1 f.l. NotI Stop rev
RR038	human Maf1 1-256 Δ49-82 (= -part of mobile insertion and fulllenght)	pET28b(+)	nt His	NotI, NdeI	hMaf1 ABC NdeI for hMaf1 f.l. NotI Stop rev hMaf1 D49-82 for hMaf1 D49-82 rev

RR039	human Maf1 1-205 Δ49-82 (= -part of mobile insertion -complete acidic tail)	pET28b(+)	nt His	NotI, NdeI	hMaf1 ABC NdeI for hMaf1 1-205 NotI Stop rev hMaf1 D49-82 for hMaf1 D49-82 rev
RR040	human Maf1 1-205 Δ49-82 (= -part of mobile insertion -complete acidic tail)	pET21b(+)	_	NotI, NdeI	hMaf1 ABC NdeI for hMaf1 1-205 NotI Stop rev hMaf1 D49-82 for hMaf1 D49-82 rev
RR041	human Maf1 1-205 Δ36-82 (= -mobile insertion -complete acidic tail) crystallized construct	pET28b(+)	nt His	NotI, NdeI	hMaf1 ABC NdeI for hMaf1 1-205 NotI Stop rev hMaf1 D36-82 for hMaf1 D36-82 rev
RR042	human Maf1 82-205 (="BC-box" - mobile insertion -complete acidic tail)	pET28b(+)	nt His	NotI, NdeI	hMaf1 BC NdeI for hMaf1 1-205 NotI Stop rev
RR043	sc Maf1 1-395 Δ41-224 (= -part of mobile insertion, adapted to crystallized human construct, fulllenght) (achieved as unspecific product of cloning)	pET28b(+)	nt His	NotI, NdeI	scMaf1 1 NdeI for scMaf1 395 NotI rev Stop scMaf1 D36-224 for scMaf1 D36-224 rev
RR044	sc Maf1 1-340 Δ41-224 (= -part of mobile insertion, adapted to crystallized human construct, -acidic tail) (achieved as unspecific product of cloning)	pET28b(+)	nt His	NotI, NdeI	scMaf1 1 NdeI for scMaf1 340 rev NotI Stop scMaf1 D36-224 for scMaf1 D36-224 rev
RR045	based on RR086: sc Maf1 1-345 Δ36-224 (= -mobile insertion, -acidic tail) equates to crystallized human construct	pET28b(+)	nt His	NotI, NdeI	scMaf1 1 for opt. NdeI scMaf1 395 rev opt. NotI stop
RR046	based on RR087: sc Maf1 1-340 Δ52-224 (= -mobile insertion, including predicted helix, -acidic tail)	pET28b(+)	nt His	NotI, NdeI	scMaf1 1 for opt. NdeI scMaf1 340 rev opt NotI Stop
RR047	based on RR086: sc Maf1 1-340 Δ36-224 (= -mobile insertion, -acidic tail)	pET28b(+)	nt His	NotI, NdeI	scMaf1 1 for opt. NdeI scMaf1 340 rev opt NotI Stop
RR048	based on RR086: sc Maf1 1-340 Δ36-224 (= -mobile insertion, -acidic tail)	pET21b(+)	_	NotI, NdeI	scMaf1 1 for opt. NdeI scMaf1 340 rev opt NotI Stop
RR049	based on RR087: sc Maf1 1-395 Δ52-224 (= -mobile insertion, including predicted helix, fulllenght)	pET28b(+)	nt His	NotI, NdeI	scMaf1 1 for opt. NdeI scMaf1 395 rev opt NotI Stop
RR050	based on RR087: sc Maf1 1-395 Δ52-224 (= -mobile insertion, including predicted helix, fulllenght)	pET21b(+)	_	NotI, NdeI	scMaf1 1 for opt. NdeI scMaf1 395 rev opt NotI Stop
RR051	based on RR087: sc Maf1 1-345 Δ52-224 (= -mobile insertion, including predicted helix, -acidic tail)	pET28b(+)	nt His	NotI, NdeI	scMaf1 1 for opt. NdeI scMaf1 345 rev opt NotI Stop
RR052	based on RR087: sc Maf1 1-345 Δ52-224 (= -mobile insertion, including predicted helix, -acidic tail)	pET21b(+)	_	NotI, NdeI	scMaf1 1 for opt. NdeI scMaf1 345 rev opt NotI Stop
RR053	based on RR086: sc Maf1 1-395 Δ36-224 (= -mobile insertion, fulllenght)	pET21b(+)	_	NotI, NdeI	scMaf1 1 for opt. NdeI scMaf1 f.l. rev opt NotI Stop
RR054	sc Maf1 1-395 D248A /D250A	pET28b(+)	nt His	NotI, NdeI	yeast Maf1 D248A D250A for yeast Maf1 D248A D250A rev
RR055	sc Maf1 1-395 D250A	pET28b(+)	nt His	NotI, NdeI quick	yeast Maf1 D250A for yeast Maf1 D250A rev
RR056	sc Maf1 1-395 D40N	pET28b(+)	nt His	NotI, NdeI	yeast Maf1 D40N for yeast Maf1 D40N rev

RR057	sc Maf1 1-395 R232H	pET28b(+)	nt His	NotI, NdeI	yeast Maf1 R232H for yeast Maf1 R232H rev
RR058	sc Maf1 1-395 E314A	pET28b(+)	nt His	NotI, NdeI	yeast Maf1 E314A for yeast Maf1 E314A rev
RR059	sc Maf1 1-395 E314A	pET21b(+)	_	NotI, NdeI	yeast Maf1 E314A for yeast Maf1 E314A rev
RR060	sc Maf1 1-395 A240R	pET28b(+)	nt His	NotI, NdeI	yeast Maf1 A240R for yeast Maf1 A240R rev
RR061	sc Maf1 1-395 A240R	pET21b(+)	_	NotI, NdeI	yeast Maf1 A240R for yeast Maf1 A240R rev
RR062	sc Maf1 1-395 E272A	pET28b(+)	nt His	NotI, NdeI	yeast Maf1 E272A for yeast Maf1 E272A rev
RR063	sc Maf1 1-395 R280A	pET28b(+)	nt His	NotI, NdeI quick	yeast Maf1 R280A for yeast Maf1 R280A rev
RR064	sc Maf1 1-395 G316E	pET28b(+)	nt His	NotI, NdeI	yeast Maf1 G316E for yeast Maf1 G316E rev
RR065	sc Maf1 1-395 K233A	pET28b(+)	nt His	NotI, NdeI	yeast Maf1 K233A for yeast Maf1 K233A rev
RR066	sc Maf1 1-395 K329A/K331A	pET28b(+)	nt His	NotI, NdeI	yeast Maf1 K329A/K331A for yeast Maf1 K329A/K331A rev
RR067	C160 1-235 (=N-terminal 235 AA of C160 RNAP III)	pET28b(+)	nt His	NotI, NdeI	C160 1 NdeI for C160 235 NotI Stop rev
RR068	scMaf1 1-395	pET21b(+)	nt Strep	NotI, NdeI	scMaf1 1 for STREP NdeI scMaf1 f.l. NotI Stop rev
RR069	scMaf1 1-395 A240R	pET21b(+)	nt Strep	NotI, NdeI	yeast Maf1 A240R for yeast Maf1 A240R rev
RR070	sc Maf1 1-395 G316E	pET21b(+)	nt Strep	NotI, NdeI	yeast Maf1 G316E for yeast Maf1 G316E rev
RR071	sc Maf1 1-395 K233A	pET21b(+)	nt Strep	NotI, NdeI	yeast Maf1 K233A for yeast Maf1 K233A rev
RR072	sc Maf1 1-395 E272A	pET21b(+)	nt Strep	NotI, NdeI	yeast Maf1 E272A for yeast Maf1 E272A rev
RR073	sc Maf1 1-395 S263R	pET21b(+)	nt Strep	NotI, NdeI	yeast Maf1 S263R for yeast Maf1 S263R rev
RR074	sc Maf1 1-395 K329A/K331A	pET21b(+)	nt Strep	NotI, NdeI	yeast Maf1 K329A/K331A for yeast Maf1 K329A/K331A rev
RR075	sc Maf1 1-395 D248A	pET21b(+)	nt Strep	NotI, NdeI	yeast Maf1 D248A for yeast Maf1 D248A rev
RR076	sc Maf1 1-395 E314A	pET21b(+)	nt Strep	NotI, NdeI	yeast Maf1 E314A for yeast Maf1 E314A rev
RR077	sc Maf1 1-395 R280A	pET21b(+)	nt Strep	NotI, NdeI	yeast Maf1 R280A for yeast Maf1 R280A rev
RR078	sc Maf1 1-395 D250A	pET21b(+)	nt Strep	NotI, NdeI	yeast Maf1 D250A for yeast Maf1 D250A rev
RR079	sc Maf1 1-345 Δ36-224 (=X-tal assigned to yeast); insert with optimized sequence for Ecoli expr	pET21b(+)	nt Strep	NotI, NdeI	scMaf1 opt 1 for STREP NdeI scMaf1 345 rev opt. NotI stop
RR080	sc Maf1 1-345 Δ52-224; insert optimized sequence for Ecoli expr	pET21b(+)	nt Strep	NotI, NdeI	scMaf1 opt 1 for STREP NdeI scMaf1 345 rev opt. NotI stop
RR081	sc Maf1 1-395 Δ36-224 insert optimized	pET21b(+)	nt Strep	NotI,	scMaf1 opt 1 for STREP NdeI scMaf1 395 rev opt.

	sequence for Ecoli expr			NdeI	NotI stop
RR082	sc Maf1 1-395 D248A/H249Q (unspecific cloning product)	pET21b(+)	nt Strep	NotI, NdeI	yeast Maf1 D248A for yeast Maf1 D248A rev
RR083	sc Maf1 1-395 E314/D40N	pET21b(+)	nt Strep	NotI, NdeI	yeast Maf1 D40A for yeast Maf1 D40A rev
RR084	sc Maf1 1-395 R232H/D248A (unspecific cloning product)	pET21b(+)	nt Strep	NotI, NdeI	yeast Maf1 R232H for yeast Maf1 R232H rev
RR085	sc Maf1 1-395	pET21b(+)	_	NotI, NdeI	scMaf1 1 for NdeI scMaf1 395 rev
RR086	ordered at Mr gene: scMaf1 1-395 Δ36-224; optimized sequece for E.Coli expression (= -mobile insertion, fulllenght)	pAM	-	NotI, NdeI	scMaf1 opt for scMaf1 395 opt rev
RR087	ordered at Mr gene: scMaf1 1-395 Δ52-224; optimized sequence for E.Coli expression (= -mobile insertion incl. Predicted helix, fulllenght)	pAM	-	NotI, NdeI	scMaf1 opt for scMaf1 395 opt rev
RR088		pRS316			
RR089	human Maf1 52-256 (="+ mobile insertion + BC-box + acidic tail")	pET28b(+)	nt His	NotI, NdeI	hMaf1 52 NdeI for hMaf1 f.l. NotI Stop rev
RR090	Brf/TBP/Brf triple fusion (George Kassavetis)	pET28b(+)	nt His		-
RR091	C53 NH 2°/ C37 f.l.1° (Alessandro Vannini)	pDuet	His		-
RR092	scMaf1 1-395 Δ52-122 Δ188-224 (ordered at Mr Gene)	pMA	-	NotI, NdeI	scMaf1 for scMaf1 395 rev
RR093	scMaf1 1-395 Δ123-187 (ordered at Mr Gene)	pMA	-	NotI, NdeI	scMaf1for scMaf1 395 rev
RR094	scMaf1 1-395 Δ52-224 (ordered at Mr Gene), optimized sequence for E.Coli expression =RR087	pAM	-	NotI, NdeI	scMaf1 opt for scMaf1 395 opt rev
RR095	scMaf1 1-395 Δ36-224 (ordered at Mr Gene), optimized sequence for E.Coli expression =RR086	pAM	-	NotI, NdeI	scMaf1 opt for scMaf1 395 opt rev
RR002	scMaf1 1-395 with endogenous *s.cer.* promoter and terminator sequence – homologous recombination	pRS316	-	SacI (only vector cutting)	Iv_HR_scPromotor_NotI_for Iv_HR_scTerminator_SalI_rev Iv_HR_scMaf1_overlap_for Iv_HR_scMaf1_395_overlap-rev
RR001	hMaf1 1-256 with endogenous *s.cer.* promoter and terminator sequence (cut with HindIII in scMaf1 sequence of RR…) - homologous recombination	pRS316	-	HindIII	Iv_HR_hMaf1_overlap_for Iv_HR_hMaf1_overlap-rev
RR003	scMaf1 1-395D36-52 with endogenous *s.cer.* promoter and terminator sequence – homologous recombination (="+ mobile insertion -helix + acidic tail")	pRS316	-	HindIII	Iv_HR_scMaf1_D36-52_for Iv_HR_scMaf1_D36-52_rev Iv_HR_scMaf1_overlap_for Iv_HR_scMaf1_395_overlap-rev
RR004	scMaf1 1-395D36-224 with endogenous *s.cer.* promoter and terminator sequence – homologous recombination (="- mobile insertion -helix +acidic tail")	pRS316	-	HindIII	Iv_HR_scMaf1_D36-224_for Iv_HR_scMaf1_D36-224_rev Iv_HR_scMaf1_overlap_for Iv_HR_scMaf1_395_overlap-rev

RR005	scMaf1 1-345 with endogenous *s.cer.* promoter and terminator sequence – homologous recombination (="-acidic tail")	pRS316	-	HindIII	Iv_HR_scMaf1_overlap_for Iv_HR_scMaf1_345_overlap-rev
RR006	scMaf1 1-345 D36-224 with endogenous *s.cer.* promoter and terminator sequence – homologous recombination (="- mobile insertion-helix -acidic tail")	pRS316	-	HindIII	Iv_HR_scMaf1_overlap_for Iv_HR_scMaf1_345_overlap-rev
RR007	scMaf1 1-345 D41-224 with endogenous *s.cer.* promoter and terminator sequence – homologous recombination (="- mobile insertion –part of helix -acidic tail")	pRS316	-	HindIII	Iv_HR_scMaf1_overlap_for Iv_HR_scMaf1_345_overlap-rev
RR098	scMaf1 1-395 K329A/K331A with endogenous *s.cer.* promoter and terminator sequence	pRS316	-	-	yeast Maf1 K329A/K331A for yeast Maf1 K329A/K331A rev
RR099	scMaf1 1-395 R232H with endogenous *s.cer.* promoter and terminator sequence	pRS316	-	-	yeast Maf1 R232H for yeast Maf1 R232H rev
RR100	scMaf1 1-395 S263R with endogenous *s.cer.* promoter and terminator sequence	pRS316	-	-	yeast Maf1 S263R for yeast Maf1 S263R rev
RR101	scMaf1 1-395 G316E with endogenous *s.cer.* promoter and terminator sequence	pRS316	-	-	yeast Maf1 G316E for yeast Maf1 G316E rev
RR102	scMaf1 1-395 K233A with endogenous *s.cer.* promoter and terminator sequence	pRS316	-	-	yeast Maf1 K233A for yeast Maf1 K233A rev
RR103	scMaf1 1-395 D250 with endogenous *s.cer.* promoter and terminator sequence	pRS316	-	-	yeast Maf1 D250A for yeast Maf1 D250A rev
RR104	scMaf1 1-395 S263R/G316E with endogenous *s.cer.* promoter and terminator sequence	pRS316	-	-	yeast Maf1 S263R/G316E for yeast Maf1 S263R/G316E rev
RR106	scMaf1 1-395 D248A/D250A with endogenous *s.cer.* promoter and terminator sequence	pRS316	-	-	yeast Maf1 D248A/D250A for yeast Maf1 D248A/D250A rev
RR107	scMaf1 1-395 D40N/R232H with endogenous *s.cer.* promoter and terminator sequence (unspecific cloning product)	pRS316	-	-	yeast Maf1 D40N for yeast Maf1 D40N rev
RR108	scMaf1 1-395 E272A with endogenous *s.cer.* promoter and terminator sequence	pRS316	-	-	yeast Maf1 E272A for yeast Maf1 E272A rev
RR109	scMaf1 1-395 D40N with endogenous *s.cer.* promoter and terminator sequence	pRS316	-	-	yeast Maf1 D40A for yeast Maf1 D40A rev
RR110	scMaf1 1-395 D248A with endogenous *s.cer.* promoter and terminator sequence	pRS316	-	-	yeast Maf1 D248A for yeast Maf1 D248A rev
RR111	scMaf1 1-395 T111P/D248A with endogenous *s.cer.* promoter and terminator sequence (unspecific cloning product)	pRS316	-	-	-

Table 5. List of primers used in this study.

ID	Primer	Sequenz (5´-3´)
RRP01	scMaf1 1 NdeI for	GGAGGAGGACATATGAAGCTATTGGAGAACTCGAGCTTG
RRP02	scMaf1 395 rev	GGAGGAGGAGCGGCCGCCTACTGTAGGGATTCTTC
RRP03	hMaf1 ABC NdeI for	GGAGGAGGACATATGAAGCTATTGGAGAACTCGAGCTTG
RRP04	hMaf1 f.l. NotI Stop rev	GGAGGAGGAGCGGCCGCCTATCAAATACAGATCACTGG
RRP05	hMaf11-205 NotI Stop rev	GGAGGAGGAGCGGCCGCTCAGGAACGGCAGCTAAA
RRP06	hMaf1 D36-82 for	AGCTACTCATGTAAGCCCCTCAGTGACAAG
RRP07	hMaf1 D36-82 rev	CTTGTCACTGAGGGGCTTACATGAGTAGCT
RRP08	scMaf1 1 for opt. NdeI	GGAGGTACCCATATGATGAAATTCATTGACGAGCTGGAC
RRP09	scMaf1 345 rev opt NotI Stop	GGAGGAGGAGCGGCCGCTTAACTATTCAGGCGGCTACAGATCAG
RRP10	hMaf1 BC NdeI for	GGAGGAGGACATATGGGCCCCCTCAGTGACAAGTGC
RRP11	hMaf1 BC NotI rev	GGAGGAGCGGCCGCTCAGGGTGTGTAGGTGGAG
RRP12	hMaf1 1-81 NotI Stop rev	GGAGGAGGAGCGGCCGCTCACTCCTCCTCACCGCCTTG
RRP13	hMaf1 1-205 NotI Stop rev	GGAGGAGGAGCGGCCGCTCAGGAACGGCAGCTAAA
RRP14	hMaf1 52 NdeI for	GGAGGAGGACATATGCAGCCCCACGTGCTGGAGGCACTT
RRP15	hMaf1 D63-78 for	GCACTTTCTCCACCCGAGGAGGAGGGCCCC
RRP16	hMaf1 D63-78 rev	GGGGCCCTCCTCCTCGGGTGGAGAAAGTGC
RRP17	hMaf1 D63-82 for	GCACTTTCTCCACCCCCCCTCAGTGACAAG
RRP18	hMaf1 D63-82 rev	CTTGTCACTGAGGGGGGGTGGAGAAAGTGC
RRP19	hMaf1 D55-78 for	GGCCAGCCCCACGAGGAGGAGGGC
RRP20	hMaf1 D55-78 rev	GCCCTCCTCCTCGTGGGGCTGGCC
RRP21	hMaf1 D55-82 for	GAGGGCCAGCCCCACCCCCTCAGTGACAAG
RRP22	hMaf1 D55-82 rev	CTTGTCACTGAGGGGGTGGGGCTGGCCCTC
RRP23	hMaf1 D49-82 for	TTCAAGCAGTTCTGCCCCCTCAGTGACAAG
RRP24	hMaf1 D49-82 rev	CTTGTCACTGAGGGGGCAGAACTGCTTGAA
RRP27	scMaf1 D36-224 for	GCGGTTGCATCAGATCCCATAAACGAACCG
RRP28	scMaf1 D36-224 rev	CGGTTCGTTTATGGGATCTGATGCAACCGC
RRP29	scMaf1 340 rev NotI Stop	GGAGGAGGAGCGGCCGCTCAGCAAATCAAGTAAAGGTA
RRP30	scMaf1 395 rev opt. NotI stop	GGAGAGCTCGCGGCCGCTTACTGCAGTGACTCCTCTTGGTCGCT
RRP31	scMaf1 340 rev opt NotI Stop	GGAGGAGGAGCGGCCGCTTAACAGATCAGATACAGATAGGCCAC
RRP34	yeast Maf1 D248A D250A for	GCTTCTTATCCTGCCCATGCTTTTTCATCGGTT
RRP35	yeast Maf1 D248A D250A rev	AACCGATGAAAAAGCATGGGCAGGATAAGAAGC
RRP36	yeast Maf1 D250A for	TCTTATCCTGACCATGCTTTTTCATCGGTTGAG
RRP37	yeast Maf1 D250A rev	CTCAACCGATGAAAAAGCATGGTCAGGATAAGA
RRP38	yeast Maf1 D40N for	AAGGCGGTTGCATCAAATAGAAAATTATATAAA
RRP39	yeast Maf1 D40N rev	TTT TAT TAA TTT TCT ATT TGA TGC AAC CGC CTT
RRP40	yeast Maf1 R232H for	AAC GAA CCG TCA AGC CAC AAA ATA TTT GCT TAT
RRP41	yeast Maf1 R232H rev	ATAAGCAAATATTTTGTGGCTTGACGGTTCGTT
RRP42	yeast Maf1 E314A for	TTGGAAGATGCGCCTGGCTATCTT
RRP43	yeast Maf1 E314A rev	AAGATAGCCAGGCGCATCTTCCAA
RRP44	yeast Maf1 A240R for	TTTGCTTATCTGATTCGTATCCTCAACGCTTCT
RRP45	yeast Maf1 A240R rev	AGAAGCGTTGAGGATACGAATCAGATAAGCAAA
RRP46	yeast Maf1 E272A for	TTTATTTCCAAATTTGCAAACACCTTATATTCT
RRP47	yeast Maf1 E272A rev	AGAATATAAGGTGTTTGCAAATTTGGAAATAAA

RRP48	yeast Maf1 R280A for	TATTCTCTTGGTGCACAACCAGAGGAA
RRP49	yeast Maf1 R280A rev	TTCCTCTGGTTGTGCACCAAGAGAATA
RRP50	yeast Maf1 G316E for	TTGGAAGATGAGCCTGAATATCTTTGGAATCTT
RRP51	yeast Maf1 G316E rev	AAGATTCCAAAGATATTCAGGCTCATCTTCCAA
RRP52	yeast Maf1 K233A for	CCGTCAAGCCGCGCAATATTTGCTTAT
RRP53	yeast Maf1 K233A rev	ATAAGCAAATATTGCGCGGCTTGACGG
RRP54	yeast Maf1 K329A/K331A for	CTTTACAACAGGGCAAGGGCAAGAGTGGCTTAC
RRP55	yeast Maf1 K329A/K331A rev	GTAAGCCACTCTTGCCCTTGCCCTGTTGTAAAG
RRP56	C160 1 NdeI for	GGAGGAGGACATATGAAGGAAGTCGTTGTAAGTGAA
RRP57	C160 235 NotI Stop rev	GGAGGAGCGGCCGCTCACTTAATTTGCTTGAAAAGATTTAAAGT
RRP58	scMaf1 1 for STREP NdeI	GGAGGTACCCATATGGCAAGCTGGAGCCACCCGCAGTTCGAA AAGGGTGCAATGAAATTTATTGATGAG
RRP60	yeast Maf1 S263R for	GATTTTGTCAAAACACGATTGAAAACTTTTATT
RRP61	yeast Maf1 S263R rev	AATAAAAGTTTTCAATCGTGTTTTGACAAAATC
RRP62	yeast Maf1 D248A for	AACGCTTCTTATCCTGCCCATGATTTTTCATCG
RRP63	yeast Maf1 D248A rev	CGATGAAAAATCATGGGCAGGATAAGAAGCGTT
RRP64	scMaf1 opt 1 for STREP NdeI	GGAGGTACCCATATGGCAAGCTGGAGCCACCCGCAGTTCGAA AAGGGTGCAATGAAATTCATTGACGAG
RRP65	yeast Maf1 D40A for	AAGGCGGTTGCATCAGCTAGAAAATTATATAAA
RRP66	yeast Maf1 D40A rev	TTTTATTAATTTTCTAGCTGATGCAACCGCCTT
RRP70	C160 1 NdeI for	GGAGGAGGACATATGAAGGAAGTCGTTGTAAGTGAA
RRP71	C160 235 NotI Stop rev	GGAGGAGCGGCCGCTCACTTAATTTGCTTGAAAAGATTTAAAGT
RRP72	Iv_HR_scPromotor_NotI_for	Acggccagtgaattgtaatacgactcactatagggcgaattggagctcgcggccgc TCCGTATTCGGTCCTCATTATATCG
RRP73	Iv_HR_scTerminator_SalI_rev	Atgattacgccaagctcggaattaaccctcactaaagggaacaaaagctgggtacc GTCGACTTGAAGTTCCGTATTCGAAAGAAACT
RRP74	Iv_HR_scMaf1_overlap_for	TAACCGCTCATTACTCCAAACGGATTTTTTTGCCTAAAGAATCACGACA ATGAAAGTATGTTATCACTCTAAAACTGCCA
RRP75	Iv_HR_scMaf1_395_overlap-rev	AACGATTATAGGTGTAAGACAAGGAAAATTCACAAATTAAAGTTTAAAA ctactgtagggattcttcttgatctgat
RRP76	Iv_HR_hMaf1_overlap_for	TAACCGCTCATTACTCCAAACGGATTTTTTTGCCTAAAGAATCACGACA ATGaagctattggagaactcgagctttgaa
RRP77	Iv_HR_hMaf1_overlap-rev	AACGATTATAGGTGTAAGACAAGGAAAATTCACAAATTAAAGTTTAAAA tcaaatacagatcactgggaccctgtcctcc
RRP78	Iv_HR_scMaf1_345_overlap-rev	AACGATTATAGGTGTAAGACAAGGAAAATTCACAAATTAAAGTTTAAAA ctacgaatttagacgcgagcaaatcaa
RRP79	Iv_HR_scMaf1_D36-52_for	CAGTTGCGATATTTTCACAACAAAGACTATTTTACAGGAAAATGAGAATTACAATGCTA
RRP80	Iv_HR_scMaf1_D36-52_rev	TAGCATTGTAATTCTCATTTTCCTGTAAAATAGTCTTTGTTGTGAAAATATCGCAACTG

2.1.4 Reagents and Consumables

Chemicals were obtained from Merck (Darmstadt, Germany), Roth (Karlsruhe, Germany) or Sigma-Aldrich (Seelze, Germany), unless otherwise stated. Cloning enzymes and reagents were obtained from Fermentas (St. Leonrot, Germany), New England Biolabs (Frankfurt am Main, Germany) or Agilent/Stratagene (Waldbronn, Germany). For DNA preparation commercial kits from Qiagen (Hilden, Germany) were used. DNA oligonucleotides were ordered at ThermoScientifc (Ulm, Germany), RNA at Metabion (Planegg, Germany). Crystallization reagents were ordered at Hampton Research (Aliso Viejo, CA, USA) and Qiagen (Hilden, Germany). Reagents and consumables were ordered at standard laboratory suppliers.

2.1.5 Media and additives

Table 6. Media for *E. coli* and *S. cerevisiae*.

Media	Application	Description
LB	*E. coli* culture	1% (w/v) tryptone; 0.5% (w/v) yeast extract; 0.5% (w/v) NaCl
LSSB	*E. coli* culture	1% (w/v) tryptone; 0.5% (w/v) yeast extract; 0.5% (w/v) NaCl; 0.7M Sorbitol; 2.5 mM Betaine
SOB	*E. coli* transformation	2% (w/v) tryptone; 0.5% (w/v) yeast extract; 8.55 mM NaCl; 2.5 mM KCl; 10 mM MgCl2
SOC	*E. coli* transformation	SOB + 20 mM glucose (before use)
YPD	Yeast culture	2% (w/v) peptone; 2% (w/v) glucose; 1% (w/v) yeast extract
YPGly	Yeast culture	2% (w/v) peptone; 2% (w/v) glycerol; 1% (w/v) yeast extract
Synthetic defined (SD)	Yeast culture	Nitrogen and carbon sources, vitamins, trace elements, minerals according to specific drop outs; only essential amino acids; pH 5.6-6.0
Synthetic complete (SC)	Yeast culture	0.69% (w/v) nitrogen base; 0.6% (w/v) CSM amino acid drop out mix; 2% (w/v) glucose; pH 5.6-6.0

Table 7. Media additives for *E. coli* and *S. cerevisiae*.

Additive	Description	Stock Solution	Applied concentration
IPTG	*E. coli* induction	1M in H_2O	0.5 mM
Ampicillin	Antibiotic	100 mg/ml in H20	100 μg/ml for *E. coli* culture, 50 μg/ml for yeast culture
Kanamycin	Antibiotic	30 mg/ml in H20	30 μg/ml for *E. coli* culture
Chloramphenicol	Antibiotic	50 mg/ml in EtOH	50 μg/ml for *E. coli* culture
Streptomycin	Antibiotic	50 mg/ml in EtOH	50 μg/ml for *E. coli* culture
Tetracyclin	Antibiotic	12.5 mg/ml in 70% EtOH	12.5 μg/ml for yeast culture

2.1.6 Buffers and solutions

Standard buffers and solutions were prepared according to Sambrook and Russell (2001).

Table 8. General buffers, dyes and solutions.

Name	Description	Application
4x Stacking gel buffer	0.5 M Tris; 0.4% (w/v) SDS; pH 6.8 at 25°C	SDS-PAGE
4x Separation gel buffer	3 M Tris; 0.4% (w/v) SDS; pH 8.9 at 25°C	SDS-PAGE
Electrophoresis buffer	25 mM Tris; 0.1% (w/v) SDS; 250 mM glycine	SDS-PAGE
5x SDS sample buffer	250 mM Tris/HCl pH 7.0 at 25°C; 50% (v/v); glycerol; 0.5% (w/v) bromophenol blue; 7.5% (w/v) SDS; 12.5% (w/v) ß-mercaptoethanol	SDS-PAGE
Gel staining solution	50% (v/v) Ethanol; 7% (v/v) acetic acid; 0.125% (w/v) Coomassie Brilliant Blue R-250	Coomassie staining
Gel destaining solution	5% (v/v) Ethanol; 7% (v/v) acetic acid	Coomassie staining
Fix solution	50% MeOH, 12% HAc, 0.05% formalin (35%	Silver staining

	Formaldehyde)	
Silver nitrate solution	0.2% $AgNO_3$, 0.076% formalin (35% Formaldehyde)	Silver staining
Developer Solution	6% Na_2CO_3, 0.05% formalin (35% Formaldehyde), 0.0004% $Na_2S_2O_3$	Silver staining
Silver stop solution	50% MeOH, 12% HAc	Silver staining
2x Western transfer buffer	2.4% (w/v) glycin; 0.8% (w/v) Tris; 40% (v/v) methanol	Western blotting
Blotting buffer	10% (v/v) methanol in ddH2O	Edman sequencing
Swelling buffer	200 mM Tris/HCl pH 8.5 at 25°C; 2% (w/v) SDS	Edman sequencing
MOPS running buffer	40 mM MOPS (buffering); 10 mM NaAc; 1 mM EDTA; pH 7.0	Gradient Bis-Tris Gels (NuPAGE, Invitrogen)
MES running buffer	50 mM Tris base, 50 mM 3–(N-Morpholino)propanesulfonic acid, 1 mM EDTA, 0.01% SDS at pH 7.3)	Gradient Bis-Tris Gels (NuPAGE, Invitrogen)
PBS buffer	137 mM NaCl; 2.7 mM KCl; 10 mM Na_2HPO_4; 1.76 mM KH_2PO_4; pH 7.4	Protein expression
100x PI	0.028 mg/ml leupeptin; 0.137 mg/ml pepstatin A; 0.017 mg/ml PMSF; 0.33 mg/ml benzamidine; in 100% EtOH p.a.	Protease inhibitor mix
10x TBE	900 mM Tris; 900 mM boric acid; 20 mM EDTA (pH 8.0, 25°C)	Agarose gels
6x Loading buffer	10 mM Tris pH 7.6; 0.0015% (w/v) bromphenol blue; 0.0015% (w/v) xylene cyanol; 60% (v/v) glycerol; 100 mM EDTA; 1% SDS	Agarose gels
TFB-1	30 mM KOAc; 50 mM MnCl2; 100 mM RbCl; 10 mM; CaCl2; 15% (v/v) glycerol; pH 5.8 at 25°C	Chemically competent cells
TFB-2	10 mM MOPS pH 7.0 at 25°C; 10 mM RbCl; 75 mM CaCl2; 15% (v/v) glycerol	Chemically competent cells
TE	1 mM Tris pH 8.0; 0.1 mM EDTA	DNA dissolving
TB	20 mM Hepes 7.6; 60 mM $(NH_4)_2SO_4$; 8 mM $MgSO_4$; 10 µM $ZnCl_2$; 10% (v/v) Glycerol; 10 mM DTT	*In vitro* RNA extension assays
RNAP III transcription buffer	40 mM Tris 8.0; 7 mM MgCl2; 5% Glycerol; 60mM NaCl; 3 mM DTT	*In vitro* RNA extension assays
5x Breaking buffer	250 mM Tris 8.0; 750 mM NaCl; 0.5% TritonX 100; 25% Glycerol; 2.5 mM DTT	*In vitro* RNA extension assay
Blocking buffer	50 mM Tris 8.0; 150 mM NaCl; 2 mM EDTA 8.0; 0.1% TritonX 100; 5% Glycerol; 0.5% BSA; 35 µM Insulin; 8.3 µM Heparin; 0.5 mM DTT	*In vitro* RNA extension assays
Factor-independent transcription buffer	40 mM Tris-HCl pH 8.0, 60 mM NaCl, 7 mM $MgCl_2$, 7% glycerol, 5 mM DTT	Initiation factor-independent *in vitro* transcription assays
2x Urea loading buffer	20% (v/v) 10x TBE; 8 M Urea	Urea gel
2x Urea loading dye	20% (v/v) 10x TBE; 8 M Urea; 0.03% (w/v) bromphenol blue; 0.03% (w/v) xylene cyanol FF	Urea gel
Urea polyacrylamid gel solution	7 M Urea nf; 20% (v/v) Acrylamid solution nf (40%/2%); 1x TBE; 0.1% (v/v) TEMED; 0.05% (w/v) APS	Urea gel
5x Transcription acetate buffer	500 mM potassium acetate 7.6; 10 mM Hepes 7.6; 5 mM EDTA; 25 mM MgOAc	Initiation factor-dependent *in vitro*

		transcription assays
Stop buffer	100 mM NaAc; 10 mM EDTA; 0.5% (w/v); 0.2 g/L tRNA	Initiation factor-dependent *in vitro* transcription assays
5x Annealing buffer	25 mM Tris 8.3; 375 mM KCl; 5mM EDTA 8.0	Initiation factor-dependent *in vitro* transcription assays
5x Synthesis buffer	250 mM Tris 8.3; 375 mM KCl; 22.5 mM MgCl2; 75 mM DTT	Initiation factor-dependent *in vitro* transcription assays
2x FQP loading dye	80% (v/v) deionized formamide; 0.1 % (w/v) bromphenol blue; 25 mM EDTA 8.0	FQP-sequencing gel
50x FQP running buffer	166.7 mM Bis-Tris; 280.1 mM Tricine; 3.29 mM EDTA (free acid); adjust to pH 7.5 with NaOH	FQP-sequencing gel
FQP gel solution	5% (v/v) Acrylamid solution nf (40%/2%); 1x FQP running buffer; 6 M Urea nf; 0.12% (v/v) TEMED; 0.1% (w/v) APS	FQP-sequencing gel

Table 8. Maf1 purification buffers.

Name	Description
Buffer A	50 mM Hepes 7.8; 0.5 M NaCl; 10 mM Imidazole; 5 mM $MgCl_2$; 10 µM EDTA; 10% Glycerol; 10 mM ß-mercaptoethanol; 1x protease inhibitor
Buffer B	50 mM Hepes 7.8; 0.5 M NaCl; 20 mM Imidazole; 5 mM $MgCl_2$; 10 µM EDTA; 10% Glycerol; 10 mM ß-mercaptoethanol; 1x protease inhibitor
Buffer C	50 mM Hepes 7.8; 5 mM $MgCl_2$; 100 µM EDTA; 10% Glycerol; 5 mM DTT
Buffer D	50 mM Hepes 7.8; 200 mM NaCl; 5 mM DTT
Buffer E	25 mM Hepes 7.8; 25 mM NaCl; 5 mM DTT
Buffer F	100 mM Tris 8.0; 150 mM NaCl; 1 mM EDTA ; 2.5 mM DTT

Table 10. RNA Polymerase III purification buffers.

Name	Description
Buffer G	200 mM Tris 8.0; 10 mM $MgCl_2$; 500 mM $(NH_4)_2SO_4$; 10% Glycerol; 10 mM ß-mercaptoethanol; 1x protease inhibitor
Buffer H	40 mM Hepes 7.8; 5 mM $MgCl_2$; 1 mM EDTA; 10% Glycerol; 10 mM ß-mercaptoethanol; 1x protease inhibitor
Buffer I	40 mM Hepes 7.8; 5 mM $MgCl_2$; 500 mM KCl; 5 mM Imidazole 8.0; 10% Glycerol; 10 mM ß-mercaptoethanol; 1x protease inhibitor
Buffer J	40 mM Hepes 7.8; 5 mM $MgCl_2$; 250 mM $(NH_4)_2SO_4$; 10 mM Imidazole 8.0; 10% Glycerol; 10 mM ß-mercaptoethanol; 1x protease inhibitor
Buffer K	40 mM Hepes 7.8; 5 mM $MgCl_2$; 20% Glycerol; 500 µM EDTA; 10 mM ß-mercaptoethanol; 1x protease inhibitor
Buffer L	40 mM Hepes 7.8; 5 mM $MgCl_2$; 10% Glycerol; 5 mM DTT
Buffer M	50 mM Hepes 7.8; 100 µM $MgCl_2$; 40 mM $(NH_4)_2SO_4$; 10 µM $ZnCl_2$; 5 mM DTT

Table 11. C53/37 purification buffers.

Name	Description
Buffer N	50 mM Tris 8.0; 200 mM NaCl; 5% Glycerin; 10 mM ß-mercaptoethanol; 1x protease inhibitor
Buffer O	50 mM Tris 8.0; 500 mM NaCl; 10 mM Imidazole; 5% Glycerol; 10 mM ß-mercaptoethanol; 1x protease inhibitor
Buffer P	50 mM Tris 8.0; 150 mM NaCl; 1 mM EDTA; 5 mM DTT

Table 12. $Brf1_c/TBP_c/Brf1_n$ purification buffers.

Name	Description
Buffer Q (Lysis)	20 mM Hepes 7.8; 25 µM EDTA; 1.14 M NaCl; 5% Glycerol; 10 mM ß-mercaptoethanol; 1x protease inhibitor
Buffer R (Ni-wash1)	20 mM Hepes 7.8; 7 mM $MgCl_2$; 0.5 M NaCl; 10 mM Imidazole; 5% Glycerol; 10 mM ß-mercaptoethanol; 1x protease inhibitor
Buffer S (Ni-wash2)	20 mM Hepes 7.8; 7 mM $MgCl_2$; 0.5 M NaCl; 20 mM Imidazole; 20% Glycerol; 10 mM ß-mercaptoethanol; 1x protease inhibitor
Buffer T (Ni-elution)	20 mM Hepes 7.8; 7 mM $MgCl_2$; 0.5 M NaCl; 200 mM Imidazole; 20% Glycerol; 10 mM ß-mercaptoethanol; 1x protease inhibitor
Buffer U (MonoS)	50 mM Hepes 7.8; 0.5 mM $MgCl_2$; 50 mM NaCl; 0.2 mM EDTA; 10% Glycerol; 5 mM DTT
Buffer V (MonoS)	20 mM Hepes 7.8; 7 mM $MgCl_2$; 2 M NaCl; 200 mM Imidazole; 20% Glycerol; 10 mM ß-mercaptoethanol; 1x protease inhibitor

2.2 General methods

2.2.1 Preparation and transformation of competent cells

Chemically competent *E. coli* cells were prepared from LB overnight pre-cultures. 200 ml LB medium (supplemented with antibiotics if appropiate) were inoculated to a start optical density at 600 nm ($OD_{600\ nm}$) of 0.05, grown at 37°C and chilled on ice for 10 min once $OD_{600\ nm}$ of 0.5 was reached. Following steps were carried out at 4°C. Cells were centrifuged at 3200g for 10 min, washed with 50 ml TFB-1 buffer, centrifuged again and the sediment resuspended in 4 ml TFB-2 buffer. Aliquots were frozen in liquid nitrogen and cells stored at -80°C. Cells were transformed by heat shock typically using 100 ng (single transformation) or 200 ng (double transformation) vector, or 5-10 μl ligation product. Cells were incubated on ice for 10 min prior to heat shock at 42°C for 1 min in a water bath. Cells were subsequently cooled on ice for 1 min, 250 μl LB medium added and incubated for 1 h at 37°C vigorously shaking in a thermomixer (Qiagen). Cells were plated onto selective plates and incubated over night at 37°C.

Chemical competent yeast cells were prepared from precultures in YPD overnight precultures grown at 30°C. One hundred ml main cultures were inoculated with a start $OD_{600\ nm}$ of 0.2 and grown until a $OD_{600\ nm}$ of 0.8-1.2 was reached. Cells were centrifuged at 1250g for 5 min at room temperatur, washed with sterile water and centrifuged again. The sediments were resuspended in 1 ml 100 mM LiAc, transferred to reaction tubes, centrifuged at 18000g for 15 sec and resuspended in 100 mM LiAc to yield 500 μl each. Cells were aliquoted to 50 μl portions and directly used for yeast transformation reacions. After centrifugation, supernatants were discarded and cells covered with 240 µL PEG 3350 (50% (v/v)), 36 μl 1 M LiAc, 50 μl pre-heated salmon sperm DNA (c= 2 mg/mL), 2 nmol PCR product and 1 nmol plasmid DNA. Samples were vortexed vigorously for 1 min, then incubated 30 min at 30°C and afterwards heat shocked for 20 min at 42°C. Samples were centrifuged at 5200g for 15 sec and sediments resuspended in 250 µL sterile H_2O. Cells were plated onto selective plates and incubated at 30°C for 2-4 days.

2.2.2 Molecular cloning and mutagenesis

Polymerase Chain Reaction (PCR)

Primers were designed by using an overhang of several nucleotides (usually 5'-ggaggagga-3') at the 5' end, followed by the restriction side and at least 20 nucleotides complementary to the sequence of the gene of interest. Purification-tags were introduced either by in-frame cloning into according vectors or by PCR. PCR reactions were carried out with the Herculase II polymerase (Stratagene), Phusion High-Fidelity DNA polymerase (Finnzymes) or Taq polymerase (Fermentas), according to requirements, in a volume of 50 µl together with the respective buffer, 200 µM of dNTP mix, 0.5 µM of each primer, variable DMSO concentrations and 1-30 ng plasmid template or 100-200 ng genomic DNA template. To introduce loop-deletions, the overlap extension method was used. Here, two overlapping PCR-products are produced with primers carrying the desired deletion flanking regions. In a second PCR reaction these products were used as a template to produce the gene of interest containing the loop deletion.

Thermocycling programs were adjusted to the specific needs of the individual reactions in terms of annealing temperature and elongation times and usually contained 30 cycles (Biometra T3000 Thermocycler). PCR products were visualized by 1% agarose gel electrophoresis and staining with Sybr Safe (Invitrogen). Purification of the DNA was carried out with the QIAquick gel extraction protocol (Quiagen).

Point mutations into vectors were introduced with the site-directed mutagenesis method. Usually, 10 ng of template vector was used in the mutational PCR with Pfu polymerase (Fermentas). Primers typically exhibited 20 complementary nucleotides neighbouring each site of the mutation. PCR reactions were performed with low annealing temperatures (40-50°C) and 2 min/kb extension time. The parental vector, containing methylated DNA, was digested by 10U *Dpn*I (Fermentas) for 1 h at 37°C and the reaction directly transformed into competent cells.

Enzymatic restriction cleavage

Purified PCR product DNA was digested using restriction endonucleases (New England Biolabs and Fermentas) as recommended by the producer. Cleaved PCR products were purified using the QIAquick PCR purification protocol, cleaved plasmids by the QIAquick gel extraction protocol (both Quiagen).

Ligation
Ligation of digested DNA into linearized vectors was carried out for 1 hour at room temperature or over nught at 16°C in a volume of 20 µL using T4 DNA ligase (Fermentas) and its corresponding buffer. Concentrations of DNA components were varied depending on the different reactions. Usually a 5- to 10-fold excess of insert, relative to linearized vector was used. Ligation products were transformed as described in 2.2.1.

Homologous recombination
In addition to restriction enzyme based cloning, *in vivo* homologous recombination in yeast was used. Therefore yeast cells were transformed as described (see 2.2.1), using PCR-generated inserts, which contained 50 bp homologous regions at its 5' and 3' ends and a plasmid harbouring selection markesr for both, yeast and *E.coli*. Growth on selective plates was performed.

Isolation of plasmid DNA
After transformation of ligation products into competent cells or after homologous recombination, single clones from selective plates were used to inoculate 5 ml overnight cultures. Yeast plasmid preparation was performed with a modified Qiagen protocol for DNA preparation from *E. coli* (Jones et al. 2001). Subsequentially, 5 µl of the purified yeast plasmid DNA was transformed into *E. coli* cells and plated on selective plates (see 2.2.1). Plasmids were isolated from the *E. coli* clones using Miniprep purification kits (Qiagen) and verified by restriction analysis and DNA sequencing (Eurofins MWG and GATC).

Electrophoretic separation of DNA
Separation of DNA was carried out in horizontal 1x TBE agarose gels containing Sybr Safe (0.7 µg/ml). Agarose concentrations varied between 1% to 2%, depending on the size of the DNA molecules to seperate. Separation was carried out in PerfectBlue Gelsystem electrophoresis chambers from Peqlab. Samples were mixed with 6x loading dye and DNA was visualized and documented using a Safe Imager blue light transilluminator from Invitrogen (λ=470 nm).

2.2.3 Protein expression in *E. coli*

Recombinant proteins were expressed in *E. coli* BL21-CodonPlus (DE3)RIL (Maf1 variants, C160, C53/37 subcomplex), in *E. coli* BL21-CodonPlus (DE3)RIPL (human mitochondrial Polymerase) or in *E. coli* BL21-(DE3)pLysS cells ($Brf1_c$/TBP_c/$Brf1_n$ construct). Therefore plasmids with desired protein variants were transformed as described in 2.2.1. Cells were grown in LSSB- (for $Brf1_c$-TBP-$Brf1_n$ protein) or LB- (for all other recombinant proteins) medium including antibiotics for *E. coli* cells and the appropriate vector at 37°C up to an $OD_{600\ nm}$ of 0.5 to 0.8 and for human mitoRNAP up to an $OD_{600\ nm}$ of < 0.4. Cells were cooled on ice for 30 min, induced by addition of 0.5 mM IPTG and grown at 18°C over night while shaking. For human mitoRNAP induction was performed with 0.1 mM IPTG and growth o.n. at 16°C. Cells were harvested by centrifugation at 4000g and 4°C for 20 min and resuspended in PBS buffer. Cells were centrifuged again and the sediments flash frozen in liquid nitrogen and stored at -80°C.
Protein purification protocols for all used recombinant proteins are described in the accordant Special procedures.

2.2.4 Protein analyses

Determination of protein concentrations

Total protein concentrations were usually determined by a Bradford assay (Bradford, 1976) at an OD of 595 nm using dye reagent (Bio-Rad) according to the manufacturer's instructions. Reference curves were generated for each new batch of dye reagent using bovine serum albumin (Fraktion V, Roth). Alternatively, protein concentrations were calculated from the absorption rate by OD_{280nm} measurement using a ND-1000 (NanoDrop) spectrophotometer. Individual molar absorption coefficients for the used proteins were calculated with the help of the ProtParam software (Gasteiger et al., 2005).

SDS-Polyacrylamid gel electrophoresis

Electrophoretic separation of protein was conducted by SDS-PAGE with 15% acrylamide gels (with acrylamide:bisacrylamide = 37.5:1) according to Laemmli (1970) in BioRad gel systems. For protein samples requiring broader or higher resolution separation, pre-casted NuPAGE Novex bis-Tris minigels (Invitrogen) were used according to the manufacturer's instructions. Normally, gels were stained with Coomassie gel staining solution for 20 min and destained over night in gel destaining solution. For very sensitive detections of protein samples or for simultaneous stainings of proteins and nucleotides silver staining of the gel was performed. Therefore, the gel was fixed 2 h in Fix solution, washed three times with 35 % (v/v) EtOH, sensitized in 0.02% $Na_2S_2O_3$ for 2 min and washed again three times in H_2O. For staining the gel was incubated 20 min in Silver nitrate solution, washed two times in H_2O and developed in Developer solution. Upon reaching a sufficient staining the reaction was stopped by adding Silver stop solution for 5 min.

Edman sequencing

N-terminal sequencing was conducted by first separating proteins on SDS-PAGE, staining with Coomassie blue and either transferring by Western blotting or by passive adsorption onto PVDF membranes. Western blotting was performed using Western transfer buffer in Mini Trans-Blot Cells (Bio-Rad) according to the manufacturer's instructions. For passive adsorption transfer, bands of interest were excised from the gel, dried in a speed-vac and rehydrated in 20 µl swelling buffer at room temperature. Next 100 µl of ddH2O was added to set up a concentration gradient together with a small piece of pre-wet (ethanol) PVDF membrane (Schleicher& Schuell). Once the solution turned blue, 10 µl of methanol was added as a catalyst and the sample incubated for 4 days. The membrane was washed 5 times with 10% methanol by vortexing for 30 sec each time. Second the protein was N-terminally sequenced from the dry membrane in a PROCISE 491 sequencer (Applied Biosystems).

2.2.5 Limited proteolysis analysis

Limited proteolysis time course experiments were performed to identify stable protein fragments. Proteolysis was conducted with chymotrypsin and trypsin at 37°C and with subtilisin at 0°C. Each sample was analyzed at 1, 3, 10, 30 and 60 min. Digests were performed using 100 μg protein samples in their gel filtration buffer containing 5 mM $MgCl_2$ and addition of 1 µg protease. The reactions were stopped by the addition of SDS sample buffer and were heated immediately to 95°C for 10 min. Sample fragments were separated on SDS-PAGE and bands analyzed by mass-spectrometry and Edman sequencing.

2.2.6 Crystallization Screening

Initial crystallization screening was performed by the sitting-drop (vapour diffusion) method using commercial screens. In-house screens were set up using a Hydra II crystallization robot producing 100 nl drops in Corning 96-well crystallization plates. Usually a reducing agent (5 mM TCEP or 10 mM DTT) was added to the drop or reservoir. Prior to setting up the screen, optimum protein concentrations for crystallization screening were determined. This was achieved by visual control of the behaviour of equal volume drops of protein solution and the no. 1 and 6 screening solutions of the Hampton Crystal Screen 1. Plates were incubated at 4 or 20°C and inspected regularly from one day up to 90 days. To a greater extend crystallization screening was performed by the Crystallization Facility at the MPI of Biochemistry, Munich. Here a number of screens were tested at 20°C and by the sitting-drop method, using a 100 nL protein drop size. The following screens were used: Index screen, Classic screen, PEG/Ion (all Hampton), Anions suite, Cations suite, Classic suite (all Qiagen), and Magic 1 and 2 sceens (MPI Martinsried). Potential protein crystals were tested by diffraction measurements with the PX Scanner from Oxford Diffraction. Promising initial crystals were refined in 24-well hanging drop plates (Easy Xtal Tool, Qiagen) by varying the pH, precipitant and additive concentrations of initial conditions.

2.2.7 Bioinformatic tools

Protein and gene sequences were retrieved from the NCBI or *Saccharomyces cerevisiae* genome (SGD) databases. Sequence data was visualized and processed using the following software applications: VectorNTI (Invitrogen) and ApE (Davis and Hammarlund, 2006). Bioinformatic analysis were performed mostly using the Bioinformatics Toolkit (Biegert et al., 2006). Multiple sequence alignments were generated using Clustal2W (Larkin et al., 2007), Espript 2.2 (Gouet et al., 1999), or Aline (Bond and Schuttelkopf, 2009). Protein secondary structures were predicted by HHpred (Soeding et al., 2005).

2.3 Specific procedures

2.3.1 Recombinant Maf1

2.3.1.1 Purification of recombinant Maf1 variants and mutants

Variants of Maf1 from the organisms *Saccharomyces cerevisiae* and *Homo sapiens* were purified each from 4 L of IPTG induced expression culture (2.2.3). Cells were lysed using a Sonifier Cell Discruptor 250 (Branson) in buffer A (see Table 8). For the purification of His-tagged Maf1-variants, imidazole was added to a final concentration of 20 mM after 1h centrifugation to the supernatant. The sample was loaded onto two 2 ml Ni-NTA columns (Qiagen) equilibrated with buffer B. The columns were washed with 20 column volumes (CVs) of buffer B and 10 CVs of buffer B containing 30 mM imidazole and 200 µM NaCl. Elution was performed with buffer B containing 300 mM imidazole and 200 µM NaCl. The fractions were analyzed for recombinant protein by SDS-PAGE (see 2.2.5). Proteins were purified by anion exchange chromatography (Mono Q, GE Healthcare). The column was equilibrated with buffer C and proteins were eluted with a linear gradient of 20 CVs from 10 mM to 1

M NaCl. Peak fractions and flowthrough of this chromatography step were checked by SDS-PAGE (2.2.5) for the presence of recombinant protein. Fractions containing the corresponding Maf1 variant were pooled and concentrated (Amicon Ultra centrifugal filter devices, cutoff 10k, Millipore). Afterwards samples were applied to a Superdex-75 size exclusion column (GE Healthcare) equilibrated with buffer D or E for crystallization experiments, or buffer M for activity assays and binding experiments. Peak fractions were pooled and concentrated to 10-50 mg/ml for crystallization, respectively 5 mg/mL for other assays.
For the purification of Strep-tagged Maf1, the supernatant after cell lysis and centrifugation was added with 3 nmol Avidin per L of cell lysate and loaded on two 1 mL Strep-Tactin columns (Iba) equilibrated in buffer F. The columns were washed with 20 CVs buffer F and Strep-tagged protein was eluted with 4 CVs buffer G. Subsequently, protein samples were purified by anion exchange and gelfiltration chromatography as described above.
Proteins without any tag were purified by fractionated ammoniumsulfate precipitation. Therefore the supernatant after cell lysis and centrifugation was dealt with 25%, 40%, 60%, and 80% of ammonium sulphate. After each titration step the sample was stirred 30 min on ice and centrifuged at 10000g and 4°C for 20 min. Sediments were resuspended in buffer C and analyzed on a SDS-PAGE. Fractions containing Maf1 were further purified with anion exchange and gelfiltration chromatography as described above.
The purification protocol was the same for *Saccharomyces cerevisiae* Maf1 variants containing point mutations, which carried a His_6- or streptavidin-tag.

2.3.1.2 Crystallization of Maf1 variants

Initial screens of crystallization conditions using different protein variants were set up and analyzed as described in 2.2.7. Promising initial crystals were refined in 24 well hanging drop plates (Easy Xtal Tool, Qiagen) by varying the concentrations of constituents of initial conditions.
Diffraction quality crystals of the Maf1 1-205 Δ36-82 variant of *Homo sapiens* were grown by mixing 1 µL of purified protein in size exclusion buffer E with a concentration of 40 mg/mL with 1 µL of reservoir solution containing 50 mM MES pH 6.0 and 175 mM sodium oxalate. Crystals were grown within two days at 20°C in hanging drop. Native crystals were transferred into reservoir solution containing 25% glycerol and were flash cooled in liquid nitrogen. Crystals were soaked for 0.5-2 minutes in a reservoir solution containing 25% glycerol and 0.5 M NaBr and flash-frozen in liquid nitrogen.
Also the Maf1 1-345 Δ52-224 variant of *Saccharomyes cerevisiae* produced nice shaped initial crystals, which were reproduced by mixing 2 µL of purified protein in size exclusion buffer D with a concentration of 30 mg/mL with 2 µL of reservoir solution containing 50 mM MES 6.0, 4% MPD, 80 mM $(NH_4)_2SO_4$, and 10% PEG 8000. Crystals were grown within 2 days, dipped into reservoir solution containing different cryo-protectants like 20-30% glycerol, 25-35% MPD, or 25-35% PEG 200 and flash frozen in liquid nitrogen.

2.3.1.3 Data collection and X-ray structure determination

Diffraction data for the Maf1 1-205 Δ36-82 variant of *Homo sapiens* were collected at 100 K on a PILATUS 6M detector at the Swiss Light Source (SLS), Villigen, Switzerland (Table 13). Three-wavelength anomalous diffraction data were collected from a bromide-soaked crystal. Data were processed with MOSFLM (Leslie et al., 1986), scaled with SCALA (Evans, 2006), and data quality was assessed with Phenix.Xtriage (Adams et al., 2010). Program Phenix.HySS (Adams et al., 2010)

identified six bromide sites that were used for phasing with program SOLVE (Terwilliger and Berendzen, 1999). Density modification was carried out with RESOLVE (Terwilliger, 2003). The model was built with COOT (Emsley and Cowtan, 2004) and refined with Phenix.Refine (Adams et al., 2010) to a free R-factor of 21% (Table 13). The structures and diffraction data of *h.s.* Maf1 1-205Δ36-82 have been deposited in the Protein Data Bank under the accession code 3NR5.
Diffraction data for the Maf1 1-345 Δ52-224 variant of *Saccharomyes cerevisiae* were collected on an ADSC Q4 CCD detector at the European Synchrotron Radiation Facility (ESRF), Grenoble, France.

2.3.1.4 Interaction assays with Maf1 variants and mutants

Protein/ protein interactions
Binding experiments of Maf1 variants and point mutants with RNAP III, its subunit C34, and with $Brf1_c/TBP_c/Brf1_n$ were carried out first to identify Maf1 parts sufficient for RNAP III binding, second to elucidate binding surfaces of Maf1 and third to investigate the functional mechanism of Maf1 induced repression. Protein interactions were analyzed with purified samples by pulldown assays or gelfiltration chromatography. For pulldown assays 10-fold molar excess of untagged or strep-tagged Maf1 was preincubated with the respective interaction partner in buffer M and incubated 20 min on ice. The samples were loaded on pre-equilibrated 30 µL Ni-beads (Promega Magnetic Beads) or 20 µL streptavidin-beads (Iba Magnetic Beads type 1) for pulldown of His-tagged or strep-tagged protein, respectively. Ni-beads were washed six times with 1 mL buffer M containing 20 mM imidazole and eluted with 25 µL buffer M containing 500 mM imidazole. Streptavidin-beads were washed six times with 1 mL buffer M and eluted with 25 µL buffer M containing 10 mM d-Desthiobiotin. Samples were analyzed by NuPAGE (Invitrogen). For gelfiltration chromatography assays pre-assembled proteins were loaded on a Superose 6 10/300 GL (GE Healthcare) column in buffer M and peaks analyzed by NuPAGE.

Competing protein/protein interactions with scaffolds
To investigate the functional mechanism of the negative regulation of RNAP III transcription by Maf1, the binding behaviour of Maf1, RNAP III, $Brf1_c/TBP_c/Brf1_n$ and DNA scaffolds was tested in order of addition experiments. RNAP III-Brf1-TBP-DNA and RNAP III-Maf1 complexes were pre-assembled using 5-fold molar excesses of Brf1-TBP-DNA and Maf1, respectively, in buffer M for 60 min at 4°C and purified by gel-filtration (Superose 6 10/300 GL, GE Healthcare) in buffer M. Purified complexes were then incubated with a five-fold molar excess of the competing factors, incubated in buffer M for 60 min at 4°C, applied again to gel filtration, and analyzed by NuPAGE (Invitrogen). For the nucleic acid binding assay, size-exclusion purified complexes were analyzed by silver-stained gels.

2.3.1.5 Coexpression and copurification

Coexpression was performed as described in 2.2.3 with *E.Coli* strains carrying two plasmids, each with one protein of interest and with or without a His6-tag, respectively. 1L of *E.coli* culture was used for Ni-NTA purifications. Cell lysates were clarified by centrifugation and copurification performed by loading the sample on a 2 mL Ni-NTA column pre-equilibrated in buffer B. Washing and elution was performed as described in 2.3.1.1. Samples were analyzed on SDS-PAGE.

2.3.1.6 Initiation factor-dependent *in vitro* transcription assays

In vitro transcription assays for the RNAP III system with purified proteins had to be established and based on protocols described by the Hahn laboratory (www.fhcrc.org/labs/hahn/). A linear 145 nt U6

scaffold with a minimal bubble at position -9 until -5 was used as a template (templateDNA:5´CCTCCTGGATCCCTGATCATCTCTGTATTGTTTCAAATTGACCAAATGTCC ACGAAGGGTTACTTCGCGAACACATAGTTGCGAAAAAAACATTTATTTATAGTAGCCGAA AATAGTGGACGAAATACTTTTCTCGAGTCCTCC3´;nontemplateDNA:5´GGAGGACTCGAGA AAAGTATTTCGTCCACTATTTTCGGCTACTATAAATAAATGTTTTTTTCGGTTGAATGTGTT CGCGAAGTAACCCTTCGTGGACATTTGGTCAATTTGAAACAATACAGAGATGATCAGGGA TCCAGGAGG3´). Transcription reactions were carried out in a 25 μL volume. The reaction mixture contained 75 pmol $Brf1_c$/TBP_c/$Brf1_n$, 5 pmol RNAP III, 1 pmol template 1x Transcription acetate buffer, 2.5 mM DTT, 192 μg of phosphocreatine, 0.2 mg of creatine phosphokinase, 10U of RNase inhibitor (GE Healthcare), and 100 µM nucleoside triphosphates. Optionally, 180 pmol Maf1 were added together with RNAP III. The reaction was incubated at 30 °C for 30 min and then stopped with 180 μl of Stop buffer. Samples were extracted with phenol–chloroform and precipitated with ethanol. Transcripts were analysed by primer extension essentially as described (Ranish and Hahn, 1991). Instead of the ^{32}P labelled lacI oligo, 0.125 pmol of a fluorescently labelled Cy5-oligo (25 nt long, starting transcription at position +50) was used. Quantification was performed with a Typhoon 9400 and the ImageQuant Software (GE Healthcare).

2.3.1.7 Initiation factor-independent *in vitro* transcription assays

For factor-independent transcription assays, 1.5 pmol of RNAP III or RNAP III-Maf1 complex were incubated for 30 min at 20ºC with 2 pmol or variable amounts of a pre-annealed tailed-template scaffold (nontemplate DNA: 5'- GGCTACTATAAATAAATGTTTTTTTC GCAACTATGTGTTCGCGAAGTAACCCTTCGTGGACATTTGGTCAATTTGAAACAATACAG AGATGATCAGCAGT-3'; template DNA: 5'- ACTGCTGATCATCTCTGTATTG TTTCAAATTGACCAAATGTCCACGAAGGGTTACTTCGCGAACACATAGTTGCGAAAAAAA CATTTATTTATAGTAGCCTGCA-3'), in the presence of 0.5 mM GpG RNA primer. Complexes were incubated for 30 min at 20ºC in the presence of 0.3 mM ATP, GTP, CTP, ^{32}P-UTP in 20 µL Factor-independent transcription buffer. Reactions were stopped by addition of an equal volume of 2x Urea loading buffer and incubation for 5 min at 95°C. RNA products were separated by denaturing gel electrophoresis and visualized with a Typhoon 9400 phosphoimager (GE Healthcare).

2.3.1.8 *In vitro* RNA extension assays

Minimal Scaffold

For RNA extension assays, 5 pmol of RNAP III or RNAP III pre-incubated (10 min at 20°C) with a five-fold molar excess of Maf1 was incubated for 30 min at 20°C with 5 pmol of a pre-annealed minimal nucleic-acid scaffold (template DNA: 3'-TTACTGGTCCGGATTCATGAACTCGA-5'; nontemplate DNA: 5'-TAAGTACTTGAG-3'; RNA: 5'-FAM-UGCAUUUCGACCAGGC-3'). Maf1 was added at a five-fold molar excess followed by incubation for 5 min at 20°C. For RNA elongation, complexes were incubated for 10 min with 1 mM NTPs at 28°C in TB. Reactions were stopped and RNA products were separated and visualized as above.

Complete Complementary scaffold (bead based)

Bead-based assays were carried out as described with some modifications (Dengl et al., 2009). Briefly, per reaction 10 pmol RNAP III, optionally pre-incubated with a 10-fold molar excess of Maf1 were added to 20 pmol of an annealed DNA/RNA scaffold (RNA: FUGCAU UUCGACCAGGC3'; template DNA:3'TGCGCACCACGCTTACTGGTCCGAACGCCTG TCCTCGACCA5´). This

mixture was incubated 15 min at 20°C and mild shaking. 40 pmol nontemplate DNA (ACGCGTGGTGCGAATGACCAGGCTTGCGGACAGGAGCTGGT–3') was added and incubated 15 min at 25°C. Beads (Dynabeads MyOneTM Streptavidin T1 from Invitrogen) were added to preassembled elongation complexes (ECs) for assembly and incubated for 30 min at 25°C. Beads were subsequently washed with TB containing 0.1% Triton-X, TB containing 0.2 M $(NH_4)2SO_4$, and with TB. Beads were re-suspended in TB. For RNA extension assays including time course experiments, different amounts of NTPs (Jena Bioscience) were added, the mixture was incubated at 28°C and reactions were stopped at different time points by addition of an equal volume of 100 mM EDTA, essentially as described (Brueckner et al., 2007; Dengl et al., 2009). The beads were transferred into urea loading buffer, samples were heated to 95°C and loaded on a 20% polyacrylamid gel containing 7 M Urea. The FAM 5'-labeled RNA products were visualized with a Typhoon 9400 scanner (GE Healthcare).

2.3.1.9 EMSA assays

Nucleic acids binding activities of *h.sapiens* and *s.cerevisiae* Maf1 were analyzed using the electrophoretic mobility shift assay (EMSA). Complexes of protein and DNA migrate through a native polyacrylamide (PAA) gel more slowly than free oligonucleotides. Nucleic acid probes included double-stranded *h.s.* U6 promoter sequence, double-or single-stranded *s.c.* U6 promoter sequence, and a random double-stranded sequence, each 60 bp long. Doublestranded DNA probes ware obtained by annealing complementary synthetic single strands. 80 pmol DNA were incubated with 5-fold molar excess of Maf1 in 20 µl buffer E for 30 min on ice as described. Bound and free probes were resolved by electrophoresis in 1% agarose gels tained with SYBR-Safe (Invitrogen) and afterwards restained in gel staining solution containing coomassie blue. This ensured colocalization of nucleic acid-protein complexes.

2.3.2 Endogenous Maf1

2.3.2.1 Yeast strains generation

Yeast strains Y03945 (maf1Δ) and Y10000/ Y00000 (wild type) were obtained from Euroscarf (see Table 3). Genomic manipulation of the maf1Δ strain in form of a kanMX cassette at the maf1 loci in the yeast genome was verified by performing colony PCR reactions with primers upstream and downstream of the mutated site and DNA sequencing after agarose gel separation and isolation of the PCR-product.

To achieve deletion or point mutants of Maf1, Y03945 cells were transformed (see 2.2.1) with digested pRS316 vector and PCR products that allowed for homologous recombination and growth of transformants on selective plates (Baudin et al., 1993). Colonies were restreaked, plasmid DNA of potential positive clones isolated (2.2.2) and verified by test digestion and sequencing.

2.3.2.2 *In vivo* phenotyping assays

Phenotype analyses of wildtype and Maf1 deletion or point mutants were performed from cultures grown to stationary phase in YPD or –Ura medium, respectively. Cells were diluted to an $OD_{600\ nm}$ of 1.0, washed, and spotted in serial dilution onto plates. Growth defect assays were performed with YPD plates, YP plates containing 3% glycerol (YPGly), and YPD plates containing 2.0 µg/mL Rapamycin at 30°C and 37°C. Yeast growth was detected after 2-5 days.

2.3.3 Endogenous RNA Polymerase III and its recombinant transcription factors

2.3.3.1 Purification of endogenous RNA Polymerase III

The purification protocol was established in the laboratory by Dr Alesssandro Vannini. The *Saccharomyces cerevisiae* strain NZ16 (Lannutti et al., 1996), carrying the gene for an N-terminally His6-FLAG4-RET1-tagged C128 subunit on the parent plasmid pYE(CEN3)30 was grown to OD_{600} = 6-7 at 30°C in YPD media in a 200 L fermenter (Infors ABEC). The cells were harvested by continuous flow centrifugation (Padberg) and lysed by bead beating in ice-cooled buffer G. All subsequent steps were performed at 4°C. Glass beads were separated by filtration prior to clearing the lysate by centrifugation (60 min, 8000 g, Sorvall SLA-1500). A whole cell extract was obtained after centrifugation at 125,000 g for 90 min (Beckman Ti45) by separating the clear upper-middle phase from the turbid lower phase. The supernatant was further processed by step-wise ammonium sulfate precipitation. 35% $(NH_4)_2SO_4$ was slowly added to the sample, allowed to stir for 30 min and cleared by centrifugation (60 min, 8000 g , Sorvall SLA-1500). The supernatant was precipitated by adding 70% $(NH_4)_2SO_4$ and left stirring over night. The pellet was recovered by centrifugation (60 min, 8000 g, Sorvall SLA-1500) and resuspended in 3 L of buffer H. The sample was applied to a 250 mL Biorex resin column (Biorad). Bound proteins were eluted with buffer I. The eluting proteins were loaded onto a 12 ml Ni-NTA Agarose (Qiagen) column. Subsequent washing steps were performed with buffer I (but 10 mM imidazole) and buffer J. Proteins were eluted with buffer J (but 250 mM imidazole) and loaded onto a HiTrap Heparin 5 mL column (GE Healthcare) and fractionated by applying a salt gradient from 250 mM to 1000 mM $(NH_4)_2SO_4$ with buffers K. The pooled RNAP III-containing fractions were diluted 5-fold with buffer K, loaded onto a Mono Q anion exchange column (Mono Q 10/100 GL, GE Healthcare), and fractionated by applying a salt gradient from 50 mM to 1000 mM $(NH_4)_2SO_4$ with buffers L. The pooled RNAP III-containing fractions were diluted to reach a final concentration of 50 mM $(NH_4)_2SO_4$, supplemented with a 4- fold molar excess of recombinant full-length C53/37 heterodimer (2.3.3.2) and incubated for 60 min to overcome the endogenous substoichiometry of this subcomplex (Lorenzen et al., 2007). The sample was concentrated to a volume of 1 ml using an Amicon Ultra-4 centrifugal filter unit (MWCO 10kDA, Millipore) and applied to gel-filtration chromatography on a Superose 6 column (Superose 6 10/300 GL, GE Healthcare) with buffer M. RNAP III containing fractions were pooled, concentrated to 1 mg/mL using an Amicon Ultra-4 centrifugal filter unit (MWCO 10kDA, Millipore) and flash-frozen in liquid N2 after addition of 10% glycerol.

2.3.3.2 Purification of recombinant C53/37 subcomplex

His_6-tagged C53/37 from *Saccharomyces cerevisiae* was purified from 6 L of IPTG induced expression culture (2.2.3). Cells were lysed using a Sonifier Cell Discruptor 250 (Branson) in buffer N (see Table X). After 1h centrifugation imidazole was added to a final concentration of 10 mM to the supernatant and the sample was loaded onto two 3 ml Ni-NTA columns (Qiagen) equilibrated with buffer O. The columns were washed with 20 column volumes (CVs) of buffer O and 10 CVs of buffer B containing 150 mM NaCl. Elution was performed with buffer O containing 300 mM imidazole and 150 mM NaCl. The fractions were analyzed for recombinant protein by SDS-PAGE (see 2.2.5). Proteins were purified by anion exchange chromatography (Mono Q, GE Healthcare). The column was equilibrated with buffer P and proteins were eluted with a linear gradient of 20 CVs from 10 mM to 1 M NaCl. Peak fractions and flowthrough of this chromatography step were checked by SDS-PAGE (2.2.5) for the presence of recombinant protein. Fractions containing C53/37 were pooled and

concentrated (Amicon Ultra centrifugal filter devices, cutoff 10k, Millipore). Afterwards samples were applied to a Superose 6 10/300 size exclusion column (GE Healthcare) equilibrated with buffer M. Peak fractions were pooled and concentrated to 1 mg/ml.

2.3.3.3 Purification of recombinant $Brf_c/TBP_c/Brf_n$ triple fusion protein

His_6-tagged $Brf_c/TBP_c/Brf_n$ from *Saccharomyces cerevisiae* was purified from 6 L of IPTG induced expression culture in LSSB medium (2.2.3). Purification was performed as described before (Kassavetis et al., 2005) using buffers Q-V.

2.3.3.4 Experimental design, assembly, and sample preparation for RNA Polymerase III PIC analysis with cryoEM

A minimal RNAP III PIC consists of RNAP III, $Brf_c/TBP_c/Brf_n$ and a dsDNA (RNA) complex. The used scaffold is 60 bp long and comprises a bubble from -11 until +2 (template DNA:3´-AAAGCCGATGATATTTTTTTACAAAAAAAGCGTTGATACACAAGCGCTTC ATTGGGAAGC-5´; nontemplate DNA: 5´- TTTCGGCTACTATAAAAAAATGTTTTTTT GCGTCGACATCGATCGCGAAGTAACCCTTCG -3´; RNA: 5´- ACUAUGU -3´).
RNAP III purification and assembly with C53/37 was performed as described (2.3.3.2). $Brf_c/TBP_c/Brf_n$ protein was supplemented after MonoS with 20-fold excess of the scaffold, incubated 30 min at 4°C and purified on a Superose 6 10/300 size exclusion column (GE Healthcare). 50 µmol purified RNAP III was added with a 10-fold molar excess of $Brf_c/TBP_c/Brf_n$-scaffold complex, diluted in buffer M to 10 mL and incubated 20 min at 4°C. After concentration (Amicon Ultra centrifugal filter devices, cutoff 10k, Millipore) the sample was loaded on a Superose 6 10/300 size exclusion column using buffer M, PIC containing fractions analyzed using SDS-Page and silver-stained gels (2.2.5), pooled and concentrated to 100-200 µg/mL concentration. CryoEM grids were frozen using a vitrification robot (Vitrobot, FEI).

2.3.4 Cryo EM specific procedure

Nanogold labelling of RNAP III-Maf1 complex and cryo-EM structure determinations of RNAP III, RNAP III EC and RNAP III-Maf1 complex were performed by Dr Anselm Kusser and Dr Alessandro Vannini as described (Vannini et al., 2010).
First reconstructions of the RNAP III-PIC were performed by Dr Anselm Kusser.

3 Results and Discussion

3.1 RNAP III EM structure reveals C82/34/31 mobility

We established a large-scale purification protocol for tagged RNAP III from the yeast *Saccharomyces cerevisiae* (2.3.3.1). Pure RNAP III samples comprised all 17 subunits, were monodisperse, and appeared homogeneous in EM with negative stain (Figure 1 A and B). We collected high-quality cryo-EM data after vitrification under native conditions.

A reconstruction of RNAP III from 20,480 single particles led to a map at 21 Å resolution (Figure 1C and E). The cryo-EM map showed good agreement with previously and later published maps (Fernandez-Tornero et al., 2007; Fernandez-Tornero et al., 2010). The core RNAP III homology model plus the C25/17 crystal structure (Jasiak et al., 2006) or the 12-subunit RNAP II crystal structure (Armache et al., 2005) could both be fitted unambiguously to the map (Figures 1E).

After this fitting, two extended additional densities remained, one on top of the clamp adjacent to C25/17, and one at the lobe near Rpb9 (Figure 1E). Densities at the lobe and clamp were attributed to subcomplexes C53/37 and C82/34/31, respectively (Fernandez-Tornero et al., 2007).
The density at the lobe was fitted with a homology model of the C53/37 dimerization module based on the crystal structure of the A49/34.5 module in RNAP I (Geiger et al., 2010) (Figure 1E and 2). Adjacent densities protruding towards the C160/C11 jaw and the funnel were explained by extensions from the dimerization module. The location of C53/37 agrees with the previously reported association of C53/37 with C11 (Chedin et al., 1998b) and with the location of the dimerization domain of TFIIF, the distant homologue of C53/37 (Cramer et al., 2008) on the RNAP II lobe (Chen et al., 2010; Eichner et al., 2010).
The additional density at the clamp could only account for a small part of the 138 kDa subcomplex C82/34/31, indicating intrinsic flexibility (Figure 1E and 2).

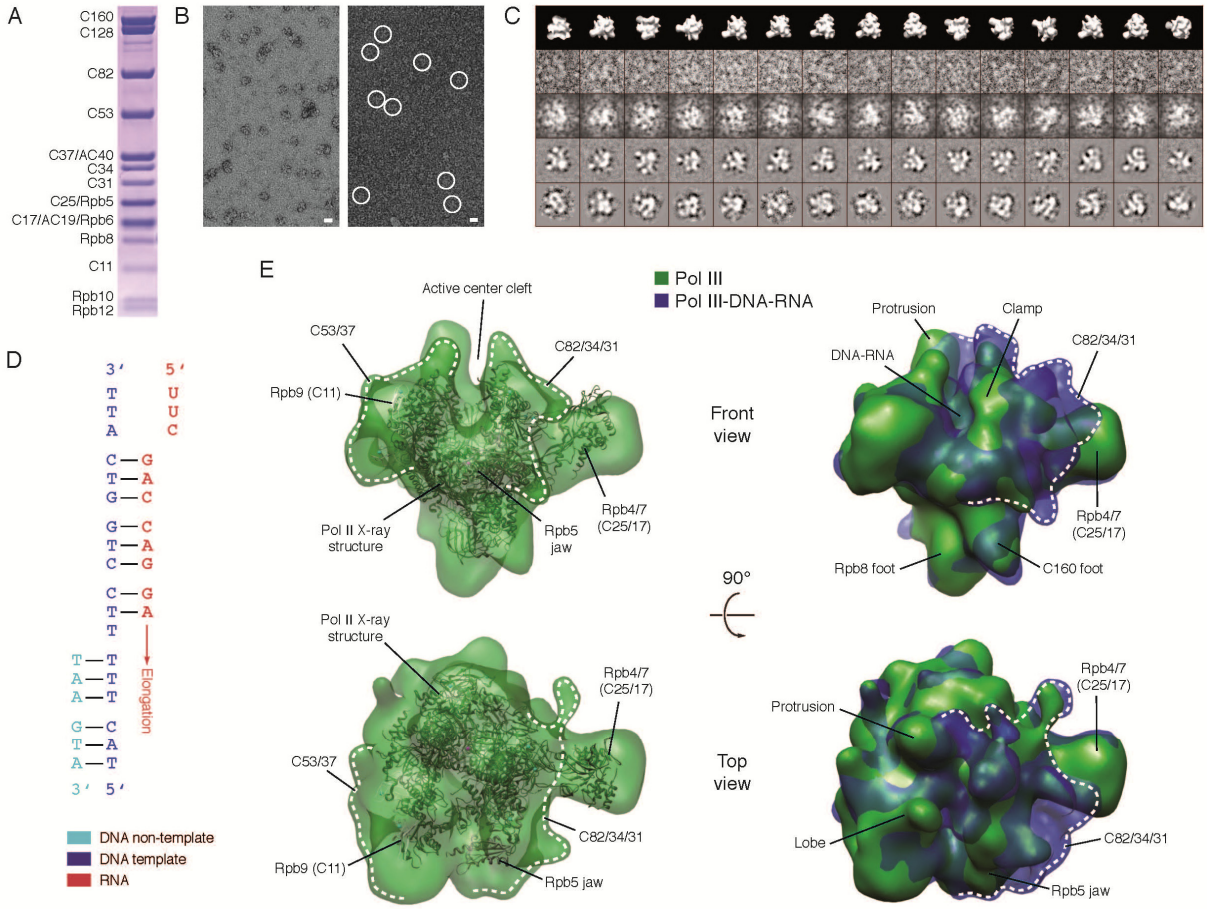

Figure 1. Cryo-EM reconstruction of RNAP III and RNAP III-DNA-RNA complexes.
(A) SDS-PAGE gel of purified yeast RNAP III. The 17 subunits are indicated. The identity of the bands was confirmed by mass spectrometry (not shown). **(B)** EM micrographs of RNAP III in negative stain (left) and vitrified ice (right). White circles indicate particles in vitrified ice. Scale bars are 10 nm in length. **(C)** Different views of the RNAP III reconstruction (first row) with corresponding raw single particle images (second row), low-pass filtered single particle images (middle row), class averages (forth row) and reference free averages (bottom row). **(D)** DNA-RNA scaffold used in the RNAP III-DNA-RNA complex (Brueckner et al., 2007). **(E)** Cryo-EM reconstruction of RNAP III (green) and RNAP III-DNA-RNA complex (blue). The 10-subunit RNAP III core homology model and the C25/17 crystal structure (Jasiak et al., 2006) were fitted to the map and are shown as ribbon models.

3.2 Nucleic acid binding restricts C82/34/31 mobility

To see how nucleic acid binding influences the RNAP III structure, we determined the cryo-EM structure of a RNAP III complex with a minimal DNA-RNA scaffold (Figure 1D, Experimental Procedures). This complex mimics an active elongation complex (Brueckner et al., 2007).

A reconstruction at 19 Å resolution was obtained from 11,965 single particles (Figures 1E, Experimental Procedures). As expected, the reconstruction revealed density for nucleic acids in the cleft, but also a structural ordering of the C82/34/31 subcomplex, giving rise to an extended density between the top of the clamp, the Rpb5 jaw, and C25/17 (Figure 1E), all the mass of the 138 kDa subcomplex. A long continous density between the clamp and the jaw (Figure 1E) could be fitted with the crystal structure of the human C82 homologue (Lefevre et al., 2011) (Figure 2A).

A prominent density remained between the clamp and the protrusion, forming a suspension over the cleft (Figures 1E and 2B). We assigned this density to subunit C34 since its two lobes fitted the structures of two winged helix (WH) domains in the N-terminal region of C34 (PDB codes 2dk5, 2dk8), and since C34 cross-links to promoter DNA around position -21 (Bartholomew et al., 1993) that is nearby in the homologous RNAP II closed and open promoter complex models (Kostrewa et al., 2009).

The remaining globular density near zinc site Zn8 in C160 between the clamp and C25/17 (Figure 2) was assigned to C31 since this position explains the known interactions with subunits C160, C82, C34, and C17 (Chedin et al., 1998b; Geiduschek and Kassavetis, 2001; Schramm and Hernandez, 2002), the requirement of the zinc site for C82/34/31 binding (Werner et al., 1992), and association of C31 with RNAP III after dissociation of the C82/34 heterodimer (Lorenzen et al., 2007).
We note that alternatively one C34 domain could be placed into the density assigned to C31, but this assignment could not explain the published biochemical data. Taken together, we could assign all RNAP III subunits to EM densities in a way that is consistent with known interactions.

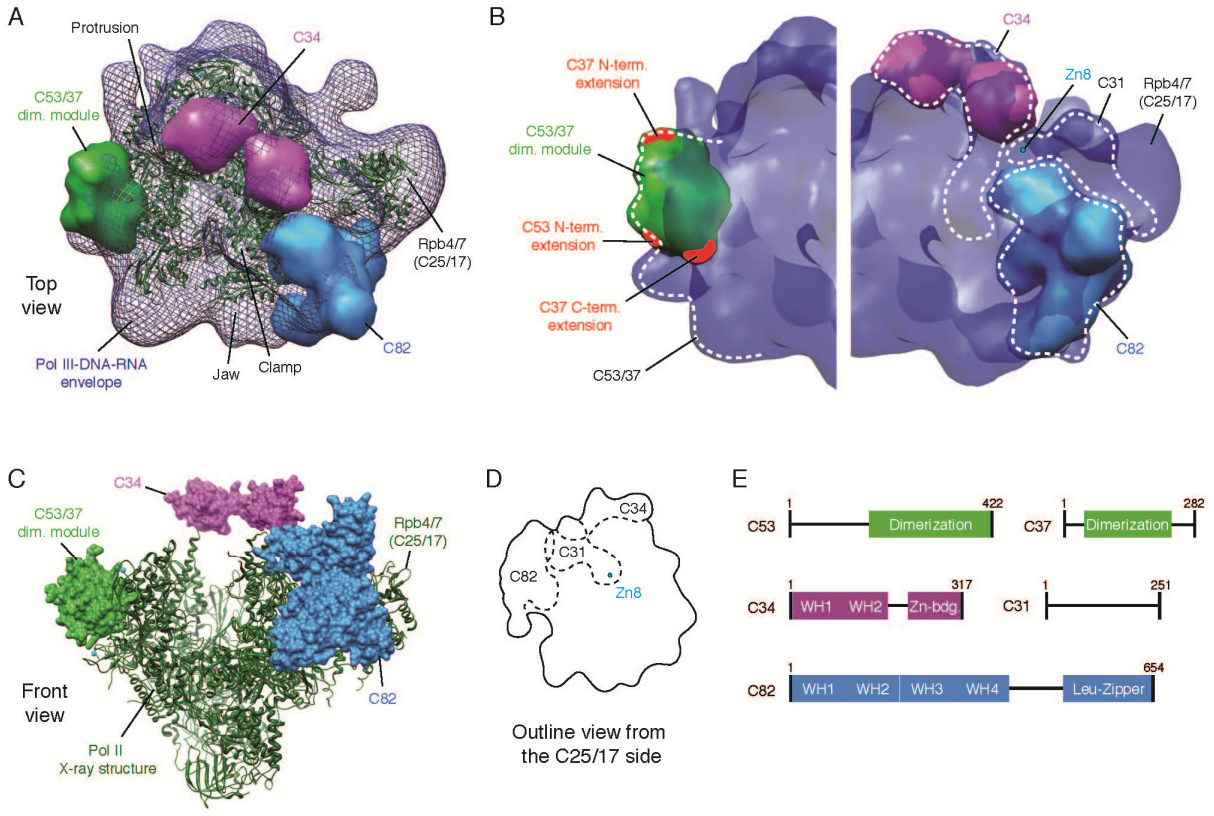

Figure 2. Subunit architecture of RNAP III.
(A) RNAP III-specific subunits placed into the cryo-EM envelope of the RNAP III-DNA-RNA complex. A homology model of the C53/37 dimerization domain (green, (Geiger et al., 2010)), the human C82 homolog crystal structure (blue, (Lefevre et al., 2011)) and the two C34 WH domain crystal structures (purple) are shown as molecular surfaces. The 10-subunit RNAP III core homology model and the C25/17 crystal structure (Jasiak et al., 2006) are shown as green ribbon models. **(B)** Close-up view of RNAP III-specific subunits fitted in the cryo-EM envelope of RNAP III-DNA-RNA complex. Terminal extensions of the C53/37 dimerization module are highlighted in red. **(C)** Localization of RNAP III-specific subunits on the core homology model and the C25/17 crystal structure (Jasiak et al., 2006). **(D)** Schematic representation of C82/34/31 subcomplex organization on RNAP III. **(E)** Domain organization of RNAP III specific subunits. Indicated domains were either revealed by homology modelling (C53, C37), X-ray crystallography (C34), or HHPred and secondary structure prediction (C82).

3.3 Maf1 structure determination

To elucidate RNAP III repression by Maf1, we determined the Maf1 structure by X-ray crystallography. We subjected recombinant *S. cerevisiae* and human Maf1 to limited proteolysis with subsequent Edman sequencing (2.2.4 and 2.2.5). Cutting sites at amino acid positions 56, 59, 72, 74, 114 in human and positions 161, 208 in *S. cerevisiae* were identified. Together with secondary structure predictions and multiple sequence alignmnents two flexible regions were revealed, a mobile insertion (human residues 50-82, yeast residues 50-224), and an acidic C-terminal tail (Figure 3 A). Based on this we constructed and purified Maf1 variants for crystallization trials.

Crystals were obtained for a human variant that lacked both mobile regions (Figure 3C). Analysis of these crystals confirmed, that they are comprised of human Maf1 1-205Δ36-82 (Figure 3B).

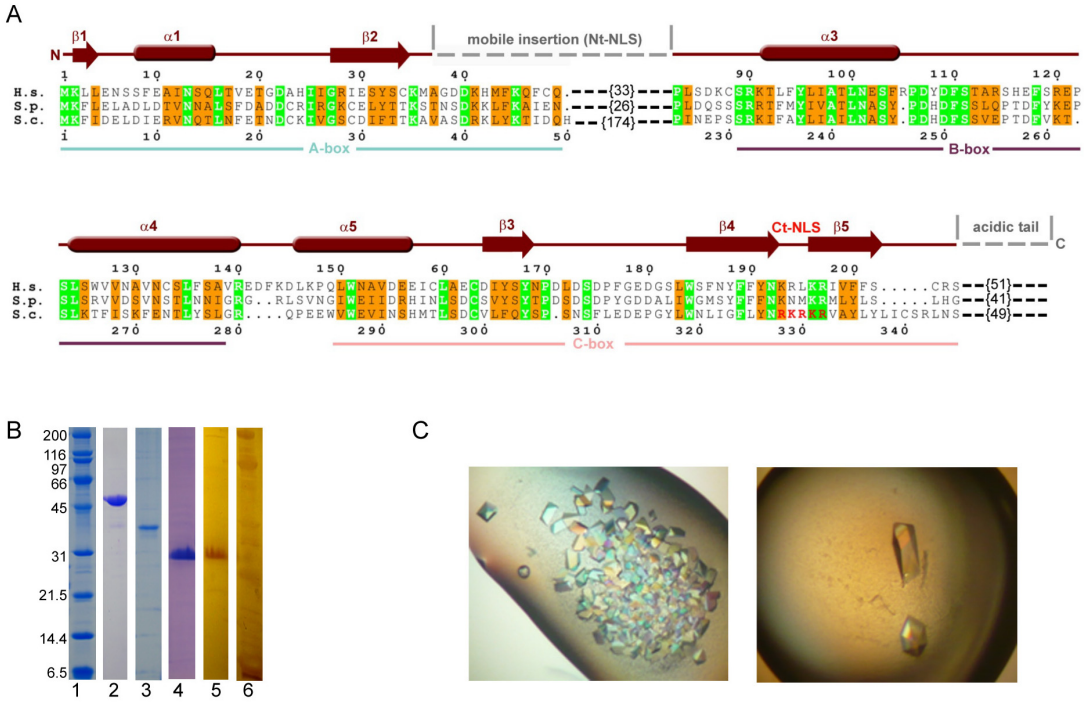

Figure 3. Maf1 crystal structure determination.
(A) Mutiple sequence alignment and structural conservation of Maf1 from *Homo sapiens* (H.s.), *Schizosaccharomyces pombe* (S.p.) and *Saccharomyces cerevisiae* (S.c.). Secondary structure elements are indicated above the sequence (cylinders for α–helices, arrows for β-strands). Red elements are included in the structure. Identical and conserved residues are highlighted in green and orange, respectively. The mobile region includes proteolytic cleavage sites (this work), phosphorylation sites (Dephoure et al., 2008; Lee et al., 2009; Moir et al., 2006), and the N-terminal NLS (Nt-NLS). The C-terminal NLS (Ct-NLS) is also indicated. Regions that are not present in the crystal structure are indicated by dashed lines. The crystallized protein was a human Maf1 variant comprising residues 1-35 and 83-205. **(B)** Purified and crystallized Maf1 variants. Lane 1 and 6 show Broad range marker, stained with coomassie and silver, respectively. Lane 2 shows purified *s.c.* Maf1 fulllenght, lane 3 purified *h.s.* Maf1 fulllenght, lane 4 purified *h.s.* Maf1 1-205Δ36-82, and lane 5 washed, dissolved and silverstained crystals of *h.s.* Maf1 1-205Δ36-82, which are shown in **(C)**. Shown crystals were grown in reservoir solution containing 50 mM MES pH 6.0, 175 mM NaOxalate or 50 mM MES pH 6.80, 250 mM NaOxalate, respectively (2.3.1.2).

The structure was solved by bromide phasing using a MAD data set with peak, remote, and inflection wavelengths. Refinment with a native data set revealed a R_{free} of 21.15% and a R_{work} of 18.81% at 1.55 Å resolution (Table 13).

Table 13. Maf1 X-ray diffraction and refinement statistic.

Data set		NaBr soak		Native
Data collection				
Space group		$P\ 2_12_12_1$		$P\ 2_12_12_1$
Unit cell axis a, b, c (Å)		48.07,48.34, 80.50		48.39,48.81, 79.32
	Peak	Remote	Inflection	
Wavelength (nm)	0.9196	0.9211	0.9200	0.91870
Resolution (Å)*	26.83-1.9	26.83-1.9	26.83-1.9	25.974-1.55
Rmerge (%)*	7.7 (50.7)	6.0 (39.2)	7.0 (51.3)	5.2 (58.9)
I/σ (I)*	22.0 (2.5)	22.7 (3.0)	22.0 (2.4)	22.3 (1.2)
Completeness (%)*	99.0 (99.5)	98.8 (99.4)	98.9 (99.5)	94.3 (87.4)
Redundancy*	3.9 (4.0)	3.8 (3.9)	3.8 (4.0)	3.0 (1.9)
Refinement				
Resolution (Å)				1.55-25.97
No. reflections				26,183
Rwork (%)				18.81
Rfree (%)				21.15
No. atoms				
Protein				1313
Water				142
B-factors (Å2)				
Protein				33.64
Water				43.95
r.m.s.d. from ideal				
Bond lengths (Å)				0.006
Bond angles (°)				0.959

*Highest resolution shell is shown in parenthesis.
Rmerge = $\Sigma |I - <I>|/\Sigma |$ where I is the integrated intensity of a given reflection.
R = $\Sigma ||Fobs| - |Fcalc||/\Sigma |Fobs|$. Rfree was calculated using 5% of data excluded from refinement.

3.4 Maf1 structure is globular, not modular

Maf1 forms a globular structure with a central five-stranded antiparallel β-sheet that is flanked by a single helix on one side, and by three helices on the other (Figure 4A). The Maf1 fold is frequently found in proteins, but not in proteins involved in transcription, as revealed by DALI (Holm and Park, 2000; Krissinel and Henrick, 2004). The Maf1 structure is apparently conserved among eukaryotes, since hydrophobic core residues are conserved from yeast to human (Figure 3A).

The Maf1 structure shows that the previously defined conserved sequence boxes A, B, and C (Desai et al., 2005; Pluta et al., 2001; Reina et al., 2006), do not correspond to structural modules or defined surface patches (Figure 4B). Thus, previous functional analyses of Maf1 deletion constructs, lacking one or more of these boxes, must be re-evaluated taking into account that the variants may adopt non-native structures.
To characterize the Maf1 structure into more detail, *in vivo* complementation assays were performed with scMaf1 deletion and point mutation strains (Appendix IV 1.1 and 1.2).

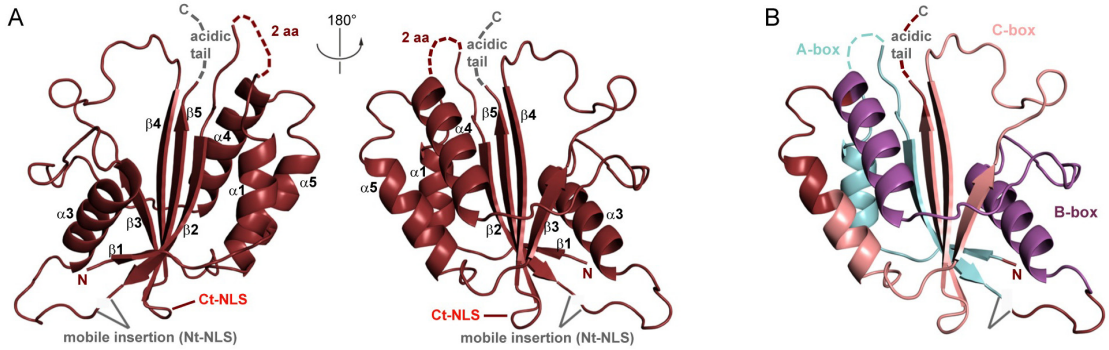

Figure 4. Maf1 crystal structure.
(A) Two views of a ribbon model of the human Maf1 crystal structure. Secondary structure elements are labelled according to A. **(B)** Ribbon model of human Maf1 with the conserved A-, B- and C-boxes highlighted in blue, purple, and rose. Colors were chosen as in Figure 3A.

3.5 Regulated Maf1 cellular localization

The Maf1 crystal structure reveals that the two NLS sequences (yeast residues 205- 208 and 328-332; (Moir et al., 2006)) are accessible on the domain surface (Figure 4A).
The C-terminal NLS (Ct-NLS) is located between strands β4 and β5, and the N-terminal NLS (Nt-NLS) is part of the directly adjacent mobile region (Figure 4A). The adjacent location suggests that phosphorylation of the mobile insertion regulates nuclear localization by masking the NLS sequences (Lee et al., 2009; Moir et al., 2006). This mechanism is apparently conserved from yeast to human, although the exact phosphorylation sites within the mobile insertion differ (Dephoure et al., 2008; Lee et al., 2009; Moir et al., 2006; Shor et al., 2010). The Ct-NLS and the residues at the mobile insertion form the only positively charged region on Maf1 (Figure 5B). Point mutants that led to defects in phosphorylation, growth on glycerol at 37°, or RNAP III repression (Moir et al., 2006; Roberts et al., 2006) (Figure 3E), cluster in this surface region.

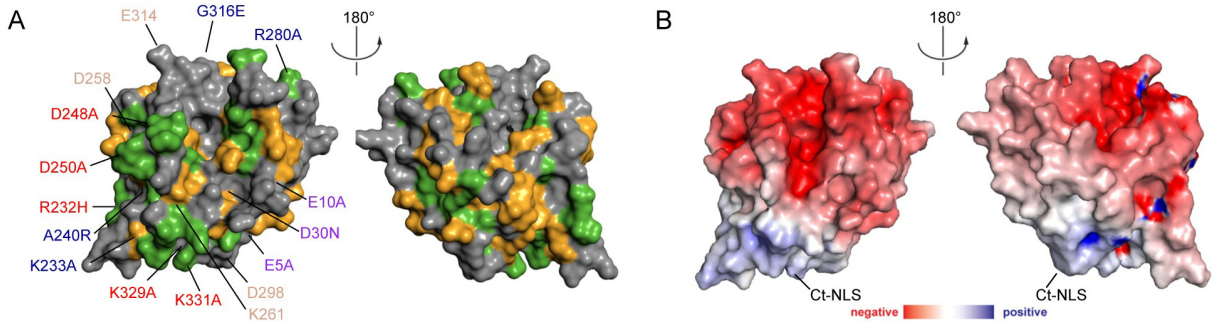

Figure 5. Maf1 crystal structure analysis.
(A) Surface conservation of Maf1. Identical and conserved residues are highlighted in green and yellow, respectively. Residues labelled in blue were analyzed for a role in RNAP III interaction (Figure 19). Residues labelled in red, pink, and wheat show severe, mild, or no phenotypes, respectively (Dephoure et al., 2008; Moir et al., 2006; Roberts et al., 2006). **(B)** Surface charge distribution of Maf1. Red, blue, and white areas indicate negative, positive, and neutral charges, respectively.

3.6 Maf1 binds the RNAP III clamp and rearranges C82/34/31

To investigate how Maf1 binds yeast RNAP III, we prepared full-length yeast Maf1 as a recombinant protein and a variant that lacked both mobile regions and corresponded to the crystallized human protein. Both variants formed a complex with RNAP III that could be purified by size-exclusion chromatography (Figure 6, lanes 3 and 4). Maf1 binding was specific, as human Maf1 did not bind yeast RNAP III (not shown). Thus, the two mobile regions are not required for RNAP III binding, and the human Maf1 crystal structure is relevant for the understanding of the RNAP III-Maf1 interaction.

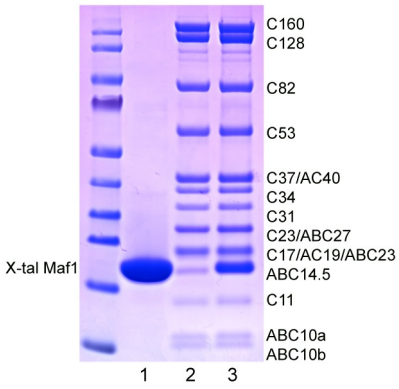

Figure 6. Binding properties of Maf1 fulllenght and crystallized construct to yeast RNAP III.
Binding experiments were performed as described in (2.3.1.4). Lane 2 shows RNAP III, lane 3 the RNAP III complex with the s.c. Maf1 variant corresponding to the crystallized human variant (s.c. Maf1 1-345Δ36-224), and lane 4 shows the RNAP III complex with full-length *sc* Maf1.

We collected cryo-EM data of the pure RNAP III-Maf1 full-length complex and used 16,974 particles to obtain a reconstruction at 18.5 Å resolution (Figures 7A).

The structure revealed a continuous density for C82/34/31, similar to the density in the RNAP III-DNA-RNA complex (Figure 7A). Maf1 was assigned to a new density on top of the clamp, with the help of calculated difference maps. The Maf1 X-ray structure fitted this density well (Figures 7A and C).

To provide additional support for the Maf1 location, we labelled the C-terminal hexahistidine tags on Maf1 and the RNAP III subunit C128 with Ni-NTA-Nanogold™ and located the labels by 2D cryo-EM image analysis. The locations of the labels were consistent with Maf1 binding on top of the clamp domain (Figure 7B). This location also agreed with published biochemical and genetic interactions of Maf1 with the N-terminal region of C160 that forms most of the clamp (Boguta et al., 1997; Oficjalska-Pham et al., 2006; Reina et al., 2006) (Figure 7D). Further consistent with this location, C160, C82, and C34 are the top interacting partners of Maf1 in the yeast interactome (Gavin et al., 2006).

A detailed comparison of the EM structures revealed that the C82/34/31 density observed in the RNAP III-Maf1 complex differed from that in the RNAP III-DNA-RNA complex. In particular, it appears that most of the density assigned to the C34 WH domains in the RNAP III-DNA-RNA complex is absent in the RNAP III-Maf1 complex, as an effect of a Maf1-dependent displacement of these domains. Probably these domains are shifted and become partially mobile, as suggested by the

presence of a shifted residual density, attributed to the second C34 WH domain (Figure 7F). The densities assigned to C31 and C82 undergo a similar change in location towards the Rpb5 jaw domain, giving rise to additional density in this region (Figures 7C and 7F).
Consistently, Maf1 overlaps with the assigned locations of the C34 second WH domain and with C82 and C31 in the RNAP III-DNA-RNA complex (Figures 7C and 7E).

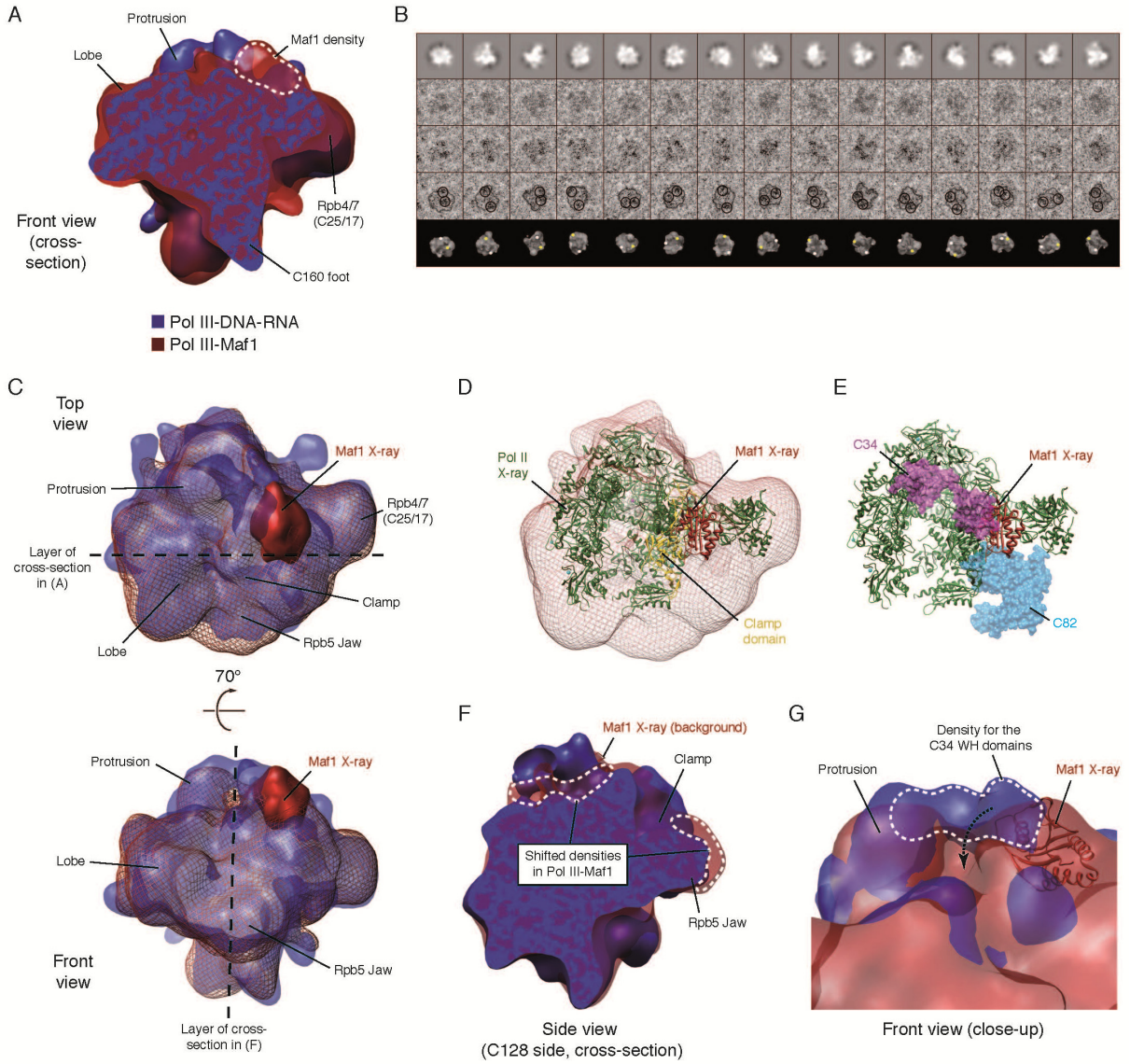

Figure 7. Cryo-EM structure of the RNAP III-Maf1 complex.
(A) Comparison of cross section of EM structures of the RNAP III-Maf1 complex (red) and the RNAP III-DNA-RNA complex (blue) reveals an additional density for Maf1. **(B)** Different views of reference projections of the RNAP III-Maf1 reconstructions (top row), corresponding thresholded Nanogold-labeled RNAP III-Maf1 particles used for alignment (second row), raw Nanogold-labeled particles (middle row), Nanogold particles with outline of RNAP III-Maf1 structure and circles indicating the location of the Nanogold labels (forth row), and surface representations of RNAP III-Maf1 reconstructions with N-terminus of C128 and location of Maf1 indicated by white and yellow dots, respectively (bottom row). The Nanogold signals are consistent with the location of Maf1 shown in A. **(C)** Fit of the Maf1 X-ray structure (red molecular surface) to the RNAP III-Maf1 EM map (red grid). For comparison, the cryo-EM map of the RNAP III-DNA-RNA complex is also shown (blue surface). **(D)** Ribbon representation of RNAP III-Maf1 complex. RNAP III homology model is depicted in green while Maf1 X-ray structure is depicted in red. The clamp domain of C160 (residues 1-245) is highlighted in yellow. The RNAP III-Maf1 cryo-EM map is shown as a red mesh. **(E)** Maf1 (red ribbon) sterically clashes with C34 (purple) and C82 (cyan) as positioned in the RNAP III-DNA-RNA complex. **(F)** Comparison of cross section of EM structures of the RNAP III-Maf1 complex (red) and the RNAP III-DNA-RNA complex (blue) reveals a shift of the density attributed to the C82/34/31 subcomplex upon Maf1 binding. **(G)** Close-up view of the region over the clamp. Most of the density attributed to the two C34 WH domains in the RNAP III-DNA-RNA complex (blue) is absent in the RNAP III-Maf1 complex (red).

3.7 Maf1 impairs closed promoter complex formation

To analyze how the structural changes induced by Maf1 binding could repress RNAP III transcription, we constructed a model for the RNAP III-Brf1-TBP closed promoter complex. Brf1 resembles the RNAP II initiation factor TFIIB in its N-terminal region, but contains a specific C-terminal extension that binds TBP (Khoo et al., 1994). We therefore combined the RNAP II-TFIIB-TBP closed promoter complex model (Kostrewa et al., 2009) with the structure of TBP bound to the Brf1 C-terminal residues 437-507 (Juo et al., 2003).

Comparison of the resulting RNAP III closed promoter complex model with the EM densities revealed that C34 was well positioned for interacting with both the Brf1 N- and C-terminal regions (Figure 8A), consistent with both regions interacting with C34 (Andrau et al., 1999; Brun et al., 1997; Khoo et al., 1994). In the RNAP III-Maf1 complex, C34 is locked in a different position that is apparently incompatible with Brf1 interaction, suggesting that Maf1 impairs RNAP III recruitment to Brf1-containing promoters (Figure 8A and B).

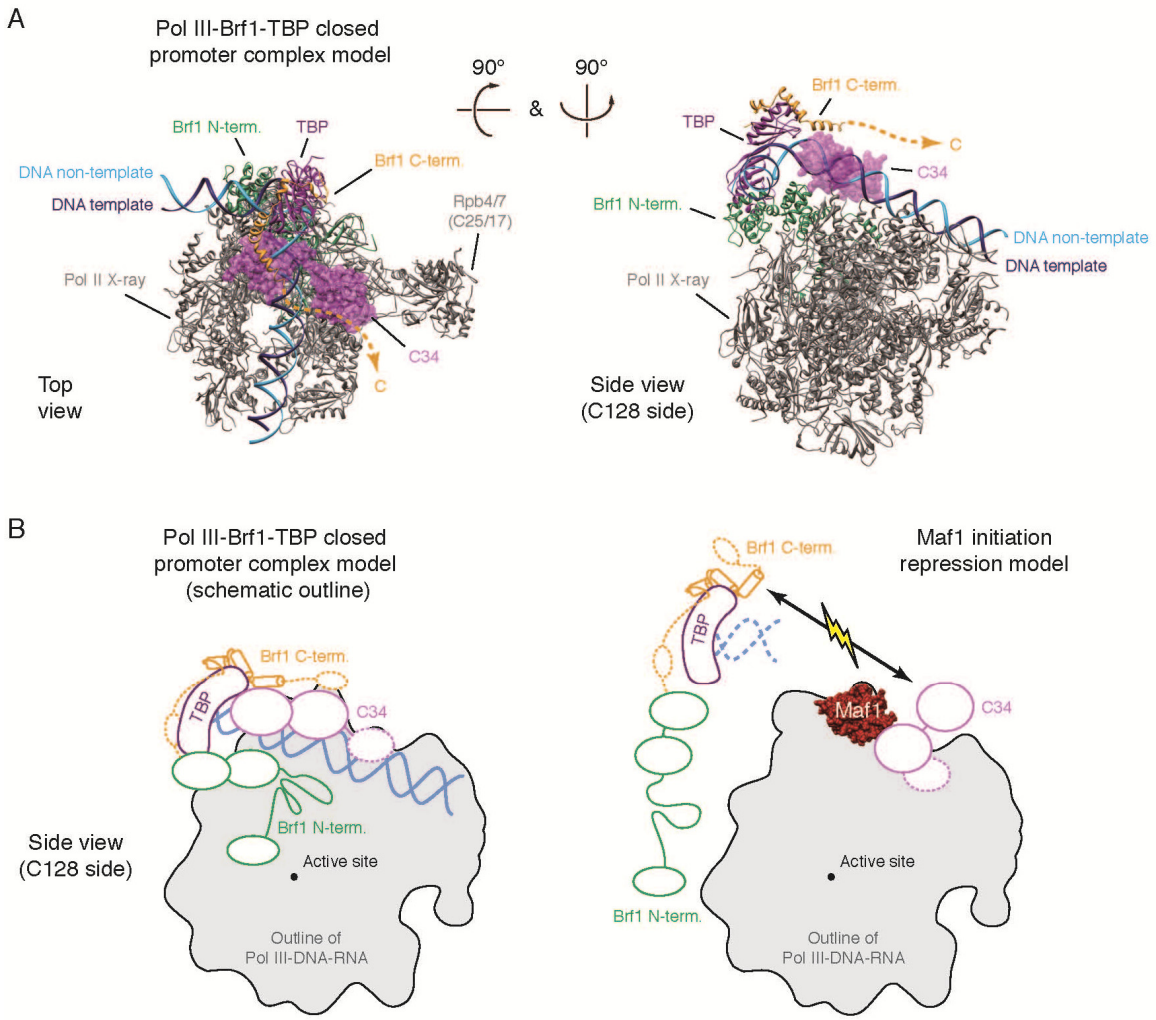

Figure 8. Mechanism of RNAP III transcription repression by Maf1.
(A) Model of RNAP III-Brf1-TBP-DNA closed promoter complex. The RNAP III core homology model and C25/17 crystal structure (Jasiak et al., 2006) are depicted as gray ribbons. The C34 WH domains are depicted as magenta surfaces. The Brf1 Nterminal domain (green ribbon) and the closed promoter DNA (cyan and blue ribbons) are based on the RNAP II-TFIIB-TBP-DNA closed promoter complex model (Kostrewa et al., 2009). TBP (dark purple) and the Brf1 C-terminal domain (orange) are depicted as ribbons and are based on the Brf1-TBP-DNA crystal structure (Juo et al., 2003). **(B)** Schematic model for Maf1-dependent repression of RNAP III-Brf1-TBP-DNA closed promoter complex formation, coloured as in A.

To test this model for the Maf1 repression mechanism, we investigated by size exclusion chromatography whether the RNAP III-Maf1 complex can bind to a preassembled, transcriptionally functional, Brf1-TBP fusion protein-DNA promoter complex (Kassavetis et al., 2005). We used U6 snRNA promoter DNA from position - 40 to +20 relative to the transcription start site +1. Whereas free RNAP III formed a stable closed promoter complex (Figure 9B, lane 3), the RNAP III-Maf1 complex did not bind the Brf1-TBP-DNA complex, even when a five-fold molar excess was used (Figure 9 lane 5). When we repeated the experiment with a mismatched bubble region at positions –11 to +2 (Figure 9A), the same result was obtained (Figure 9B, lanes 6 and 7). Further, pre-assembled RNAP III-Brf1-TBP promoter complexes were unable to bind Maf1, even when a five-fold molar excess was used (lane 4).

These experiments indicate that the interaction of RNAP III with Maf1 and a Brf1-TBP-DNA complex are mutually exclusive, showing that Maf1 impairs formation of a closed promoter complex. This is consistent with evidence that Maf1 binds RNAP III and prevents promoter interaction (Desai et al., 2005; Moir et al., 2006; Roberts et al., 2006).

3.8 Maf1 does not inhibit RNAP III activity

The above model predicts that Maf1 inhibits binding of promoter DNA over the active center cleft but not in the cleft.

To test this, we compared pure RNAP III and RNAP III-Maf1 complexes in an initiation factor-independent transcription assay using a 3'-tailed DNA template and a priming RNA dinucleotide ((Bardeleben et al., 1994), 2.3.1.7) that bind directly in the cleft. Consistent with the model, both complexes were equally active in RNA synthesis, and an excess of Maf1 or DNA did not change activity (Figure 9C).

We additionally performed RNA extension assays using a minimal DNA-RNA scaffold (Damsma and Cramer, 2009). The presence of Maf1 neither prevented scaffold binding nor elongation to the end of the template, and this was independent of the order of factor addition (Figure 9D).

To rule out that nucleic acids displace Maf1 from RNAP III or prevent its binding, we tested by size-exclusion chromatography whether RNAP III is capable of binding Maf1 and nucleic acids simultaneously. RNAP III-Maf1 complexes with 3'-tailed template or bubble scaffold could be purified, independent of the order of addition (Figure 9E). Thus, Maf1 neither prevents nucleic acid binding in the active center cleft nor DNA dependent RNA synthesis. The observation that RNAP III can simultaneously bind Maf1 and nucleic acids suggests that the increased Maf1 occupancy at RNAP III genes under repressive conditions (Geiduschek and Kassavetis, 2006; Oficjalska-Pham et al., 2006; Roberts et al., 2006) is due to Maf1 binding to RNAP III elongation complexes. Such Maf1-containing RNAP III elongation complexes would be unable to re-initiate, explaining the observation that Maf1 represses multiple-round but not single-round transcription by RNAP III (Cabart et al., 2008).

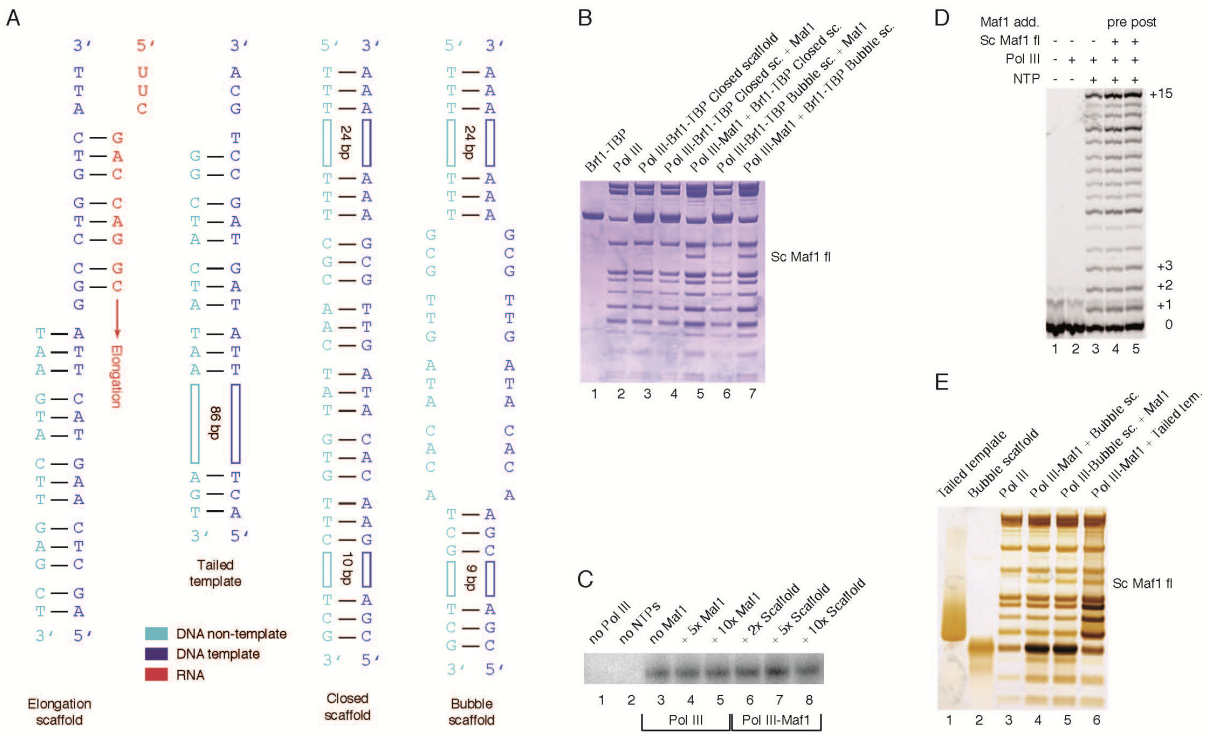

Figure 9. Maf1 impairs closed promoter complex formation but not RNAP III activity.
(A) Nucleic acid scaffolds. **(B)** Competition assays reveal that Maf1 impairs binding of RNAP III to a Brf1-TBP-DNA complex. Preassembled RNAP III-Brf1-TBP-DNA or RNAP III-Maf1 complexes were incubated with a 5-fold molar excess of competing factor or complex as indicated and subjected to gel filtration, and the peak fraction was analyzed by SDS-PAGE. In lanes 3, 4, and 6, the presence of DNA was revealed by the high A260/A280 ratio (~1) compared to the A260/280 ratio (~0.6) in lanes 2, 5, and 7. **(C)** Factor-independent RNAP III transcription assays. Preincubated RNAP III-DNA (lanes 3–5) and RNAP III-Maf1 complexes (lanes 6–8) efficiently transcribe the tailed template (A). Addition of increasing amounts of Maf1 to preincubated RNAP III-DNA complexes does not impair transcription (lanes 4 and 5). Increased amounts of scaffold have no effect (lanes 6–8). **(D)** RNA extension assay. The elongation scaffold (A) was efficiently transcribed to produce run-off product (+15) by RNAP III upon addition of NTPs (lane 3). Preincubation or addition of Maf1 (lanes 4 or 5, respectively) did not impair activity. **(E)** RNAP III can simultaneously bind Maf1 and nucleic acids. Preassembled RNAP III-Maf1 and RNAP III-DNA complexes were incubated with 5-fold molar excess of DNA or Maf1, respectively, and subjected to gel filtration, and the peak fraction was analyzed by SDS-PAGE and silver staining. Staining of a RNAP III-Maf1 complex (without DNA) is identical to that in lanes 4, 5, and 6.

4 Conclusions and Outlook

Our results complement the published data on the mechanism of RNAP III-specific transcription repression by Maf1. Cellular stress leads to dephosphorylation of a mobile surface region in Maf1 that unmasks adjacent NLS sequences, leading to nuclear import of Maf1. In the nucleus, Maf1 binds free RNAP III at its clamp domain and rearranges the C82/34/31 subcomplex. This impairs RNAP III binding to a TBP-Brf1-promoter complex and specifically abolishes initiation from RNAP III promoters, which require Brf1. Maf1 also binds RNAP III that is engaged in transcription elongation, leaving activity intact but preventing reinitiation. Since RNAP III genes are short and elongation is fast, this leads to rapid shutdown of all RNAP III transcription.

Based on this repression mechanism of RNAP III transcription by Maf1 new questions and starting points for follow up projects arise.

Firstly, the Maf1 protein itself can be analyzed into more detail. Important residues which are not included in the crystal structure due to construct design could be identified and their function investigated. Phosphorylation/dephosphorylation in the cytoplasm and in the nucleolus as well as nuclear import/export has to be regulated by binding to kinases/phosphatases, masking/demasking of the NLS sequences, and by interaction with transporter proteins (Ciesla et al., 2007; Moir et al., 2006; Oficjalska-Pham et al., 2006; Reina et al., 2006; Roberts et al., 2006; Towpik et al., 2008; Wei and Zheng, 2010). Presumably, different regions, binding surfaces and conformational states of Maf1 play a role here. Deletion mutants of Maf1 can be designed based on the structure and used in *in vivo* phenotyping assays and in binding assays with regulatory proteins to elucidate these functional parts and binding surfaces. First experiments have already been performed and preliminary results are shown in the appendix (Appendix IV).

Additionally, Maf1 structures of other species can explain observed differences in its activity, like repression of TBP expression by human Maf1 (Johnson et al., 2007). Also, from an evolutionary perspective, these structures may shed light on species specific regulatory mechanisms in the RNAP systems. Crystallization of a *Saccharomyces cerevisiae* Maf1 variant was successful in this study, but structure solution failed (Appendix IV 1.5). These results can serve as a starting point for successive projects.

Secondly, the Maf1/RNAP III interaction can be analyzed further. We were able to position Maf1 on the RNAP III complex with the help of cryo EM. However, no information about the orientation and only scant information about directly interacting subunits were available (Gavin et al., 2006; Oficjalska-Pham et al., 2006). Maf1 point mutants and analysis of its RNAP III binding properties can be used to identify interacting surfaces of Maf1. Initial trials with Maf1 point mutants were used in this study for *in vivo* phenotyping assays and binding studies to RNAP III (Appendix IV 1.2). Additionally, binding studies of scMaf1 fl to interacting RNAP III subunits should be perfomed. In this study only binding to C34 and C160 was analyzed (Appendix IV 1.3).

Thirdly, the interaction of Maf1 with TFIIIB can be the focus of further analysis. It was shown that human and yeast Maf1 bind to Brf1 very weakly (Desai et al., 2005; Reina et al., 2006; Rollins et al., 2007). Whether this interaction plays a physiological role and how the binding looks on

an atomic level is not known. Therfore assembly of a stoichiometrically bound complex is a first step for subsequential structure investigation. Preliminary trials are summed up in the appendix (Appendix 1.3).

A more longterm perspective would be to understand the molecular interactions of the potential tumor suppressor Maf1 with RNAP III, TFIIIB, and regulatory proteins, like kinases, phosphatases, and transporter proteins, and may help to develop therapies against diseases with uncontrolled rRNA and tRNA levels (White, 2008).

Additionally, a cryo EM reconstruction of a minimal RNAP III PIC should be focus of further studies, allowing the mechanism of transcription initiation and its regulation on a molecular level to be elucidated. So far only binding site mapping of a RNAP PIC could be obtained (Chen et al., 2010; Cramer, 2007; Kassavetis et al., 2003). This is probably due to its flexibility in different conformational intermediate states and thereby generating heterogeneous samples. Recent findings, that an enlarged bubble (-16 until +2) compared to a normal bubble (-9 until +2) in the RNAP II leads to a more homogeneous sample assembly and bubble position ((Andrecka et al., 2009) and unpublished results) may solve this problem.
Our published results comprise a RNAP III EC cryo EM reconstruction whith better defined RNAP III specific subunits, compared to RNAP III reconstructions. Also assembly of the triple fusion protein $Brf1_N$-TBP_C-$Brf1_C$ with RNAP III is possible (Vannini et al., 2010). Altogether these data serve as a good starting point for extensive studies of a minimal RNAP III PIC. RNAP III, $Brf1_N$-TBP_C-$Brf1_C$, and a promoter scaffold with enlarged bubble can be used to assemble a minimal PIC. Analysis with cryo EM can potentially lead to a first structure of a minimal eukaryotic PIC. Experimental design, complex assembly and first reconstructions were performed in this study (Appendix IV 2).

III

■ ■ ■

Structure of human mitochondrial RNA polymerase

1 Introduction

1.1 Mitochondrial functions

Mitochondria are dynamic subcellular organelles with cell type-specific appearance (Westermann, 2010). They are responsible for metabolic energy production in the form of ATP. This is generated by oxidative phosphorylation using the electron transport chain (ETC) in the inner mitochondrial membrane and coupled chemiosmosis. Furthermore, mitochondria are involved in a number of catabolic and anabolic reactions, including the citric acid cycle, β-oxidation of fatty acids, and the biosynthesis of certain phospholipids and other metabolites (Scheffler, 2001). Additionally, mitochondria play an important role as key regulators in apoptosis and are suggested to be a major initiator and target of reactive oxygen species (ROS) -mediated aging and integrator of stress-evoked mitochondrial pathways, which can lead to longevity (Bonawitz et al., 2006; Durieux et al., 2011).

This plethora of functions already indicates the impact of mitochondria in disease. Mutations and deletion of mtDNA in yeast lead to cells showing a petite phenotype, since *Saccharomyces cerevisiae* can survive on fermentable carbon sources (Bernardi et al., 1970). In mammals many diseases are suggested to be linked to mutations in mtDNA, but are hard to investigate, since cells often show heteroplasmy and only accumulation and segregation of these genomes result in a phenotype (Ono et al., 2001). Mitochondrial diseases are often age-associated and mostly affect cells with high energy consumptions, like muscle cells and neurons. Neuromuscular disorders, certain tumors, and diabetes as well as Parkinson's, Alzheimer's, and Huntington's disease are linked to mutations in mtDNA (Narendra and Youle, 2011; Wallace, 2005).

1.2 The mitochondrial genome

As described above the mitochondrion originates most likely from an α-proteobacterium, which developed early in evolution a symbiotic relationship with a primitive eukaryotic cell (Andersson et al., 2003). Based on phylogenetic relationships, a monophyletic origin is supposed (Gray et al., 1999). Gene content and organization in eukaryotes is very diverse, mostly ranging from 15-60 kbps and from circular to linear molecules, with the human mitochondrial genome comprising of 16,600 bps (Burger et al., 2003). Mammalian mitochondria show significant diversification in the sequence of individual genes to enable compatible interactions of its proteins with nuclear-encoded proteins (Boore, 1999).

Gene transfer took place from the mitochondrion to the nuclear genome and only a small number remained in the mitochondrion. In humans, about 1000 mitochondrial proteins are encoded in the nucleus and just 13 proteins, which are involved in oxidative phosphorylation, are encoded in the mammalian mtDNA (Scheffler, 2001). Genes which encode for essential mitochondrial transcription and translation proteins are nuclear (Adams and Palmer, 2003). The 1000-10000 copies of mtDNA in human cells encode additionally two rRNAs and 22 tRNAs that are used during mitochondrial translation, and have just one longer non-coding region, which contains the control elements for transcription and replication (Gaspari et al., 2004b).

The two mtDNA strains differ in their G+T content and can be separated into a heavy (H)- and light (L)-strand. Each strand harbours only one promoter for transcriptional initiation. Transcription initiation by usage of the transcription factors TFB2M and TFAM as well as mitochondrial RNAP regulation was described earlier (General Introduction 2.2).

The transcription product of each strand is a polycistronic precursor RNA, which are processed to tRNA, rRNA and mRNA (Bonawitz et al., 2006; Falkenberg et al., 2007).

Maturation of mitochondrial transcripts and mitochondrial DNA replication

In human, the two polycistronic precursor RNAs are processed by endonucleolytic cleavage into individual rRNAs, mRNAs and intervening tRNAs (Ojala et al., 1981). According to the "tRNA punctuation model" endonucleolytic excision of tRNA sequences also generates matured mRNAs and rRNAs (Ojala et al., 1981). Cleavage of 5´ ends of tRNA is catalyzed by a mitochondrial RNase P, consisting of three proteins only (Holzmann and Rossmanith, 2009), subsequent generation of 3´ends is performed by a 3´ processing activity (Manam and Van Tuyle, 1987). Further processing of mRNAs involves polyadenylation of the 3´end, which is performed by human mitochondrial poly(A) polymerase (Tomecki et al., 2004). This produces an UAA stop codon in many mitochondrial mRNAs (Anderson et al., 1981) and increased mRNA stability (Temperley et al., 2003). tRNAs undergo base modifications and addition of a CCA tail at the 3´end, whereas rRNAs become oligoadenylated at their 3´ends (Taanman, 1999).

Interestingly, the mitochondrial RNAP also assists mtDNA replication by synthesis of primers, thereby serving as a primase (Fuste et al., 2010). According to the strand-displacement model, *de novo* primer synthesis starts at the L-strand promoter (OriH) and terminates at a conserved sequence block II 100 bps downstream (Pham et al., 2006), where mitoRNAP dissociates and transfers the primer with an unknown mechanism to the replication machinery. The mitochondrial replication machinery consists of the Twinkle helicase, DNAPγ, and single-strand DNA binding protein, which are all encoded in the nucleus. Twinkle and DNAPγ likely share ancestry with T7 phage proteins (Shutt and Gray, 2006).

The replication machinery uses the synthesized primer to replicate the leading strand (Chang and Clayton, 1985). When reaching the second replication start site (OriL) on the H-strand, DNA forms a single-stranded hairpin, and mitoRNAP transcribes, without the help of TFAM and TFB2M, a second primer in reverse direction, which gets 25-35 nt long before DNAPγ takes over again and replicates the missing DNA strand (Fuste et al., 2010). Replication is completed when the DNA circles are ligated to form continuous strands (Shadel and Clayton, 1997). Since changing energetic needs of cells lead to varying amounts of mitochondria and mtDNA (Wallace, 2001) and also the localization of the mitochondrion in the cell plays a role for the replication probability (Davis and Clayton, 1996), regulation of this replication process in an adaptive and signal-dependent manner is needed and likely performed at least partly by regulating mitoRNAP activity.

1.3 Mitochondrial RNA polymerase

Regulated expression of the mitochondrial genome is crucial for cell viability and the ability to adapt to changing energetic needs (Wallace, 2005). Transcription of the mitochondrial genome is driven by the nuclear-encoded DNA-dependent mitoRNAP. This RNAP belongs to a family of ss RNAPs that is distinct from the multisubunit cellular RNAPs and also includes chloroplast RNAP and RNAPs from bacteriophages such as T7 and N4.

Comparison with known ss RNAP structures

All ss RNAPs share high sequence homology in their carboxy-terminal domains (CTD) that form a fold resembling a right hand (Jeruzalmi and Steitz, 1998). The conserved palm and the mobile fingers subdomain of the CTD comprise the catalytic core of these enzymes. The CTD fingers subdomain also contains the specificity loop, a β-hairpin that binds the major groove of promoter DNA and forms base-specific contacts (Cheetham et al., 1999). The third subdomain in the CTD is the thumb, with a long α helix that takes part in RNA/DNA heteroduplex separation (Yin and Steitz, 2004).

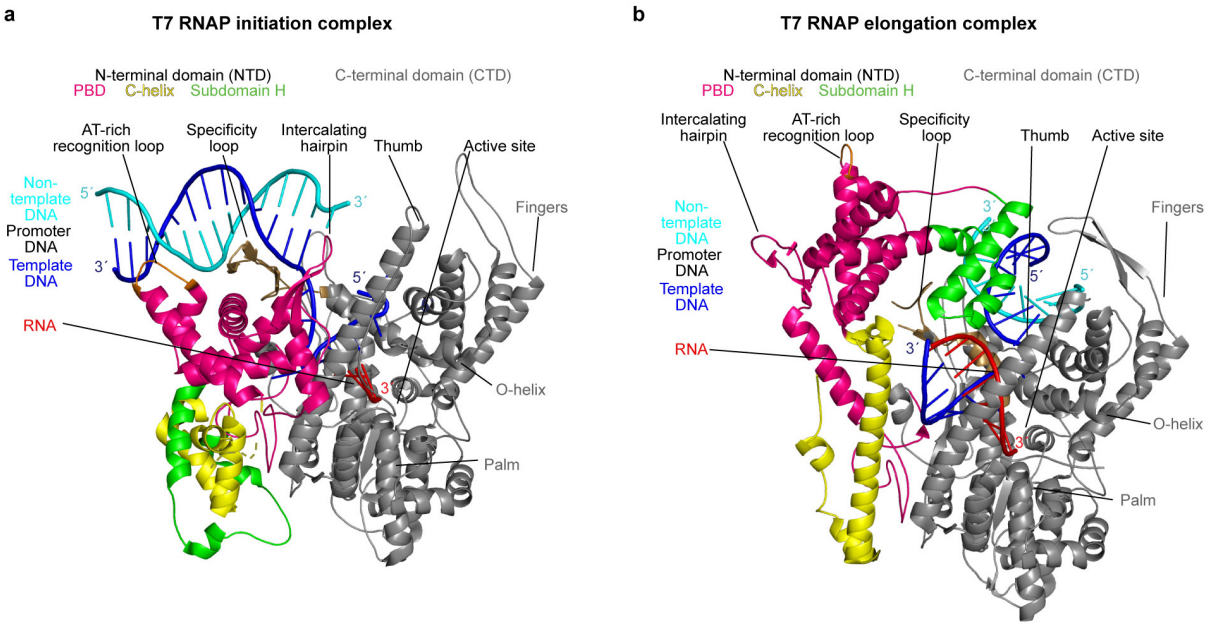

Figure 10. T7 RNAP structures.
(a) Structure of T7 RNAP initiation complex (PDB 1QLN) with a 17/22mer DNA (blue for template strand and cyan for non-template strand) and 3mer RNA (red). Three loops are essential for promoter recognition, binding and melting, which are indicated as AT-rich recognition loop (organge), specificity loop (brown) and intercalating hairpin. The CTD is shown in gray and consists of the thumb, palm, and fingers subdomains, which also bild the active center, including the O-helix. Te active site is in an open, inactive state. The NTD consists of the protein binding domain (PBD) (pink), the C-helix (yellow), and the subdomain H (green) and undergoes major refolding in the transition from initiation to the elongation state, shown in (**b**). (**b**) Structure of T7 RNAP elongation complex (PDB 1H38) with 18/10 mer DNA and 12mer RNA (just 8 nt of RNA were seen in electron density). The colour code is the same as in (a). The CTD is in a closed, active state. The refolding of the NTD leads to lost of promoter DNA contacts, seen in the positional changes of the three loops and to the formation of an RNA exit tunnel by the subdomain H and the CTD specificity loop,

Structural studies with T7 RNAPs elucidated the mechanisms of the four steps in the nucleotide addition cycle during elongation (Tahirov et al., 2002; Temiakov et al., 2004; Yin and Steitz, 2002; Yin and Steitz, 2004).
The substrate NTP binds with its triphosphates to Lys631 and Arg627 of the fingers O-helix and initially base-pairs in an open conformation (pre-insertion substrate complex) (Temiakov et al., 2004). Conformational changes by a rotation of five helices in the fingers subdomain around a pivot point in the O-helix result in a closed conformation of the active center, so that the substrate NTP is properly positioned for insertion (insertion substrate complex) (Yin and Steitz, 2004). Nucleotide addition can take place with the help of two catalytic Mg^{2+}-ions and leads to a closed product complex with bound pyrophosphate forming an ionic crosslink between the Mg^{2+}-coordinated Asp537 and Arg627 (Yin and Steitz, 2004). Dissociation of the PP_i results in an open complex again and accompanied translocation of the DNA/RNA heteroduplex (post-translocation complex) (Tahirov et al., 2002; Yin and Steitz, 2002). The conformational changes in the fingers subdomain resulting from PP_i dissociation is associated with the unwinding of the downstream heteroduplex by one bp at the Y-helix concomitant with translocation by 3.4 Å (Yin and Steitz, 2004). In the post-translocation conformation the Tyr639 is stacked on the primer template bases, inhibiting backtracking and blocking the insertion site. Only after binding of the next substrate NTP in the pre-insertion site can another round of nucleotide addition take place.

Since all catalytic residues are conserved also in mitoRNAP, one can expect similar nucleotide binding and addition mechanisms. However, there are some differences in the product length of initiation RNA (8 nt in T7 RNAP and 13 nt in yeast mitoRNAP) and abortive initiation which may be explained by structural adaptions.

In contrast, the amino-terminal regions of ss RNAPs show very limited homology and differ in size. In phage RNAPs, they contain a promoter binding domain (PBD) (Durniak et al., 2008; Gleghorn et al., 2008). In T7 RNAP, the PBD forms a six-helix bundle that includes two DNA-binding elements, the intercalating hairpin and the AT-rich recognition loop (Cheetham et al., 1999; Durniak et al., 2008) (Figure 10a). The intercalating hairpin separates DNA strands during promoter melting and interacts with the DNA template strand (Cheetham et al., 1999; Gleghorn et al., 2008). The AT-rich recognition loop binds the minor groove of upstream promoter DNA (Cheetham et al., 1999). In N4 RNAP, the AT-rich recognition loop is altered, to specifically recognize hairpin promoters (Davydova et al., 2007; Gleghorn et al., 2008).

Structural studies with T7 RNAPs show that the N-terminal domain (NTD) refolds massively in the transition from initiation to elongation (Figure 10). In the elongation state promoter DNA contacts are lost and processive transcription is enabled through formation of a RNA exit tunnel by the subdmain H, PBD, and specificity loop (Tahirov et al., 2002; Yin and Steitz, 2002).

Since the amino-terminal regions of mitochondrial and chloroplast RNAPs share essentially no sequence homology with phage RNAPs it is unknown whether they contain similar structural elements with a role in promoter recognition and transcription processivity.

Human mitoRNAP relies on two essential transcription factors, TFAM and TFB2M (Gaspari et al., 2004b; Litonin et al., 2010), which are described in more detail in part 2.2 of this work. These factors likely control promoter binding and melting during transcription initiation (sin-Cayuela and Gustafsson, 2007; Sologub et al., 2009). A similar functional role was demonstrated for the yeast

TFB2M analog, Mtf1, whose C-terminus was shown to contact the template strand in an active initiation complex at nt positions -3/-4 (Savkina et al., 2010). Importantly, the structure of Mtf1 was solved before (Schubot et al., 2001). While the components of the transcription initiation complex (IC) are known, their spatial arrangement and the molecular mechanisms of promoter binding and melting remain unknown.

No structure of any mitoRNAP has been solved yet, which would hopefully reveal the mechanistic adaptations that occurred during evolution of a self-sufficient T7-like RNAP to become regulated by transcription initiation factors.

PPR motif

MitoRNAP has two putative pentatricopeptide repreat (PPR) motifs in its N-terminal region (Rodeheffer et al., 2001). Genome wide analysis for a variety of organisms revealed that PPR motifs are specific to eukaryotes and most prominent in plants, with 441 PPR motif containing proteins predicted in *A.thaliana*, 7 in *H.sapiens*, and 5 in *S.cerevisiae* (Lurin et al., 2004, Mili et al., 2003). Each of these proteins contains 2 to 26 PPR motifs per molecule (Small and Peeters, 2000). Only few PPR proteins are characterized so far but are all implicated in RNA-processing in mitochondria and chloroplasts (Mili and Pinol-Roma, 2003). Prediction programs reveal that nearly 65% of all PPR proteins are targeted to mitochondria and another 16% to plastids and targeting experiments with 45 randomly chosen PPR proteins show that mitochondria or plastids are the only observed subcellular localization (Lurin et al., 2004). The seven human PPR proteins are all predicted to be mitochondrial (Lurin et al., 2004).

The function of PPR proteins remains unclear and only few individual proteins were analyzed so far. Interestingly, mutants pet309 and cya5 in yeast and *N.crassa* are affected in stability and translation of mitochondrial cytochrome c oxidase subunit 1 (Cox1) transcripts, a similar phenotype to a mutation in a human PPR motif containing gene (*LRPPRC*) which is linked to Cox1 deficiency (Coffin et al., 1997; Manthey et al., 1998; Mootha et al., 2003). Also Crp1, a PPR protein of *Z.mays*, plays a role in processing and translation of plastid transcripts (Fisk et al., 1999). And recently RNA processing factor 1 (Rpf1), a PPR protein in *A.thaliana*, was characterized to play a role in processing the 5´ends of mRNA transcripts (Holzle et al., 2011). Additionally, also the third protein subunit of human mitochondrial RNAse P, MRPPR3, which is involved in tRNA maturation, has two tandem PPR-motifs (Holzmann and Rossmanith, 2009).
These examples illustrate that PPR proteins play a role in organelle gene expression. Additionally, initial nucleic acid binding studies show preferential binding of poly(G) RNAs (Lurin et al., 2004). Therefore it suggests that PPR proteins operate in protein/RNA interactions.

The 35-amino acid PPR motif is predicted to consist of two α helices and in contrast to tetratricopeptide (TPR) motifs, which form a related and well-studied protein class, the PPR motifs show sequence conservation in their connecting loops, likely building a conserved positively charged groove on top of the helices. Speculatively, this groove could be part of the suggested RNA-binding activity of PPR motifs. So far no structure of any PPR motif containing protein was solved, but could help to elucidate conserved structural elements, which explain the suggested functions.

1.4 Aims and Scope

Mitochondrial RNAPs evolved from interaction of three distinct entities, namely the host cell, a bacterium and a phage. Therefore mitochondrial transcription shares a number of features with phage, bacterial, and eukaryotic transcription and is unique among well studied bacteriophage and multi-subunit RNAPs (Table 2, General introduction). On the one hand mitochondrial RNAPs recognize its promoters in a self-sufficient manner like T7 RNAPs. On the other hand they need transcription factors for efficient initiation (Cheetham et al., 1999; Gaspari et al., 2004b; Shutt et al., 2010). Additionally, transcription in mitochondria is highly regulated by additional transcription factors and cofactors (Woo and Shadel, 2011). This regulated initiation resembles the structurally unrelated multi-subunit RNAPs.

Thereby, investigation of mitochondrial RNAP´s molecular transcription and regulation mechanisms establishes ties between the evolutionary diversification of RNAPs and is very meaningful in this perspective. To date no structural data for any mitochondrial RNAP is available. Since structures of multi-subunit RNAPs in bacteria, archaea, and eukaryotes as well as structures of ss RNAPs, like bacteriophage T7, were solved over the last decades, the structure of the mitochondrial RNAP will fill the last remaining gap.

Furthermore, mitochondrial dysfunctions lead to aging and a number of human diseases (Narendra and Youle, 2011; Wallace, 2005). Therefore investigation of mitochondrial RNAP functions and molecular mechanisms will also help to understand human disease related dysfunctions of mitochondria.

The aim of this study was to solve the structure of mitochondrial RNAP by X-ray crystallography. This can help to understand the unique features of mitochondrial RNAPs on a molecular level and to shed a light on its transcription activity mechanism.

Subsequent structure analysis by comparing a mitochondrial RNAP structure with other ss RNAP structures like T7 and N4 RNAPs, and model building of functional states can help to reveal the mechanistic adaptations that occurred during evolution of a self-sufficient T7-like RNAP to become regulated by transcription initiation factors.

Accordingly, this structure can serve as a basis for new experimental designs to elucidate a complete picture of the mitochondrial transcription system. New mitochondrial RNAP variants can be designed and analyzed in functional assays to obtain more structure/function relationships.
Additionally, the structure can be used as a model for structural follow up projects, i.e. to elucidate structures of mitochondrial RNAP in different functional states or structures of complexes with transcription and regulation factors.

In a more long term view the deeper understanding of the molecular mechanisms and unique features of transcription by mitochondrial RNAP can help in future to find more effective mitochondrial-targeting and antiviral drugs.

2 Materials and Methods

2.1 Materials

2.1.1 Bacterial strains

Table 14. *E. coli* strains.

Strain	Genotype	Source
XL-1 Blue	*rec1A*; *endA1*; *gyrA96* ; *thi-1* ; *hsdR17*; *supE44* ; *relA1* ; *lac*[F´*proAB lacI* qZD*M15* Tn*10*(Tetr)]	Stratagene
BL21-CodonPlus (DE3)RIPL	B F– *ompT hsdS*(rB– mB–) *dcm*+ Tetr *gal* λ(DE3); *endA;* Hte [*argU proL* Camr] [*argU ileY leuW* Strep/Specr]	Stratagene

2.1.2 Plasmids and primers

Table 15. List of vectors used in this study.

Vector	Inserts/ Description	Type	Tag	Restr. sites	Primer
RR096	cloning vector (mutation in NcoI cutting site)	pProExHtb	-	-	-
RR097	Intein_RNAP (AA 109-1230) plasmid (by Dmitry Temiakov)				
RR105	RNAP 760-1230	pProExHtb	Nt His	XhoI, NcoI	AM 37 for AM 37 rev

Table 16. List of primers used in this study.

ID	Primer	Sequenz (5´- 3´)
RRP01	AM 37 for	GTTCCATGGGTCATCACCATCACCATCACGAGCTGGCGCACT
RRP02	AM 37 rev	GGTGGTCTCGAGTTATCAGCTGAAGAAGTAGGTGGAACGCT

2.1.3 Media and additives

Media and additives were used as in chapter II.

2.1.4 Buffers and solutions

Table 17. Human mitochondrial RNA Polymerase purification buffers.

Name	Description
Buffer A	50 mM Tris 8.0; 0.25 M NaCl; 5% Glycerol; 5 mM ß-mercaptoethanol; 1x protease inhibitor
Buffer B	40 mM Tris 8.0; 1.5 M NaCl; 15 mM Imidazole; 5% Glycerol; 5 mM ß-mercaptoethanol; 1x protease inhibitor
Buffer C	40 mM Tris 8.0; 1.5 M NaCl; 200 mM Imidazole; 5% Glycerol; 5 mM ß-mercaptoethanol; 1x protease inhibitor
Buffer D	40 mM Tris 8.5; 0.3 M NaCl; 5% Glycerol; 1mM EDTA; 10 mM ß-mercaptoethanol
Buffer E	100 mM Tris 7.7; 300 mM NaCl; 5% Glycerol ; 1 mM EDTA ; 10 mM DTT

2.2 General methods

General methods were used as described in chapter II. Cloning of all human mitoRNAP constructs was performed by Dmitry Temiakov (UMDNJ, New Jersey, USA).

2.3 Specific procedures

2.3.1 Purification of recombinant human mitochondrial RNA polymerase variants

Variants of human mitoRNAP were purified from 20 L of IPTG induced expression culture (I 2.2.3). Cells were resuspended in 500 mL buffer A (see Table 17) and lysed using a Sonifier Cell Discruptor 250 (Branson).

After centrifugation the supernatant was loaded onto two 750 µL Ni-NTA columns (Qiagen) equilibrated with buffer B. Each column was washed with 20 mL of buffer B. Elution was performed with 8 mL buffer C for each column. The fractions were analyzed for recombinant protein by SDS-PAGE (see 2.2.5). Dialysis of protein fractions was performed in buffer D o.n. at 4°C. Proteins were purified by cation exchange chromatography (HiTrap Heparin 5mL column, GE Healthcare). The column was equilibrated with buffer D and proteins were eluted with a linear gradient of 8 CVs from 300 mM to 1.5 M NaCl. Peak fractions were checked by SDS-PAGE (2.2.5) for the presence of recombinant protein. Fractions containing the corresponding human mitoRNAP variant were pooled and concentrated (Amicon Ultra centrifugal filter devices, cutoff 50k, Millipore). Afterwards samples were applied to a Superdex-200 16/10 size exclusion column (GE Healthcare) equilibrated with buffer E for crystallization experiments. Peak fractions were pooled and concentrated to 4-9 mg/ml for crystallization.

2.3.2 Crystallization of human mitochondrial RNA polymerase variants

An intial search for crystallization conditions using different protein variants was performed (MPI Martinsried, Department of E. Conti) with crystallization screens supplemented with 10% glycerol to prevent excessive precipitation, and analyzed as described in 2.2.7. Promising hits were refined in 24 well sitting or hanging drop plates (Easy Xtal Tool, Qiagen) by varying precipitant and/or salt concentrations. Diffraction quality crystals of mitoRNAP variant D150 were obtained by *in situ* proteolysis crystallization and subsequent seeding. Thereafter the purified protein at a concentration of 9.5 mg/mL was mixed with trypsin in a molar ratio of 900:1 (RNAP:trypsin) in size exclusion buffer E and incubated on ice for 1h. 2 µL of trypsin-treated protein was mixed with 2 µL of reservoir solution containing 40 mM MES pH 6.5, 97.5 mM $(NH_4)_2SO_4$, 12% PEG5000, 12.5% Xylitol, and 120 mM DTT. Initial crystals appeared within two days at 20°C in hanging drops and used for subsequent microseeding. Crystal seed stocks were produced by crushing initial crystals by dilution with 50 µl of the respective reservoir solution and vortexing in a Seed Bead microcentrifuge tube (Hampton Research). Seeds were diluted 10-1000 times in reservoir solution. Plates were set up by mixing 2 µL proteolysed protein with 2 µL seed stock solution of different dilutions. Microseeding produced diffracting crystals, approximately 250x90µm in size after 3 days (Figure 1B). Crystals were transferred into reservoir solution containing 15% glycerol and 25% PEG4000 and were flash cooled in liquid nitrogen.

2.3.3 Data collection, X-ray structure determination and refinement

Diffraction data for *in situ* proteolysed human mitochondrial RNAP variant D150 were collected in 0.5° increments at 100 K on a MarCCD or PILATUS 6M detector at the Swiss Light Source (SLS), Villigen, Switzerland (Table 18). Raw data were integrated with MOSFLM (Leslie et al., 1986), the spacegroup confirmed with POINTLESS (Evans, 2006), and scaled with SCALA (Evans, 2006). The structure was solved by molecular replacement with the program PHASER (McCoy et al., 2007), by using the structure of T7 RNAP (PDB 1QLN). 1QLN was mutated to a poly-alanine sequence (program Chainsaw) and reduced to residues 246-354, 392-568, 691-741, 766-883. The molecular replacement solution was subjected to rigid body refinement with Refmac5 (Murshudov et al., 1997) and revealed initial R factors of R_{work}= 43.2% and R_{free}= 44.1%. The model was iteratively built with COOT (Emsley and Cowtan, 2004) and refined with autoBuster (Global Phasing Ltd) and phenix.refine (Adams et al., 2010), using TLS. TLS groups were determined with TLSMD (Painter and Merritt, 2006), and the model refined to a final free R-factor of 22.2% (Table 18). Evaluation of the X-ray structure with MolProbity (Davis et al., 2004) revealed 1.06% residues as outliers and 95.87% residues in highly favoured regions of the Ramachandran plot. The structure and diffraction data of *h.s.* mitochondrial RNAP have been deposited in the Protein Data Bank under the accession code 3SPA. Figures were prepared with Pymol (Schrödinger, LLC).

2.3.4 Transcription run-off assay

Transcription run-off reactions were performed by the laboratory of Prof Dmitry Temiakov, (UMDNJ-SOMStratford, NJ, USA) and were carried out using synthetic DNA templates containing LSP promoter as described elsewhere (Sologub et al., 2009).

3 Results and Discussion

3.1 Structure determination of human mitochondrial RNAP

We determined the structure of human mitoRNAP by X-ray crystallography. Limited proteolysis experiments and subsequential Edman sequencing with human mitoRNAP variants and trypsin or chymotrypsin revealed cutting sites at amino acid positions 154, 157, 598, 761, 776, 1089, and 1111. Together with secondary structure prediction and sequence alignments with bacteriophage T7 RNAP this revealed flexible regions in the N-terminal region (AA 1-150), the intercalating hairpin (AA 591-624), the thumb region (AA 730-790), and the specificity loop (AA 1085-1108) (see Appendix IV 4). A variant lacking the first 150 AA (mitoRNAPΔ150) or the first 104 AA (mitoRNAPΔ104) showed improved solubility and the latter is fully functional, as it requires the presence of both TFAM and TFB2M for efficient transcription initiation on double-stranded promoter DNA (Figure 24 in Appendix IV 3).

Both variants were used for crystallization trials and *in situ* proteolysis with trypsin or Arg C and revealed crystals (Figure 11A and B and 2.3.2). Analysis of mitoRNAPΔ150 crystals, which grew after *in situ* proteolysis with trypsin, showed, that they are comprised of at least two RNAP fragments and do not contain trypsin (Figure 11C). Trypsin- and Arg C-digested mitoRNAPΔ150 and Δ104 produced crystals in same conditions and with same shape.

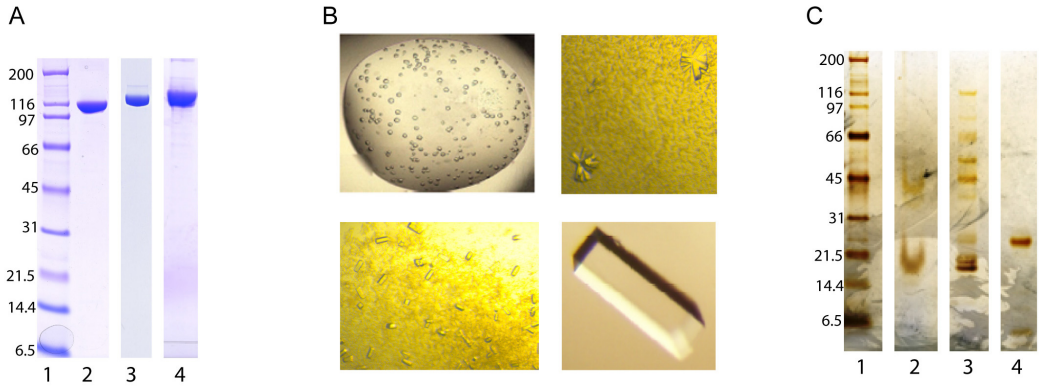

Figure 11. Human mitoRNAP crystallization.
(A) Purified and crystallized RNAP variants. Lane 1 shows Broad range marker. Lane 2, 3, and 4 show purified human mitoRNAP variants 150-1230, 104-1230, and 44-1230, respectively, stained with coomassie. **(B)** Crystallization trials with in situ proteolysis. Upper left picture shows spherulite crystals grown in 96 well plate at 20°C in reservoir solution (20% PEG 3350; 0.2M Potassium phosphate) using human mitoRNAP variant 150-1230 (c= 9 mg/mL) proteolysed with trypsin (ration (m/m) = 750:1) for 1 h on ice before seting drops. Upper right picture shows crystals in 24 well plate at 20° in reservoir solution (40 mM Mes 6.5; 97.5 mM $(NH_4)_2SO_4$; 12% PEG 5000; 12.5% Xylitol; 120 mM DTT) using using human mitoRNAP variant 150-1230 (c= 9 mg/mL) proteolyzed with trypsin (ration (m/m) = 900:1) for 2 h on ice before seting drops. Lower left picture shows crystals in 24 well plate at 20° in reservoir solution (40 mM Mes 6.5; 80 mM $(NH_4)_2SO_4$; 12% PEG 5000; 12.5% Xylitol; 120 mM DTT) after microseeding. Lower right picture shows single crystal, which grew after 2-3 days up to 250x90 µm. **(C)** Crystal content analysis. Lane 1 shows Broad range marker. Lane 2 shows washed, dissolved and silverstained crystals of human mitoRNAP 150-1230 (*in situ* proteolysed), which are shown in **(B**, lower panel**)**. Lane 3 and 4 show the digestion pattern of human mitoRNAP 150-1230 with trypsin and used trypsin protein, respectively.

A first structure (data set A3, mitoRNAPΔ150 treated with trypsin, crystal size 250x70x20 µm) was solved by molecular replacement using T7 RNAP core (pdb 1QLN and AA 246-354, 392-568, 691-741, 766-883 all as poly Alanin sequence) as searchmodel. Phaser revealed a rotation function Z (RTZ)-score of 16.69 and a translation function Z (TFZ)-score of 38.2 for the best solution and rigid body refinement with Refmac5 (Murshudov et al., 1997) revealed initial R factors of R_{work}= 43.2% and R_{free}= 44.1%. Iterative model building and refinement with autoBuster revealed a final R_{free} of 25.92% for this first data set.

Subsequently, this model was used for molecular replacement with a second data set (data set J1, mitoRNAPΔ104 treated with ArgC, crystal size 250x90x40 µm), which showed improoved data collection statistics, probably because of a larger crystal size. The final model was refined to a R_{work}= 18.47% and R_{free}= 22.20% at 2.4 Å resolution (Table 18 and 2.3.3). This model was used for subsequent structure analysis and interpretation.
Evaluation of the X-ray structure with MolProbity (Davis et al., 2004) revealed 1.06% of the residues as Ramachandran outliers and 95.87% Ramachandran favoured residues, as well as 0% bad bonds, 1.04% bad angles, and 4.03% poor rotamers, mostly in loop regions with high B-factor sidechains and missing electron density.

Table 18. Human mitochondrial RNAP X-ray diffraction and refinement statistic

Data set	Native (A3)	Native (J1)
Data collection		
Space group	I 4_1	I 4_1
Unit cell axis a, b, c (Å)	212.24, 212.24, 60,44	211.26, 211.26, 60.46
Unit cell angles α, β, γ (°)	90, 90, 90	90, 90, 90
Wavelength (nm)	1.0717	1.0000
Resolution (Å)*	41.99-2.80	58.128-2.40
Rmerge (%)*	8.8 (90.7)	5.1 (89.6)
I/σ (I)*	7.0 (1.2)	14.2 (1.4)
Completeness (%)*	99.5 (99.4)	99.8 (99.3)
Redundancy*	3.3 (3.3)	3.8 (3.8)
Refinement		
Resolution (Å)	41.99-2.81	24.00-2.40**
No. reflections	32879	52497
Rwork (%)	22.94	18.47
Rfree (%)	25.92	22.20
No. atoms		
Protein	7069	7588
Ligand/ion	1	2
Water	-	228
B-factors (Å2)		
Protein	105.3	92.7
Ligand/ion	135	132
Water	-	73.9
r.m.s.d. from ideal		
Bond lengths (Å)	0.009	0.009
Bond angles (°)	1.37	1.18

*Highest resolution shell is shown in parenthesis.
Rmerge = $\Sigma |I - \langle I \rangle| / \Sigma |$ where I is the integrated intensity of a given reflection.
R = $\Sigma ||Fobs| - |Fcalc|| / \Sigma |Fobs|$. Rfree was calculated using 5% of data excluded from refinement.
** AutoBuster deleted 50 low resolution reflections during refinement leading to a lower (24 Å) high resolution limit.

Visible in the structure are amino acids 218-1230, just lacking a loop adjacent to the intercalating hairpin (AA 592-602), the tip of the intercalating hairpin (AA 613-614), parts of the thumb (AA 736-769) and the specificity loop (AA 1086-1105) (Figure 12). This is consistent with flexible and protease-digested parts. To elucidate wether some of these non-visible parts are lacking because of protease-digestion, point mutations in human mitoRNAP were introduced at Arg residues adjacent to these breaks and providing enough space in crystal packing (R598A, R601A, R613A and R1108A). The solved structure (data set B4) of this mutant did not provide additional density in the missing parts, pointing to flexibility

Interestingly, density for one additionally bound negatively loaded ligand was found in the active center. Since the crystallization buffer only revealed $(NH_4)_2SO_4$ as a salt, SO_4^{2-} was build in this density.

3.2 Conserved C-terminal catalytic domain

MitoRNAP belongs to the pol A family of nucleotidyltransferases and shows the characteristic shape of a right hand with palm, fingers, and thumb subdomains (Figure 12).

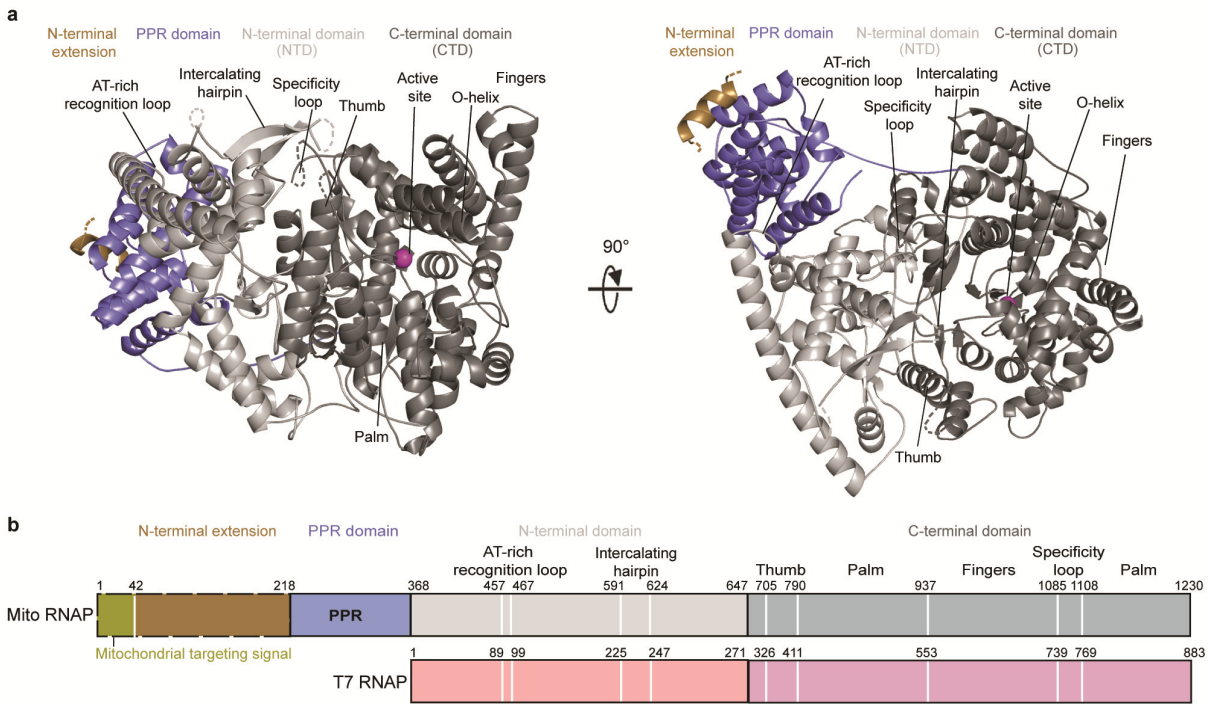

Figure 12. Crystal structure of human mitoRNAP.
(a) Two views of a ribbon model of the human mitoRNAP structure with the major domains and structural elements indicated. The C-terminal domain (CTD) that is conserved in all ss RNAPs is coloured in dark gray, the N-terminal domain (NTD) is in silver, and the PPR domain is in blue. The N-terminal extension helix is shown in sand. The active site is indicated by a magenta sphere for a modelled catalytic metal ion. **(b)** Schematic comparison of mito and T7 (PDB 1QLN) RNAPs. Prominent structural elements are indicated. MitoRNAP-specific residues 1-368 include the mitochondrial targeting signal, the N-terminal extension, and the PPR-domain. Regions in mitoRNAP that are not visible in the crystal structure include residues 592-602, 736-769, and 1086-1105.

Note that throughout this manuscript, we use the canonical polymerase domain nomenclature, and also the previously defined names for T7 RNAP functional elements (Cheetham et al., 1999; Durniak et al.,

2008), even if these names include a functional implication that is specific for T7 RNAP and not born out in mitoRNAP.

The highly conserved palm in the CTD superimposes well with the corresponding palm in T7 RNAP (r.m.s.d. 1.0 Å over 121 backbone atoms). The high conservation of the active center, including the O-helix, suggests that the mechanisms of substrate binding and selection are conserved between mitoRNAP and T7 RNAP (Temiakov et al., 2004; Yin and Steitz, 2004). The O-helix binds a sulphate ion with its residues R987, K991, and K853 of the palm subdomain (Figure 13a and b) near the position of the phosphate groups of an incoming nucleoside triphosphate (NTP) in the T7 RNAP elongation complex (EC) (Temiakov et al., 2004; Yin and Steitz, 2004). While a portion of the thumb (residues 736-769) and the flexible specificity loop (residues 1086-1105) are not visible in the mitoRNAP structure, the adjacent elements in the CTD occupy almost identical positions as in T7 RNAP, suggesting a similar orientation and functional role for these elements.

The most notable difference between the CTD of T7 RNAP and mitoRNAP is the position of the fingers subdomain, which is rotated ~25° as a rigid body approximately around the axis of the O-helix, accompanied by a tilting of the O- and Y-helices (Figure 13a). These movements result in a 15 Å translation of the N-terminus of the Y-helix towards the PBD. The observed position of the fingers domain is distinct from the previously observed positions in the 'closed' EC structure of T7 RNAP, in which the O-helix is positioned to deliver the substrate NTP into the active site (Yin and Steitz, 2004) (Figure 13b). We refer to this novel RNAP conformation as 'clenched'. In the clenched conformation, the entrance to the active site is occluded by Y-helix residue Y1004, a conserved residue in ss RNAPs implicated in downstream duplex melting (Tahirov et al., 2002; Yin and Steitz, 2002). Thus, the clenched conformation is unlikely to occur during the nucleotide addition cycle.

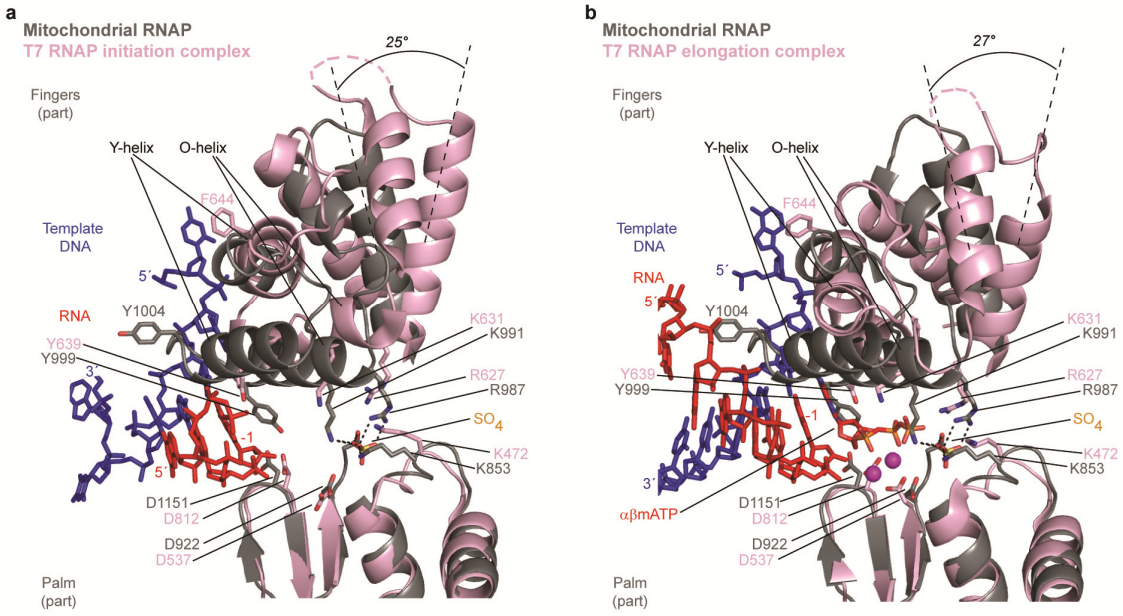

Figure 13. Active center region.
(a) A superimposition of the active center regions of mitoRNAP (gray) and the T7 RNAP initiation complex (PDB 1QLN) (light pink) reveals a rigid body rotation of the fingers domain around the O helix axis. Template DNA is in blue, RNA is in red. The clenched, catalytically incompetent conformation of the fingers domain in mitoRNAP results from a ~25° rotation around the O-helix. Conserved catalytic residues, residues implicated in NTP binding, and a sulphate ion are shown with sticks. **(b)** A superimposition of the active center regions of human mitoRNAP (gray) and the T7 RNAP elongation complex (PBD 1S76) (light pink) reveals the difference between the clenched (mitoRNAP) and closed conformation (T7 RNAP) of the fingers domain. The incoming ATP and the catalytic Mg2+ ions (magenta spheres) in the T7 structure are depicted.

3.3 Distinct N-terminal domain

The large N-terminal region of mitoRNAP (residues 1-647, Figure 12b) shares no sequence homology with T7 RNAP. Nonetheless, the C-terminal part of this region (residues 369-647) is structurally similar to the N-terminal domain of phage RNAPs, and we thus refer to it as N-terminal domain (NTD). In particular, the six-helix bundle of the PBD in phage RNAPs, which includes helices D, E, F, G, I and J, has a counterpart in mitoRNAP (Figure 14). However, there are notable changes in the orientation of the helices in the PBDs of mitoRNAP and T7 RNAP, resulting in a very high r.m.s.d. value of 9 Å for 109 backbone atoms. Compared to T7 RNAP, the N-terminal part of the PBD (residues 425-519) is rotated by 32°, whereas the C-terminal part (residues 567-654) is rotated by 24° in mitoRNAP.

The structure reveals the loops corresponding to the intercalating hairpin and the AT-rich recognition loop of T7 RNAP. The hairpin connects the conserved helices I and J, and has a 14- residue insertion that is partially visible in the mitoRNAP structure (Figure 14a). The loop that connects helices D and E of the PBD corresponds to the AT-rich recognition loop, but is shorter, whereas the D-helix is extended as compared to T7 RNAP (Figure 14b and c). Other significant differences in the NTD of mitoRNAP involve the absence of a distal helix C, shortening of the F and G helices, and an alternative fold of the region located at the position of subdomain H in T7 RNAP. In contrast to N4 RNAP, where subdomain H is absent (Figure 14d), it is likely that this structural element of the mitoRNAP NTD undergoes refolding during the transition from initiation to elongation, to form a part of an RNA exit pore, as described for T7 RNAP (Tahirov et al., 2002; Yin and Steitz, 2004).

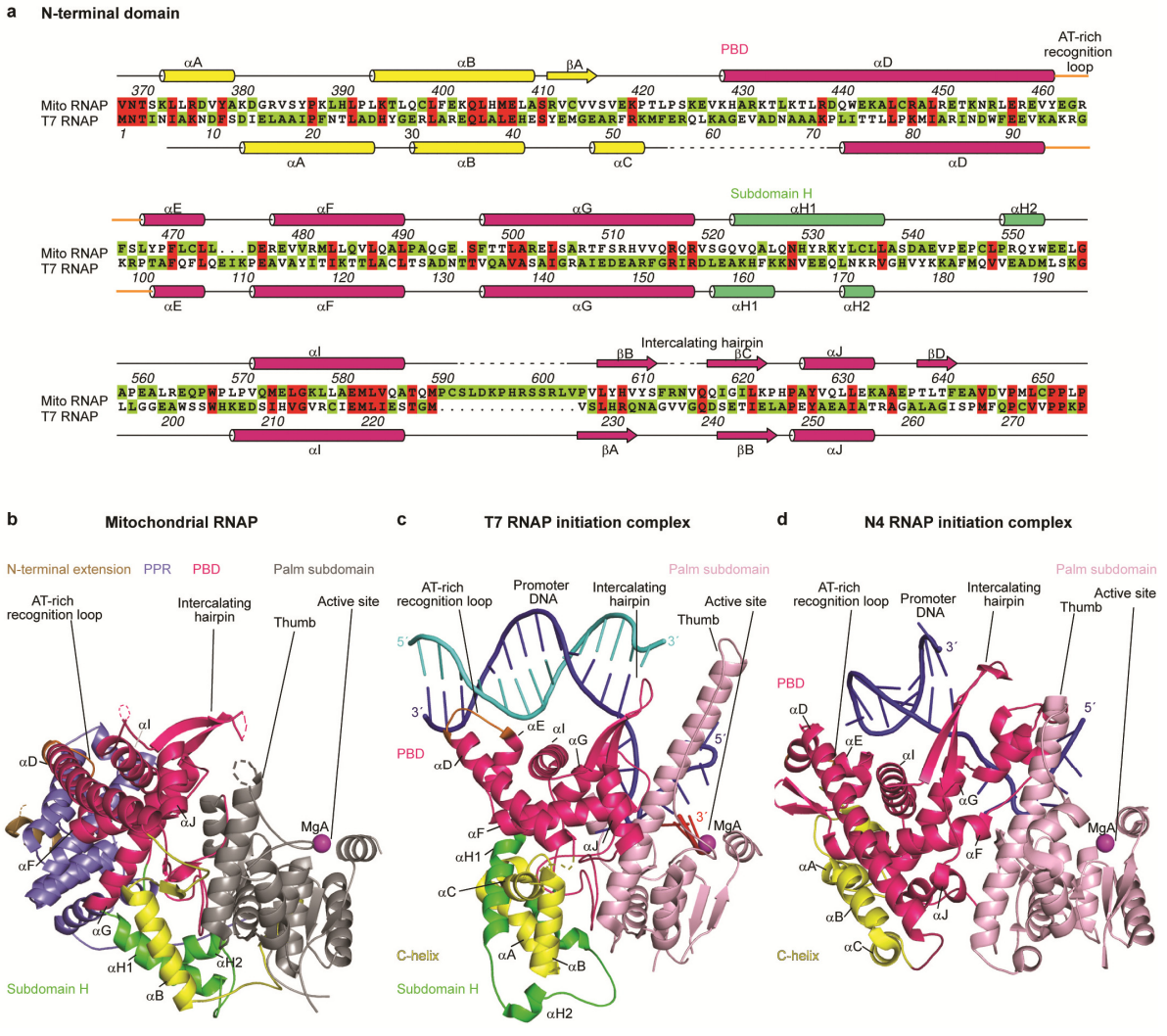

Figure 14. Variation in RNAP N-terminal domains.
(a) Sequence alignment and structural conservation of human mitoRNAP and T7 RNAP (PBD code 1QLN). Secondary structure elements are indicated above and below the sequences for mitoRNAP (residues 368-654) and T7 RNAP, respectively (cylinders for α-helices, arrows for β-strands, lines for loops). The promoter-binding domain (PBD) is in pink, the C-helix in yellow, and subdomain H in green. The AT-rich recognition loop (orange) and the intercalating hairpin are indicated. Identical residues are highlighted in red. Dashed lines indicate regions that are not visible in the mitoRNAP structure. **(b-d)** Comparison of the NTDs of mitoRNAP (residues 368-676) with ICs of T7 RNAP (PBD 1QLN) and N4 RNAP (PBD 3Q24). Structures are aligned with respect to their conserved palm subdomains. Colour code and residue borders of the elements of the NTD are the same as in **(a)**. RNA is in red, the template strand DNA in blue, and the non-template strand in cyan. From the CTD (gray or light pink), only the palm subdomain (residues 790-831, 911-937, and 1125-1178) and the thumb (residues 677-790) are shown.

3.4 Unique PPR domain and N-terminal extension

The NTD of mitoRNAP is connected through a rigid proline-rich linker to a unique helical domain (Figure 15). This domain (residues 218-368) consists of nine α-helices, of which four compose two PPR motifs found in plant and mitochondrial proteins (Lightowlers and Chrzanowska-Lightowlers, 2008; Small and Peeters, 2000). We therefore refer to this domain as the 'PPR motif-containing' domain, or PPR-domain. PPR motif-containing proteins are suggested to be involved in RNA editing or processing (Aphasizheva et al., 2011; Hammani et al., 2011), but their structures are unknown.

Our structure of the PPR domain shows that the conserved residues of the PPR motif form the hydrophobic core of a helix-turn-helix fold, and the interface between antiparallel α- helices (αD′ with αE′, αE′ with αF′, and αF′ with αG′) and parallel helices (αE′ with αG′) (Figure 15a, b). The PPR domain is tightly attached to the NTD as the helices αA′ and αB′ form a large hydrophobic interface (~950 $Å^2$) with the tip of the AT-rich recognition loop and its flanking helices αE and αD (Figure 15c). The interactions of the PPR domain with the NTD are stabilized by a salt bridge between R225 and E574 and numerous hydrogen bonds (Figure 15c).

It was reported that the gene encoding mitoRNAP undergoes alternative splicing, resulting in a truncated version (spRNAP IV, residues 263-1230) that lacks a mitochondrial targeting signal and localizes to the nucleus (Kravchenko et al., 2005). The structure of mitoRNAP suggests that removal of the first 262 residues will truncate and disconnect the PPR domain from the mitoRNAP body. This would expose large hydrophobic surfaces on both the N-terminal domain and the PPR motif 1 (more than 1000 $Å^2$). Consistent with this, attempts to express a previously described nuclear single-polypeptide RNAP IV (Kravchenko et al., 2005) in both prokaryotic and eukaryotic systems resulted in an insoluble protein (Sologub and Temiakov, personal communication).

Most of the region N-terminal of the PPR domain, called here the N-terminal extension, is invisible in the structure, except a single unassigned α-helix bound to a hydrophobic pocket formed by αF′ and αG′ of the PPR domain (Figure 15b). The mobile N-terminal extension of human mitoRNAP is required for function since deletion of the N-terminal 200 residues results in a truncated polymerase that is catalytically active but unable to initiate promoter-directed transcription (Figure 24 in Appendix IV 3). This is in contrast to yeast mitoRNAP (RPO41) in which even a larger deletion of the N-terminal region (270 residues) has no effect on transcription activity (Paratkar et al., 2011).

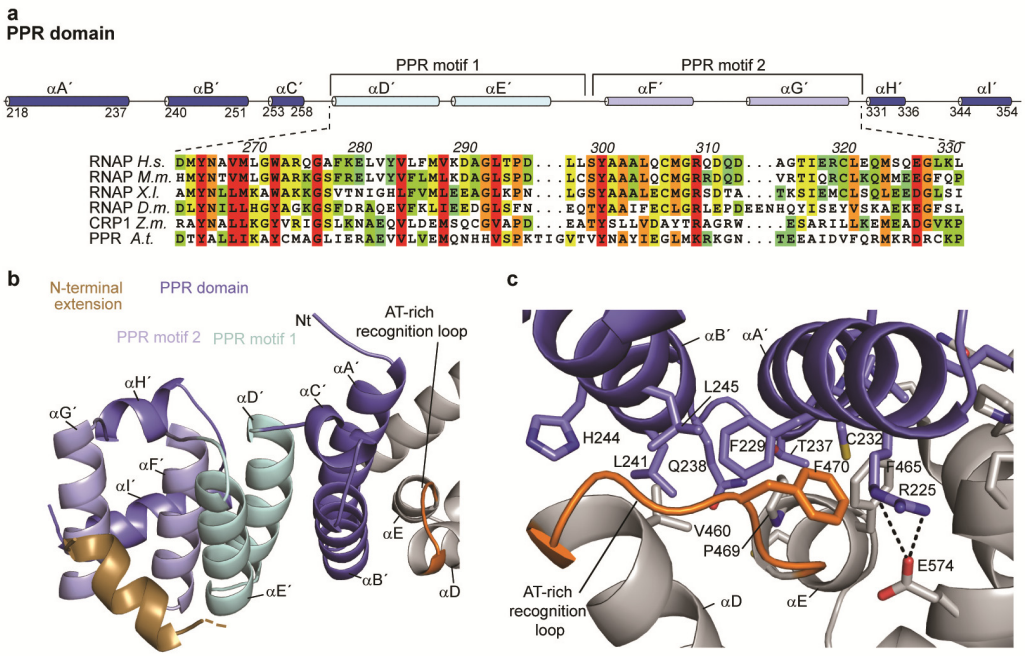

Figure 15. PPR domain.
(a) Sequence alignment of human mitoRNAP PPR domain, including PPR motifs 1 and 2, with predicted PPR motifs in mitoRNAPs of different species (lines 2-4), and chloroplast-targeting proteins of plants (lines 5,6). Abbreviations are as follows: H.s. *Homo sapiens*, M.m. *Mus musculus*, X.l. *Xenopus laevis*, D.m. *Drosophila melanogaster*, Z.m. *Zea mays*, A.t. *Arabidopsis thaliana*. Residues that are identical, highly conserved, conserved, or distinct, are highlighted in red, orange, yellow, and green, respectively. **(b)** Structure of PPR domain (blue) with PPR motif 1 (light cyan) and 2 (light blue). Each PPR motif shows a helix turn helix fold. Helices αA´ and αB´ are adjacent to the NTD (silver) and interact with the AT-rich recognition loop (orange). PPR motif 1 interacts with a helix in the N-terminal extension (sand). **(c)** Interface between PPR domain and NTD. Colours are as in **(a)**. Interface residues are shown in stick representation.

3.5 Promoter binding

An intriguing question in mitochondrial transcription is what structural changes in mitoRNAP, relative to T7 RNAP, render mitoRNAP reliant on the initiation factors TFAM and TFB2M. Foot-printing experiments suggest that mitoRNAP (in complex with TFB2M) occupies a relatively small region of upstream DNA when compared to T7 RNAP - 14 vs. 17 bps, respectively (Gaspari et al., 2004a; Sologub et al., 2009) (Figure 16a). The rest of the upstream promoter region in mammalian mitoDNA (-35 to -15) is covered by a TFAM dimer (Gangelhoff et al., 2009; Gaspari et al., 2004a) suggesting that mitoRNAP and T7 RNAP use different modes of promoter binding.

To explore this, we modeled the putative trajectory of upstream promoter DNA in mitoRNAP by superimposing the palm subdomains of mitoRNAP and the T7 RNAP IC (Figure 16b). In the model, upstream promoter DNA runs along the NTD, and the template single strand descends into the mitoRNAP active site (Figure 16b and 13). The model predicts that the tip of the specificity loop may reach into the major groove of promoter DNA and read the sequence between -6 and -11 bps while its base may interact with the phosphodiester backbone of a single-stranded DNA, similar to its role in phage RNAPs (Cheetham et al., 1999; Gleghorn et al., 2008). This is consistent with functional analysis of point mutations in the specificity loop of yeast RPO41 (Nayak et al., 2009).

The model further indicates that the AT-rich recognition loop has distinct functions in the two systems. Compared to T7 RNAP, helix D is rotated away from the minor groove of DNA by 45° and the tip of the AT-rich recognition loop is shifted by 22 Å in mitoRNAP (Figure 16c). The loop is sequestered by extensive interactions with the PPR domain (Figure 15c) and cannot bind DNA during initiation. Consistent with this, a mitoRNAP variant that lacks the PPR domain cannot initiate transcription (Figure 24 in Appendix IV 3) although it is predicted to contain a free AT-rich recognition loop. The positively charged residues important for promoter interactions by T7 RNAP are not conserved in the mitoRNAP loop (Figure 16d), and mutations R458A/R464A have no effect on transcription activity (Figure 25 in Appendix IV 3). These results indicate that human mitoRNAP does not use its AT-rich recognition loop for promoter binding, explaining why it depends on transcription factors for initiation. The AT-rich recognition loop also has a different structure and function in RNAP of phage N4, where it recognizes a hairpin promoter (Gleghorn et al., 2008) (Figure 14d).

Unlike human mitoRNAP, yeast RPO41 does not require a TFAM homolog for initiation (Dairaghi et al., 1995a). Foot-printing data indicate that the DNA region from -17 to -13 in the AT-rich yeast promoter is protected from DNase I cleavage by RPO41/Mtf1 (Schinkel et al., 1988) (Figure 16a). Analysis of the putative AT-rich recognition loop of RPO41 from various yeast RNAPs indicates the presence of a highly conserved arginine at a position analogous to T7 RNAP R99, which is responsible for interactions with the phosphodiester backbone in promoter DNA between bases -16 and -17 (Cheetham and Steitz, 1999) (Figure 16d). Thus mitoRNAPs from lower eukaryotes may use the AT-rich recognition loop for promoter binding. In addition, the PPR domain may contribute to promoter binding as suggested by its close proximity to upstream DNA in the IC model (Figure 16b).

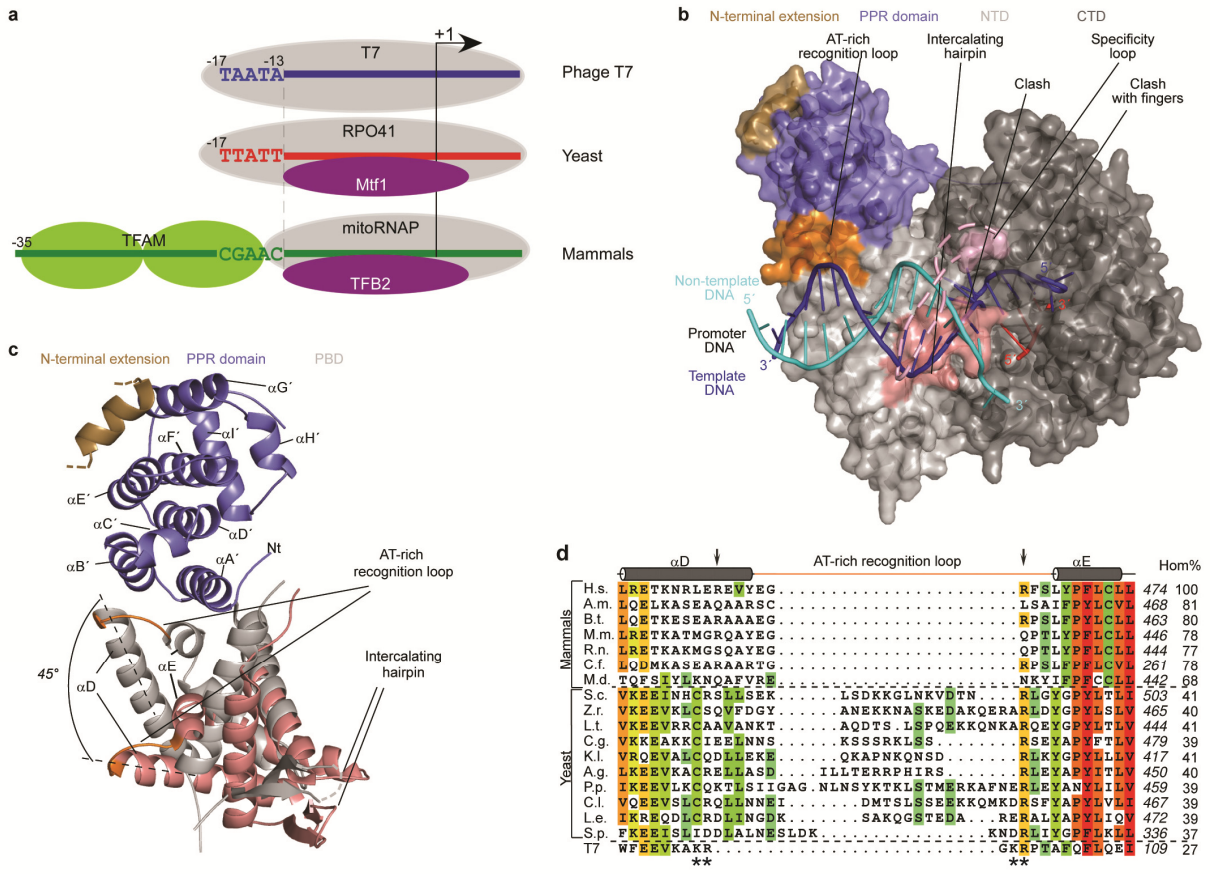

Figure 16. Promoter binding.

(a) Differences in topology of the ICs of T7, yeast and mammalian mitochondrial transcription machineries, based on foot-printing data and functional assays. Mammalian mitochondrial transcription critically depends on the presence of TFB2M and TFAM that occupies upstream promoter region, whereas yeast RPO41 requires only Mtf1 for efficient transcription. **(b)** Modelled location of upstream promoter DNA on mitoRNAP, based on a superimposition with the T7 RNAP IC structure (PDB ID 1QLN). MitoRNAP is depicted as a molecular surface. Loops in mitoRNAP that interact with DNA in the T7 system are indicated. The portion of the specificity loop not visible in the structure is modelled based on the corresponding T7 loop (dashed line). The AT-rich recognition loop is buried by the PPR domain (blue) and not seen. The intercalating hairpin (rose) is shifted by 7 Å compared to its position in T7 RNAP, and clashes with the template DNA strand. The clash is also observed between the fingers domain and the +1 template base. **(c)** Superposition of the PBDs of mitoRNAP (silver) and T7 RNAP (PBD 1QLN, salmon). The AT-rich recognition loop (orange) is shifted and rotated by 45°. **(d)** Sequence alignment of AT-rich recognition loop and adjacent helices in mitoRNAPs of mammals and yeast, and in T7 RNAP. Abbreviations are the following: H.s. *Homo sapiens;* A.m. *Ailuropoda melanoleuca;* B.t. *Bos taurus;* M.m. *Mus musculus;* R.n. *Rattus norvegicus;* C.f. *Canis lupus familiaris;* M.d. *Musca domestica;* S.c. *Saccharomyces cerevisiae;* Z.r. *Zygosaccharomyces rouxii;* L.t. *Lachancea thermotolerans;* C.g. *Candida glabrata;* K.l. *Kluyveromyces lactis;* A.g. *Ashbya gossypii;* P.p. *Pichia pastoris;* C.l. *Candida lusitaniae;* L.e. *Lodderomyces elongisporus;* S.p *Schizosaccharomyces pombe*. The colour scheme is the same as in Figure 4. Percent homology is indicated to the right of the panel. The positions of nonconserved arginines in human mitoRNAP AT-rich recognition loop are indicated by arrows. Asterisks indicate residues in T7 RNAP involved in promoter interactions.

3.6 Promoter melting

The mitoRNAP structure reveals two major differences to T7 RNAP that help rationalize the loss of the enzyme's ability to melt DNA by itself, explaining why TFB2M is required for promoter melting. First, the position of the intercalating hairpin is not compatible with promoter melting as observed in T7 RNAP (Figure 14b and c). The tip of the loop is translated 7 Å away from its position in T7 and clashes with the template strand of DNA (Figure 16b). Second, a 25° rotation of the fingers domain towards the NTD (Figure 13a) blocks access of the single-stranded DNA to the active site. This brings the tip of the intercalating hairpin within contact distance of the Y helix, suggesting that rearrangements of these two elements may be coupled (Figure 12).

Two mechanisms of promoter melting may be anticipated that involve TFB2M. First, binding of TFB2M may reposition the intercalating hairpin so it can function as in T7 and N4 RNAP (Cheetham et al., 1999; Gleghorn et al., 2008). Second, unlike the situation in phage RNAPs, the intercalating loop may not function in DNA melting, and instead an unidentified structural element in TFB2M may trigger melting.

To investigate this, we constructed variants of mitoRNAP lacking five residues at the tip of the intercalating hairpin (Δ613−618), or an insertion to this loop (Δ591-601) that is not present in phage RNAPs. We found that these enzymes had an activity similar to the wild type on a premelted 'bubble' LSP promoter template (Figure 17a). However, when analyzed in run-off assays using double-stranded LSP, the activity of the mutant RNAPs was dramatically decreased suggesting defects in promoter melting and thus the importance of the intercalating hairpin region for this process (Figure 17a).
These results indicate that TFB2M binding to mitoRNAP repositions the intercalating hairpin so it can participate in DNA melting.

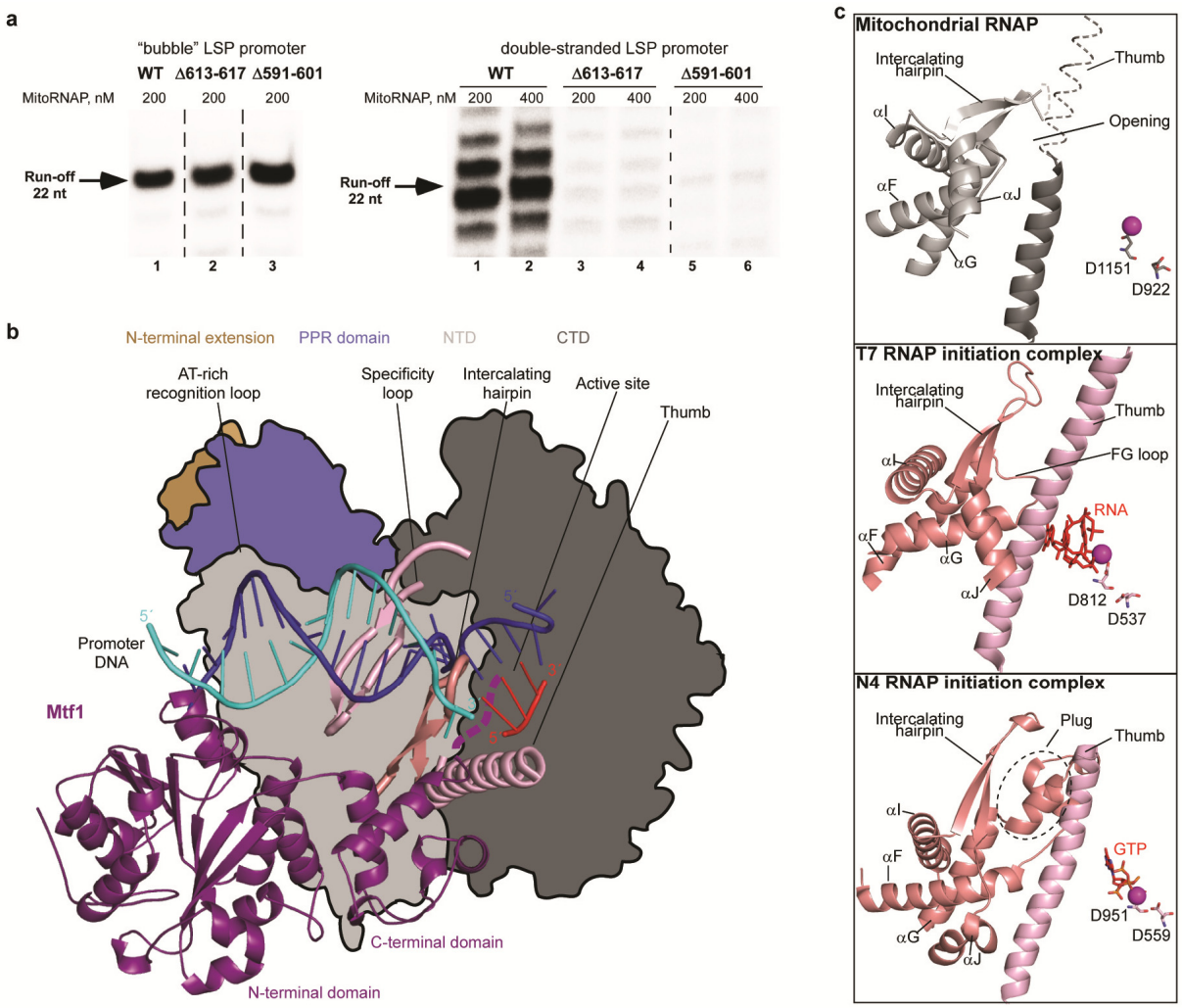

Figure 17. Promoter melting.
(a) An intercalating hairpin region is required for promoter melting in mitoRNAP. Transcription run-off assays with wild-type and mutant RNAPs were performed using bubble (left panel) and double stranded (right panel) LSP promoter templates for 30 min at 35°C. Transcription factors TFAM (50nM) and TFB2M (150 nM) were added to the reactions that involved the double stranded template (right panel, lanes 1-6) while transcription using the bubble template was factor-independent (left panel, lanes 1-3). Products of the reaction were resolved using 20% PAGE containing 6M urea, and analyzed using a PhospoImager. **(b)** Model of mitochondrial transcription IC. The Mtf1 yeast homolog structure (PDB 1I4W) is shown as a violet ribbon. MitoRNAP is shown as an outline and the promoter DNA was modelled as in Fig. 5. The intercalating hairpin and specificity loop (light pink ribbon) are shown to occupy positions as in T7 RNAP IC. Positioning of Mtf1 was done as described in the text, enabling the C-terminal tail of Mtf1 to use the passage between the thumb and the intercalating hairpin to reach the active site. **(c)** Opening for TFB2M insertion region passage to the mitoRNAP active site. Regions in mitochondrial, T7 and N4 RNAPs involving the thumb, intercalating hairpin and adjacent helices are presented in the same orientation of the corresponding CTDs. Note that only in mitoRNAP there is an opening for the Mtf1/TFB2M insertion region to reach the active site.

3.7 Initiation complex model

To further explore the initiation mechanism, and to rationalize the available biochemical and genetic data, we built a model of a mitochondrial transcription IC.

Since the human TFB2M structure is unknown, we combined the structure of its yeast homolog (Schubot et al., 2001) with the human mitoRNAP, which is expected to closely resemble its yeast counterpart RPO41 (Figure 17b). During modeling, we placed Mtf1 onto mitoRNAP without generating steric clashes, and assumed that the Mtf1 N-terminal region contains RNAP-binding determinants (Shadel and Clayton, 1995), that the Mtf1 C-terminal domain reaches the active site (Savkina et al., 2010), that the 16 most C-terminal residues of Mtf1 contact promoter DNA (Savkina et al., 2010; Schubot et al., 2001), that Mtf1 binding involves the specificity loop and intercalating hairpin (Cliften et al., 2000), and that Mf1 interacts mostly with the promoter at positions -7 to +3 (Savkina et al., 2010). We further assumed that binding of Mtf1 involves the NTD of mitoRNAP that likely undergoes refolding upon the transition from IC to EC as in T7 RNAP, thereby displacing Mtf1 upon RNA synthesis (Mangus et al., 1994).

The model suggests that the Mtf1 C-terminal 'insertion' domain reaches the templating +1 DNA base via a narrow opening between the intercalating hairpin and the thumb domain (Figure. 17b). The mobile extension of the insertion domain may occupy the predicted RNA path, consistent with biochemical data (Savkina et al., 2010; Sologub et al., 2009). The region that constitutes the opening for Mtf1/TFB2M passage is substantially different in structures of phage RNAPs. In T7 RNAP, the opening is blocked by the loop between helices F and G (FG loop) and helix J at the base of the thumb (Figure 17c). In N4 RNAP, a large insertion into the FG loop ('plug', Figure 17c) occludes the RNA/DNA hybrid binding cavity (Gleghorn et al., 2008; Murakami et al., 2008).

These considerations indicate that penetration of TFB2M into the opening leading to the active site could reposition the intercalating hairpin and the fingers subdomain, such that these elements function in promoter melting. In addition, TFB2M may stabilize an early transcribing complex by binding to the melted template strand and/or the incoming NTPs as suggested previously (Sologub et al., 2009).

4 Conclusions and Outlook

The first structure of a mitoRNAP reveals N- and C-terminal domains that are related to phage RNAPs, but also contain pronounced structural differences, and a novel PPR domain and a flexible N-terminal extension. Some surface loops that function in phage RNAPs to bind and melt promoter DNA are structurally trapped or altered, explaining the need for initiation factors. During evolution, an early phage-like mitoRNAP apparently acquired additional structural features, and lost functions in promoter binding and melting, that are now provided by initiation factors *in trans*. This may have enabled regulation of mitochondrial gene transcription and adaptation of mitochondrial function to changes in the environment. Similarly, multisubunit cellular RNAPs use a large variety of initiation factors to enable transcription regulation and to create promoter specificity.

Based on the structure of human mitoRNAP and the elucidated structural adaptions that enable mitoRNAP to become regulated by transcription initiation factors, new starting points for follow up projects arise. These should help to elucidate a complete picture of the mitochondrial transcription system.

Functional assays to elucidate mitoRNAP specific mechanisms into more detail

This work established the structural basis for the unique transcription initiation mechanism by mitoRNAP, assisted by TFAM and TFB2M. To confirm the hypotheses drawn from the structure, new mitochondrial RNAP mutants should be designed and analyzed in functional assays.
Namely, it was already shown in this work by mutation of R458A/R464A, that the AT-rich recognition loop lost its function, at least in this mitoRNAP conformation. Additionally, the tip of the intercalating hairpin (Δ613-717) and the adjacent loop (Δ591-601) were deleted and transcription activity tested. Defects in promoter melting show the importance of these regions for melting and indicate that TFB2M binding to mitoRNAP probably repositions the intercalating hairpin so it can participate in DNA melting. Since V237 in the intercalating hairpin of T7 RNAP was shown to separate the template and non-template strand of DNA, mutation of V615 at the tip of mitoRNAP hairpin would probably have a similar functional role.
Hence transcription assays with mitoRNAP carrying mutations in the specificity loop and intercalating hairpin should be performed. A likely conserved function of the specificity loop, a sequence-specific recognition of promoters, and identification of essential residues can be investigated with these mutants.

Structural investigations of full length or of larger variants of mitoRNAP

Since this work finished with the published mitoRNAP structure, which misses the N-terminal extension (AA 1-217), and parts of the thumb (AA 736-769) and specificity loop (AA 1086-1105) (see also Appendix IV 4), a new focus should lie on investigation of full-length mitoRNAP.

An analysis of the N-terminal extension could be highly rewarding. It was shown in this work that mitoRNAPΔ200 (deletion of AA 1-200) is catalytically active but unable to initiate promoter directed transcription. Since the same deletion in yeast mitoRNAP has no effect on transcription activity (Paratkar et al., 2011), the N-terminal extension in human mitoRNAP may contain additional elements required for transcription initiation. Additionally, a splicing variant, which lacks the AA 1-262 (nuclear single-polypeptide RNAP IV) was identified and showed transcription activity in the nucleus (Kravchenko et al., 2005). Nevertheless, deletion of the N-terminal parts (sp RNAP IV) leads to insoluble protein (unpublished data by Sologub and Temiakov).

To crystallize a larger variant of mitoRNAP, co-crystallization with nucleic acids or interacting proteins like TFB2M and/or TFAM should be used, since previous crystallization trials with the apo-enzyme were part of this study and only produced very tiny crystals. They grew to only 50-80 µm long needle-like crystals, diffracting only up to 14 Å and therefore were not sufficient for structure determination.

Also parts of the thumb, specificity loop and AT-rich recognition loop adjacent regions were not resolved in the structure. Attempts in this study to mutate possible cutting sites of the used trypsin/Arg C proteases in these regions (R598, R601, R613, and R1108) did not help to resolve the missing residues, suggesting that flexibility is the reason for the failure. Structure solution of these parts will be simplified by crystallization of mitoRNAP with scaffolds, since these motifs are adjacent and will hopefully be stabilized by nucleic acids.

Structure/ function analysis of the novel PPR domain

The structure of mitoRNAP also presents the first atomic model for a PPR-motif containing domain. However the proposed function as a RNA-binding domain or other functions still have to be investigated. The mitoRNAP structure reveals a positively charged surface patch on the PPR domain, which indicates a possible enlarged trajectory for promoter DNA or a role of the PPR domain in building a RNA binding surface comparable with the RNA exit tunnel found in T7 RNAP ECs. A structure of mitoRNAP with a bound promoter DNA or longer elongation scaffolds would help to establish a functional role of the PPR domain. Also binding and transcription assays of promoter DNA or elongation scaffolds with mitoRNAP proteins, whose PPR residues that build the surface accessible charged patch are mutated, can help to identify these possible roles of PPR domains.

Crystallization of mitoRNAP in numerous functional states and in complex with transcription factors

Furthermore the structure should serve as a model for structural follow up projects to elucidate structures of mitochondrial RNAP trapped in different functional states.

Experimental strategies can be copied from the T7 RNAP field. By binding of mitoRNAP to different RNA/DNA bubble scaffolds and adding either nonhydrolyzable substrate NTPs or 3´deoxyNTP and PP_i, elongation states can be mimicked, like an insertion (substrate) complex, pre-translocation (product) complex (compare (Yin and Steitz, 2004)), post-translocation complex (Tahirov et al., 2002; Yin and Steitz, 2002), and a pre-insertion (substrate) complex (Temiakov et al.,

2004). Structural changes at the active site of mitoRNAP during one nucleotide addition cycle can be analyzed and the exact substrate selection, binding, nucleotidyl transfer reaction and translocation mechanisms investigated. Since ss RNAPs do not have proofreading activity (Huang et al., 2000), these steps are extremely important to impede extended misincorporations. Although all catalytic residues are conserved between mitoRNAP and T7 RNAP, these mechanisms may differ, since a unique, "clenched" active site conformation was found in the structure of mitoRNAP (movements of fingers subdomain and F/G-helices, and occlusion of active site by Y1004).

Also initiation states of the mitochondrial transcription system should be structurally analyzed in future projects. IC conformations involve binding of mitoRNAP to promoter ds DNA, TFB2M and TFAM, whereby TFB2M interacts with both TFAM and mitoRNAP as well as with promoter DNA and possibly bridges and stabilizes promoter contacts during initiation (Litonin et al., 2010; Sologub et al., 2009). Both transcription factors can be purified recombinantly (Sologub et al., 2009) and used for *in vitro* IC reconstitutions and crystallization trials. Possible ICs, described subsequently from low to higher complexity, include the complex of mitoRNAP and TFB2M, the complex of mitoRNAP with TFB2M and a bubble ds DNA and the complex of the complete IC with mitoRNAP, TFB2M, TFAM, and ds DNA.

An interesting feature of mitoRNAP is its activity as a primase for mitoDNA replication. Molecular details of the initiation of primer synthesis in the replication process can be structurally investigated. Since mitoRNAP transcribes the reverse primer at the second replication start site (OriL) on the H-strand, where DNA forms a single-stranded hairpin, without the help of TFAM and TFB2M this hairpin promoter can be used to elucidate this special initiation process.

It is suggested that transition from initiation to elongation takes place, when the growing RNA clashes with the F/G helices, leading to abortive initiation and in the case of T7 RNAP, refolding of the N-terminus. For mitoRNAP, maybe the same transition releases TFB2M. To elucidate transition from initiation to elongation into more detail, scaffolds with different lengths of RNA can help to identify and crystallize transition states, like an intermediate state, where the mitoRNAP is bound to both the promoter and downstream DNA (compare (Steitz, 2009)). Thereby possible refolding of the N-terminal domain, as found in T7 RNAP, can be structurally investigated as well as subsequent changes and loss of the interaction with (TFAM and) TFB2M.

Crystallization of mitoRNAP with regulatory proteins

Furthermore, complex structures with regulatory factors (and DNA) beside the decribed TFAM and TFB2M can be attempted. For example mTERF is an interesting candidate. In human four mTERF proteins are predicted (Linder et al., 2005) and suggested to have termination activity. However direct association with mitoRNAP was not tested so far (Gaspari et al., 2004b).

IV

■ ■ ■

Appendix

Unpublished results to part II

Beside the published Maf1 structure and functional and biochemical assays, which were combined with cryo EM reconstructions of RNAP III, RNAP III EC and RNAP III/Maf1 and thereby led to the investigation of the molecular basis of RNAP III transcription repression by Maf1, additional experiments were carried out. First the Maf1 structure and protein was characterized into more detail and second initial trials of the structural investigation of RNAP III-PIC were performed. This chapter can serve as an overview and for experimental design of future projects.

1 Further Maf1 analysis

1.1 Maf1 activity is possibly controlled by an internal 16 AA predicted helix

The Maf1 protein was analyzed into more detail. ScMaf1 variants, which lacked striking parts of the protein, were designed based on the structure. Analyzed scMaf1 variants corresponded completely or partially to the crystallized *h.s.* Maf1 variant and fulllenght *h.s.* Maf1 and were used for *in vivo* phenotyping with complementation assays in yeast (Figure 18). MafΔ strains show a temperature sensitive growth defect on YPGly (Boguta et al., 1997). Interestingly, scMaf1 1-345, which lacks the complete acidic tail of 50 AA, fulfils normal Maf1-function under this stress condition. In contrast, the truncated crystallized Maf1 variant (sc Maf1 1-345Δ36-224), which is able to bind to RNAP III (Figure 6), has a maf1Δ phenotype. This underlines the importance of the flexible linker, which was cut for crystallization reasons, *in vivo*. This linker comprises regulatory PKA-phosphosites and the Nt-NLS sequence. Since scMaf1 mutants with destroyed NLS sequences or PKA-posphosites were shown to exhibit a wt growth on YPGly (37°C) (Moir et al., 2006), this phenotype is not explainable by deletion of these sequence motifs but rather by other effects. Additionally, also scMaf1 1-396Δ36-52, which misses just a predicted helix at the N-terminus of the cut flexible linker, has a maf1Δ phenotype. Thereby AA 36-52 are essential for the *in vivo* function of Maf1 but not for *in vitro* binding to RNAP III. Possible functions of this predicted helix include the binding of upstream regulators (phosphatases), of nuclear transport factors or of target proteins beside RNAP III (TFIIIB) and have to be further elucidated.
Concordantly to binding experiments human Maf1 fl. is not able to complement the scMaf1 protein in yeast.

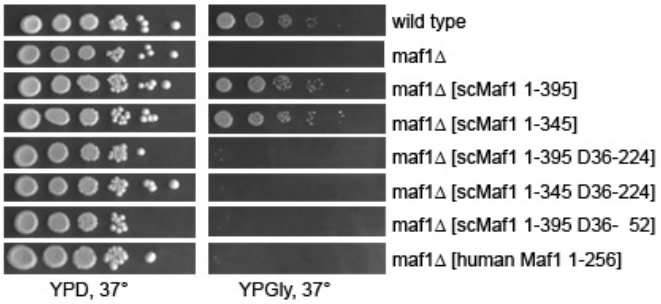

Figure 18. *In vivo* properties of Maf1 variants.
Described variants of *s.cer.* and *h.s.* Maf1 were analyzed in *in vivo* phenotyping assays as described (2.3.2.2). On the left panel serial spot dilutions on a YPD plate incubated at 37°C with normal growth of all yeast strains are shown. Right hand panel shows spot dilutions on a YPGly plate incubated 37°, indicating phenotyping effects with maf1Δ and some Maf1 variants.

1.2 Single point mutations in Maf1 have no effect *in vivo* nor on RNAP III binding

We wanted to analyze if single aminoacid residues on the Maf1 surface could influence scMaf1 properties *in vivo* or its´ binding to RNAP III *in vitro*. Thereby one may identify residues, which are essential for Maf1´s activity.

Based on the structure and sequence analysis of Maf1, conserved surface residues were mutated. Some of these residue mutations were already described in literature (Moir et al., 2006; Roberts et al., 2006). Namely, we could reproduce the *in vivo* phenotyping results that D248A, D250A, K329A/K331A showed no effect in glycerol growth assays (Figure 19C). Additionally, we investigated novel mutants, E272A, K233A, G316E, S263R, and D40N/R232H, which all did not change the phenotype and conclusively the Maf1 activity. May slight effects could be found with the point mutation R232H and D40A (Figure 19C), convergent with published observations of a growth phenotype of D40A/R41A and R232H (Moir et al., 2006; Roberts et al., 2006). Anyway, these phenotypes are probably not strong enough to draw any conclusion. Unfortunatly, the slight phenotypic mutants R232H and D40A were not tested in pulldown assays.

Consequentially to a wild type phenotype of mutants D248A, K233A, and G316E also did not abolish RNAP III binding *in vitro* (Figure 19B).

Since no tested single point mutation showed a deficient *in vivo* phenotype nor reduced binding to RNAP III, the Maf1 binding surface to RNAP III and regulatory proteins is not affected. Propably, a larger surface takes part in this interaction.

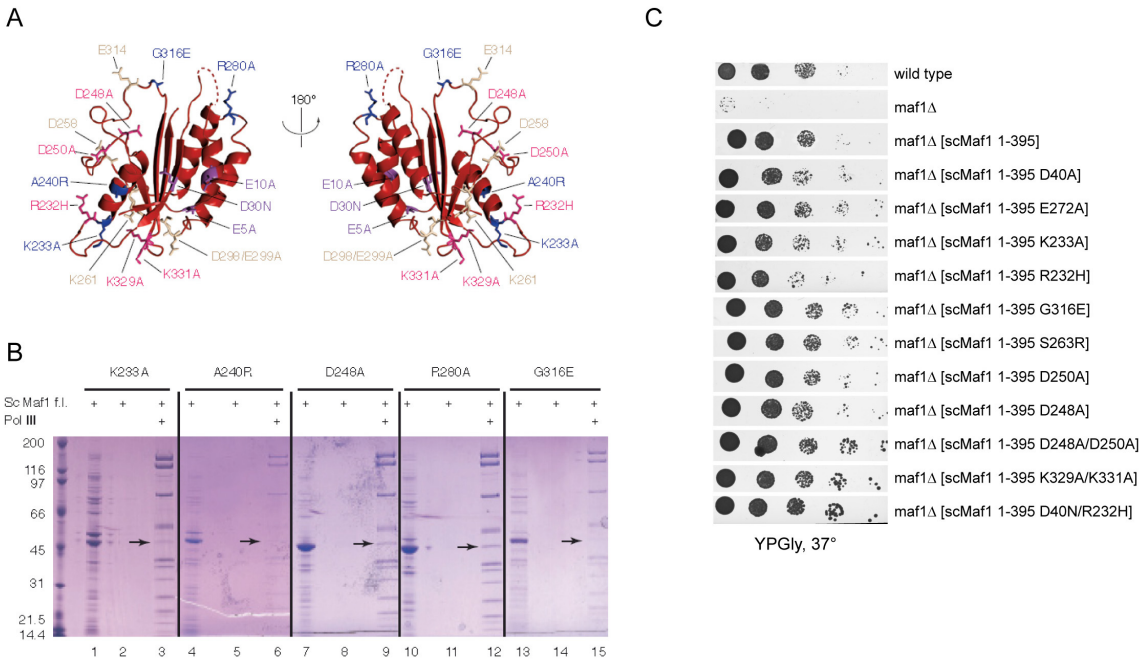

Figure 19. Analysis of Maf1 single point mutants.

(A) Ribbon model of Maf1 structure (1-205Δ36-82). Investigated residues are shown in ball and stick representation. Residues labeled in blue were analyzed by pulldowns in this study and did not abolish RNAP III binding. Other indicated residues were analyzed in *in vivo* phenotypic assays (see (C)). **(B)** Pulldown assays with endogenous RNAP III and recombinantly expressed and partly purified scMaf1 mutants. Gels show partly purified Maf1 mutants used for binding (lanes 1, 4, 7, 12), negative control of unspecific Maf1 binding to the resin (lanes 2, 5, 8, 13) and the eluted fractions, indicating that all point mutants can still bind RNAP III (lanes 3, 6, 9, 14). **(C)** Described point mutants of yeast Maf1 f.l. were analyzed in *in vivo* phenotyping assays as described in (2.3.2.2). Serial spot dilutions of each Maf1 point mutant are shown in each line, respectively and growth on YPGly at 37°C was documented after 4 days.

1.3 Binding of scMaf1 to RNAP III is stronger than to TFIIIB and probably supported by interactions with multiple RNAP III subunits

ScMaf1 binds recombinant Brf1 very weakly but specifically, which was shown in pulldown assays with autoradiography (Desai et al., 2005). Also human Maf1 associates weakly with Brf1, whereas binding to Brf2 is inconsistently found and even weaker (Reina et al., 2006; Rollins et al., 2007).
For *in vitro* binding competition and transcription assays, we used the triple fusion protein $Brf1_N$-TBP_C-$Brf1_C$. We performed size exclusion chromatography experiments (2.3.1.4) to first check if we can detect binding of scMaf1 with $Brf1_N$-TBP_C-$Brf1_C$ and to compare the affinity with RNAP III binding. And secondly, to figure out if DNA-binding of $Brf1_N$-TBP_C-$Brf1_C$ potentially increases its affinity to Maf1, since this was not tested before but could be part of the inhibition mechanism.
Under the chosen conditions no binding of $Brf1_N$-TBP_C-$Brf1_C$ with or without ds DNA could be detected, confirming a lower affinity compared to RNAP III and impairing a DNA-induced increase of affinity for TFIIIB (Figure 20A). Additionally, heavy degradation of $Brf1_N$-TBP_C-$Brf1_C$ in the absence of DNA could be detected (Figure 20A left panel).

Additionally, we wanted to elucidate RNAP III subunits, which participate in Maf1 binding, into more detail, since a strong binding of scMaf1 to the complete RNAP III complex was shown (Figure 6).
Firstly, the RNAP III subunit C34, which was found as one top interacting partner of Maf1 in the yeast interactome (Gavin et al., 2006), was analyzed. Pulldown and size exclusion binding experiments of scMaf1 fl with recombinantly purified C34 were performed (2.3.1.4). No binding could be detected (Figure 20B).
Secondly, the N-terminal part of C160 (AA 1-235), which shows genetic interactions (Pluta et al., 2001) and whose N-terminal 235 AA coimmunopurify with Maf1 from crude extracts in western blots (Oficjalska-Pham et al., 2006), was analyzed (2.3.1.5). The N-terminal part of C160 (AA 1-235) was cloned with a His_6-Tag and cotransformed with a plasmid carrying scMaf1 fl. Coexpression and copurification did not succeed (Figure 20C). Possible reasons for failure can be suboptimal expression conditions, insufficient detection sensitivity (Coomassie-staining vs immunoblotting), and unproper folding of Nt-C160.
These results may indicate that rather an overlapping binding surface of RNAP III can be expected to take part with multiple interactions in scMaf1 binding or a direct binding to C82, that was not tested or posttranslational modifications on RNAP III.

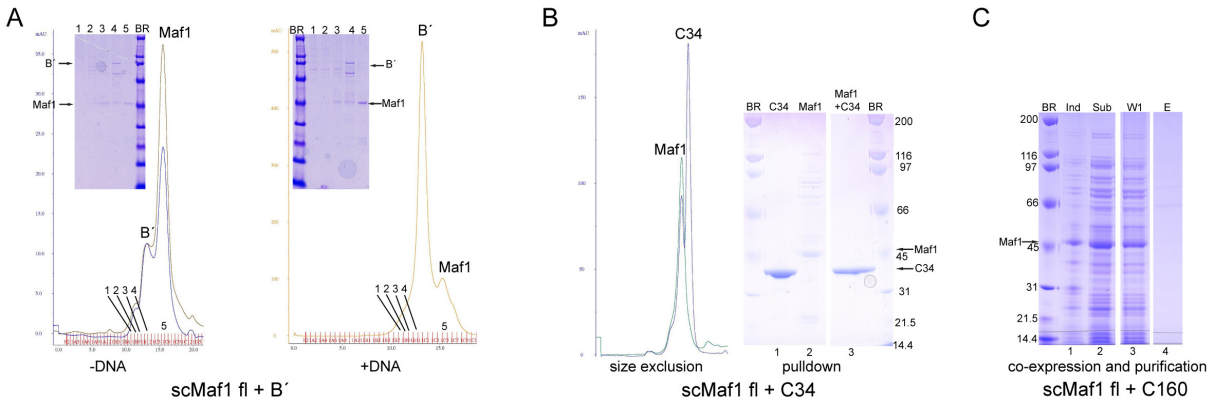

Figure 20. Binding of scMaf1 fl to $Brf1_N$-TBP_C-$Brf1_C$ and RNAP III subunits.
(A) Binding of sc Maf1 fl to the triple fusion protein $Brf1_N$-TBP_C-$Brf1_C$ (B´). Sample preparation and size exclusion runs on a Superdex 200 (10/300) column (GE Helathcare) were carried out with or without adding a 60 bp scaffold to $Brf1_N$-TBP_C-$Brf1_C$ in advance (2.3.1.4 and 2.3.3.4). Each experiment was carried out with 2.5 nmol $Brf1_N$-TBP_C-$Brf1_C$, a 2-fold molar excess of scMaf1 fl and a 2-fold molar excess of scaffold, when indicated. The left chromatogram shows the Maf1 control

curve (brown) and the assembled complex curve (blue). The right chromatogram shows only the complex assembly (orange curve). Peaks were analyzed by overlaying curves and on SDS-PAGEs. **(B)** Binding of scMaf1fl to scC34fl. Sample preparation, size exclusion runs on a Superose 12 (10/300) column (GE Helathcare), and pulldown assays were performed as described (2.3.1.4). The chromatrogram shows a control run with scMaf1 fl (green curve) and the assembled complex (blue curve). The SDS-PAGE of the pulldown experiment shows purified scC34fl (lane 1), partly purified scMaf1 fl (lane 2), and the pulldown sample of preassembled Maf1 and C34 (lane 3). **(C)** Binding of scMaf1fl to scC160 (1-235). Coexpression and purification was performed as described (2.3.1.4) with N-terminal His-tagged C160 and Maf1 without tag. The SDS-PAGE shows a sample after induction (lane 1), the soluble supernatant (lane 2), the first washing step on a Ni-column (lane 3), and eluted proteins (lane 4). Maf1 could be identified on the SDS-PAGE, C160 (M= 26 kDa) was not detected after overexpression or in later purification steps.

1.4 Maf1 binds nucleic acids unspecifically

Purification of Maf1 variants co-incidenced often with nucleic acids contaminations. ChIP experiments revealed an increased Maf1 occupancy on RNAP III-transcribed genes upon stress conditions (Oficjalska-Pham et al., 2006; Roberts et al., 2006), conversely to published data, which could not detect any direct or indirect interaction of Maf1 with DNA (Desai et al., 2005).

To find out, if Maf1 can bind nucleic acids specifically, EMSA assays were performed (2.3.1.9). Since the Maf1 structure revealed positively charged surfaces, nucleic acid binding is supported and specificity can be assigned only sequence-wise. Double-stranded and single-stranded U6- and random-sequence DNA were tested with scMaf1 fl and human Maf1 fl proteins (Figure 21). A band shift of double- and single-stranded scU6 DNA with increasing amounts of scMaf1 fl can be detected (Figure 21A, left panel), indicating nucleic-acid binding properties of scMaf1 fl. Anyway, also double- and single-stranded random DNA bound to scMaf1 fl and led to band shifts (Figure 21A, right panel). Conclusively, scMaf1 fl binds ds and ss DNA in significant amounts but this binding is sequence unspecifically. Therefore it cannot be concluded if this binding is due to unspecific interactions with the positively charged surface or if it points to a scMaf1-property *in vivo*, for example a kind of scanning mechnism on DNA.

Also human Maf1 fl protein binds to ds and ss U6 promoter DNA but to a much less extend (Figure 21B). Maybe human Maf1 exhibits *in vivo* different properties compared to yeast, namely a reduced abilty to bind (U6 promoter) DNA. Different species-specific properties of Maf1 were described before, i.e. the ability of human Maf1 to repress TBP gene transcription (Johnson et al., 2007). Additionally, it was suggested, that human Maf1 does not affect transcription from U6 promoters ((Reina et al., 2006) and unpublished data), thereby indicating a human specific mechanism on U6 promoters. Or yeast Maf1 specific properties, like the longer flexible linker, leads just in *in vitro* EMSA assays to different results, thereby indicating non-specific and non-meaningful interactions with DNA.

To elucidate these open questions more DNA-binding assays, including different promoter types have to be performed.

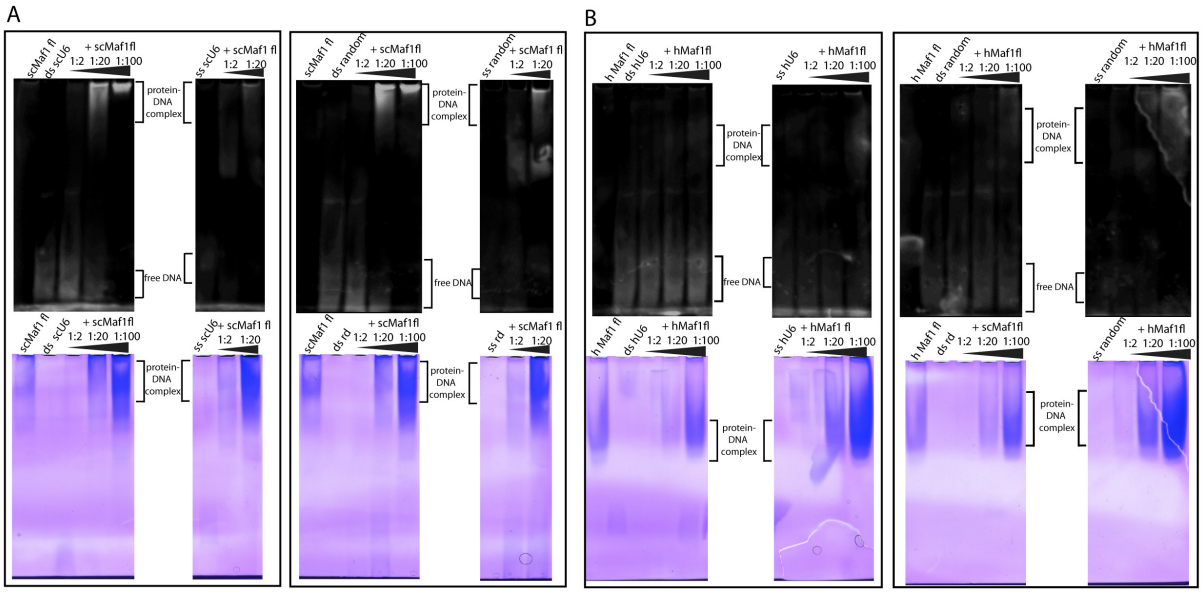

Figure 21. Maf1 binding to nucleic acids.
(A) Purified sc Maf1 fl protein was used for EMSA assays with ds and ss scU6 promoter DNA. Band shifts were inspected on 7.5% native polyacrylamidgels, stained first with SybrSafe (Invitrogen) (top row) and sequentially with Coomassie (bottom row). Gels On top on bottom are the same, respectively. 450 pmol sc or human Maf1 were loaded as negative controls (first lanes in boxes) and for each binding reaction and negative control 22.5 pmol DNA were used. **(B)** Same as (A), just human Maf1 fl instead of scMaf1 fl and human U6 promoter DNA instead of scU6 promoter DNA.

1.5 Crystallization of sc Maf1 1-345Δ52-224

After solving the structure of a human variant of Maf1 (1-205Δ36-82) we focused in a side project on crystallization of yeast variants. Thereby new structural and evolutional insights could be gained, namely by including missing parts of the Maf1 structure (missing α-helix 2 or acidic tail) and solving the structure of another species, which we also had to use for all binding and activity experiments with yeast polymerase.
The minimal soluble yeast variant was identified and lacked the flexible acidic tail (1-345). Since this construct failed in crystallization, we tested various constructs with different lengths of internal deletions spanning the flexible insertion and/ or predicted α-helix 2, as done in human Maf1. Yeast variant 1-345Δ52-224 gave initial crystals, which could be reproduced and improved by additives up to 250 µm and nice shape (Figure 22). Crystals were measured at the synchrotron, but diffracted just up to 4 Å and revealed high mosaicity. No structure determination could be obtained with collected data sets. Since reproducibility of growing nice crystals was not always given, future attemps should focus on crystallization protocols and improvement of freezing procedure.

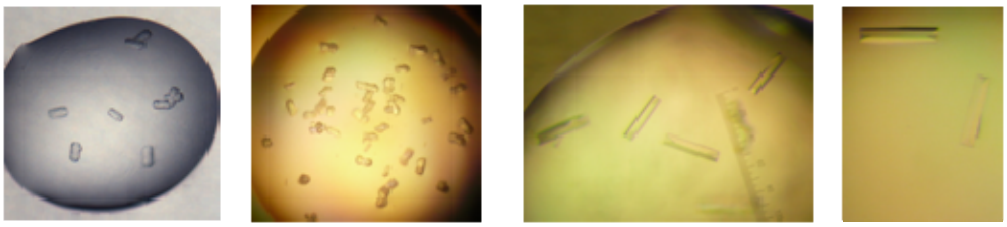

Fig 22. Reproduction and optimization of *s. cer.* Maf1 1-345Δ52-224 crystals.
Left picture shows initial hits in crystallization facility in conditions 50mM MES pH6, 4% MPD, 80 mM NH42SO4, 10 % PEG 8000 with 30 mg/mL protein concentration Right pictures show reproduced crystals (conditions see above, c(protein)= 11 mg/mL, which grow up to ~200µm crystals in 50 mM MES 6.0, 80 mM $(NH_4)_2SO_4$, 10%PEG8000, 12% MPD (third picture) and up to ~250µm crystals in conditions additionally adding 10 mM NaCl (right picture).

1.6 Transcription assays

The activity of Maf1 to repress RNAP III transcription was successfully investigated with an *in vitro* RNA extension assay using a minmal scaffold (2.3.1.8) and with an initiation factor-independent *in vitro* transcription assay using a tailed template and GpG RNA primer (2.3.1.7) (for results see Figure 9).
Anyway, in the course of this study also *in vitro* RNA extension assays with complete complementary scaffolds (bead based) (2.3.1.8) and initiation factor-dependent *in vitro* transcription assays (2.3.1.6) were tried to establish. With the latter assay effects of transcription factors together with Maf1 can get analyzed in a more *in vivo*-like situation using $Brf1_N$-TBP_C-$Brf1_C$ and a template with a minimal bubble (-9 until -5) (Kassavetis et al., 2001). Unfortunatly, both assays did not work. Probably more effort has to be made to optimize the protocols for the RNAP III transcripton system.

2 Cryo EM of minimal RNAP III PIC

The minimal RNAP III PIC consists of promoter DNA bound to TFIIIB and recruited RNAP III (Joazeiro et al., 1994; Kassavetis et al., 1990). This complex composition is in highly purified systems sufficient to transcribe DNA of type III genes, which exhibit a strong TATA box, for example U6 RNA genes (SNR6) (Gerlach et al., 1995). It was shown that the triple fusion protein $Brf1_N$-TBP_C-$Brf1_C$ retains TBP and Brf1 function *in vitro* and is dedicated to RNAP III transcription (Kassavetis et al., 2005). The scaffold design based on recent findings, that an enlarged bubble (-16 until +2) compared to a normal bubble (-9 until +2) in the RNAP II leads to a more homogeneous sample assembly and bubble position ((Andrecka et al., 2009) and unpublished results). Additionally, TFIIIB footprinting results were used to design the U6 scaffold (Joazeiro et al., 1994). A 7mer RNA was used since the structure of RNAP II-TFIIB and a RNAP II PIC model (Kostrewa et al., 2009) revealed that a 8mer RNA still fits before transition from initiation to elongation and release of TFIIB takes place.
A minimal RNAP III PIC was assembled (2.3.3.4). The peak fractions after size exclusion showed an A260/A280 ratio close to 1, a clear indication for binding of nucleic acids (Figure 23B). Coomassie and silver stained gels followed by MS-analysis confirmed the presence of all RNAP III subunits, the triple fusion protein $Brf1_N$-TBP_C-$Brf1_C$, as well as the used scaffold (Figure 23C). The micrographs of the 100 µg/ml concentrated sample allowed careful particle picking and subsequent cryo EM reconstructions (Figure 23D and E). A reconstruction at 23 Å resolution from 10783 particles was performed by Dr. Anselm Kusser.

The resulting cryo EM structure of RNAP III generally agrees with the published RNAP III-DNA-RNA complex (RNAP III EC) map (Vannini et al., 2010). Namely, the reconstruction revealed density for nucleic acids in the cleft and, compared to RNAP II, additional densities for C82/34/31 and C53/37 (Figure 23E), which were fitted according to unpublished crosslinking data (Stefan Jennebach). The well defined density for C53/37 at the lobe, which is larger as the corresponding part in the published RNAP-EC, demonstrates the quality of this reconstruction. Interestingly, density assigned to C82 is slightly shifted from the clamp to the Rpb5 jaw (middle and right panel of Figure 23E). Two C34 winged helix domains (PDB 2dk5 and 2dk8) were positioned on top of the clamp.
Since the triple fusion protein $Brf1_N$-TBP_C-$Brf1_C$ adds another 90 kDa to the PIC, additional density should be observed. Additional density compared to RNAP III-EC can be seen at the protrusion. Different folded parts can be observed close to the dock and wall domain. The RNAP III-Brf1-TBP

closed promoter complex model suggests that Brf1 can be expected here. However the additional density does not account for 90 kDa, which can be explained most probably with the flexibility of Brf1 (Juo et al., 2003; Kassavetis et al., 1997) and substoichiometric issues imposed to the complex upon freezing on the grid.

Interestingly, another area with additional density compared to RNAP III can be clearly seen at the funnel. This was described before for the RNAP III EC, but appears even more prominently in this reconstruction of the RNAP III PIC. Due to the lack of data this density cannot be explained for the time being.

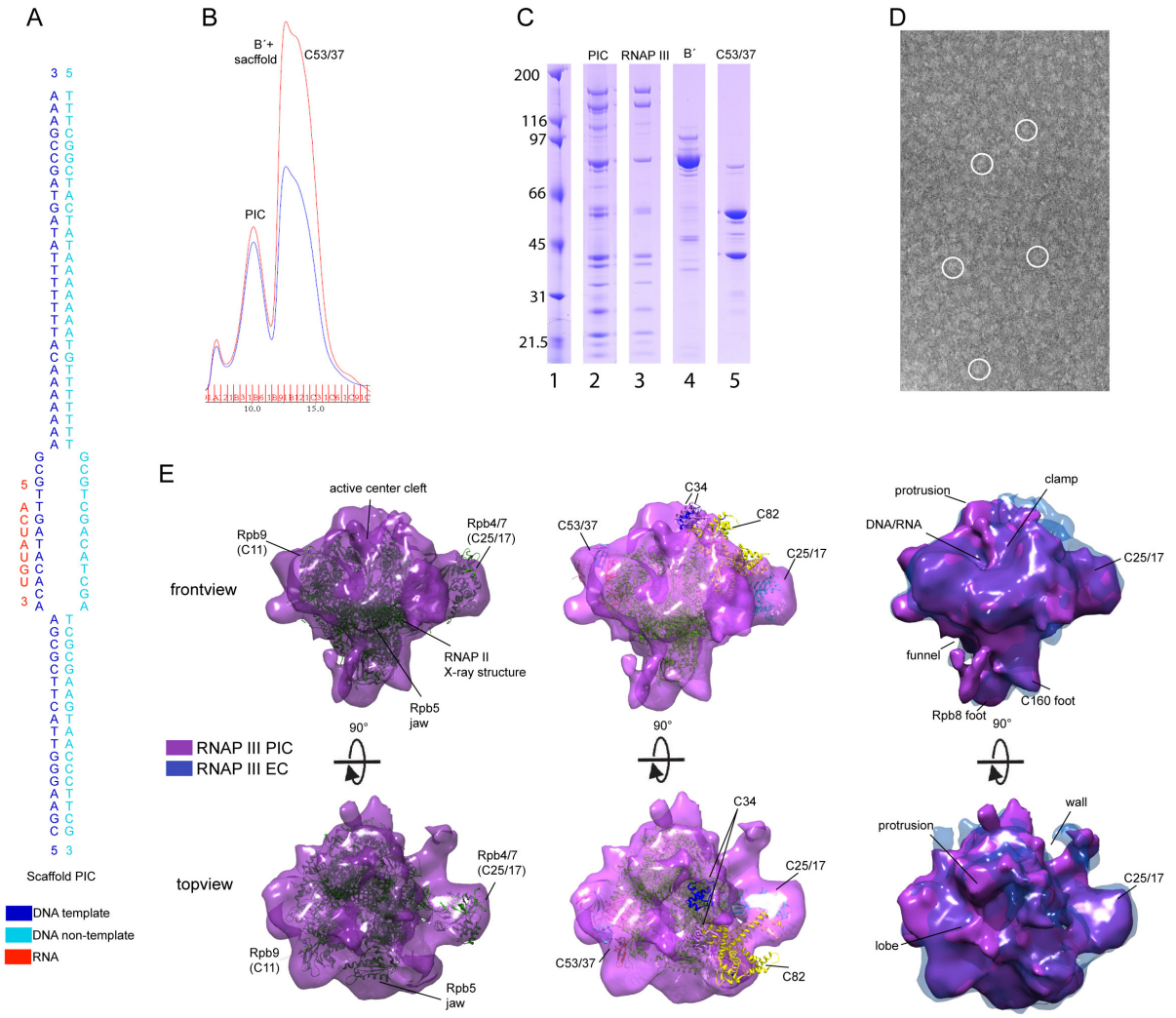

Figure 23. Cryo-EM reconstruction of RNAP III PIC complex.
(A) 60 bp scaffold used for PIC assembly. **(B)** Size-exclusion chromatogram of PIC assembly, constituting of 50 µmol RNAP III supplemented with C53/37, 500 µmol Brf_c/TBP_c/Brf_n and scaffold. For exact procedure see 2.3.3.4. **(C)** SDS-PAGE gel of purified yeast RNAP III. Lane 2 shows the assembled PIC after size-exclusion. The identity of the bands was confirmed by mass spectrometry (not shown). The 17 subunits are present in lane 3. Lane 4 shows recombinantly purified Brf_c/TBP_c/Brf_n . Recombinantly purified C53/37 subunits are shown in lane 5 and were supplemented to endogenous purified RNAP III. **(D)** EM micrograph of RNAP III in vitrified ice. White circles indicate particles. **(E)** Cryo-EM reconstruction of RNAP III (purple) and RNAP III-DNA-RNA (EC) complex (blue). The 12 subunit RNAP II crystal structure (ref…) or the 10-subunit RNAP III core homology model and the C25/17 crystal structure (Jasiak et al., 2006) were fitted to the map and are shown as ribbon models in the left and middle panel, respectively. The locations of C82 and C34 were assigned by combining unpublished crosslinking results with the published envelope of the RNAP III EC complex (Vannini et al) to localize these subunits more accurately (Stefan Jennebach, unpublished results).

Supplemental and unpublished results to part III

3 Characterization of human mitoRNAP mutants in run-off assays

In order to analyze the functional activity of the crystallized human mitoRNAP mutant (AA 105-1230) and of mutants, which miss the N-terminal extension (1-200) and additionally the PPR domoin (1-368), run-off transcription assays were performed in the laboratory of D. Temiakov. Results and discussion are described in chapter 3 part III of this work and part of the submitted manuscript.

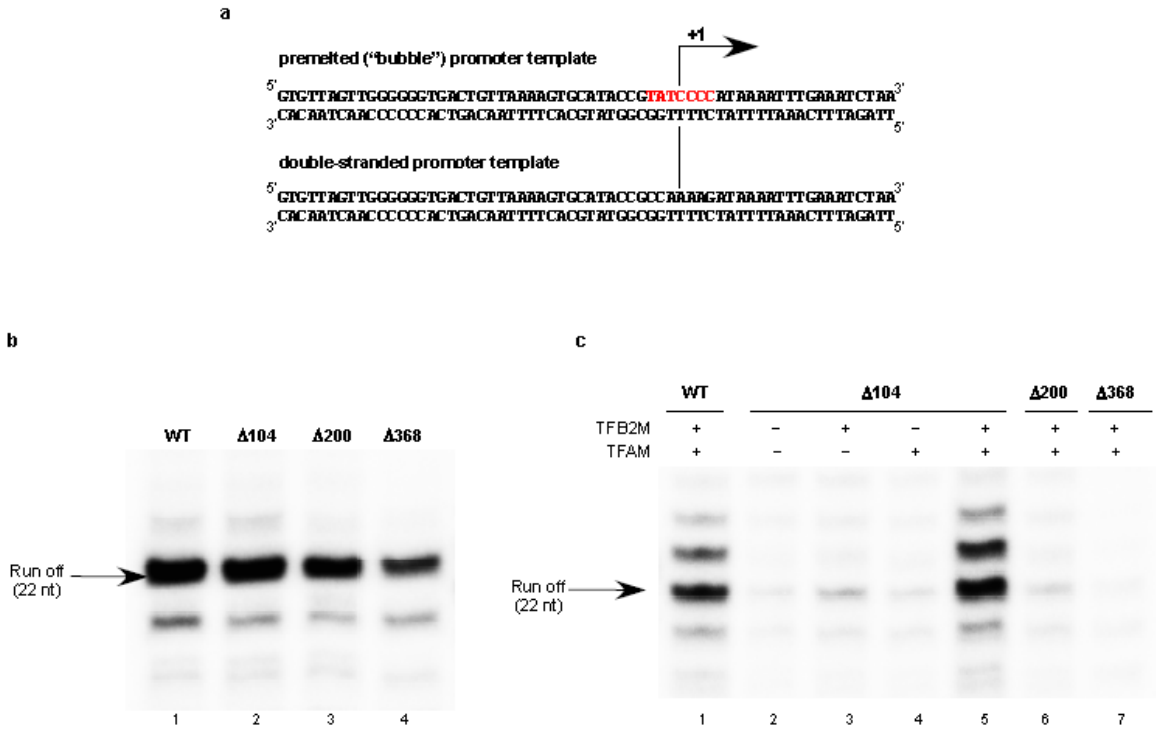

Figure 24. Activity of the N-terminal deletion mutants of human mitoRNAP.
(a) Templates used in the transcription assays. The light strand promoter (LSP) templates were prepared as described (Sologub et al., 2009) using synthetic oligonucleotides. The pre-melted ("bubble") template contains a 7 bps mismatched region in the non-template strand (highlighted in red). **(b)** Activity of deletion mutants on a pre-melted "bubble" promoter template. Transcriptions reactions were carried out as described (Sologub et al., 2009) using wild-type (WT), D104 (residues 105-1230), D200 (201-1230) and D368 (369-1230) mitoRNAPs for 30 min at 35°C in the absence of transcription factors TFAM and TFB2M. **(c)** Activity of deletion mutants on a double-stranded promoter template. Transcriptions reactions were carried out with WT (lane 1) and mutant mitoRNAPs (lane 2-7) in the presence or absence of TFAM and TFB2M as described (Sologub et al., 2009).

To characterize the function of the AT-rich recognition loop into more detail, run off transcription assays were preformed using a human mitoRNAP with mutations R458A/R464A (compare Figure 5d).

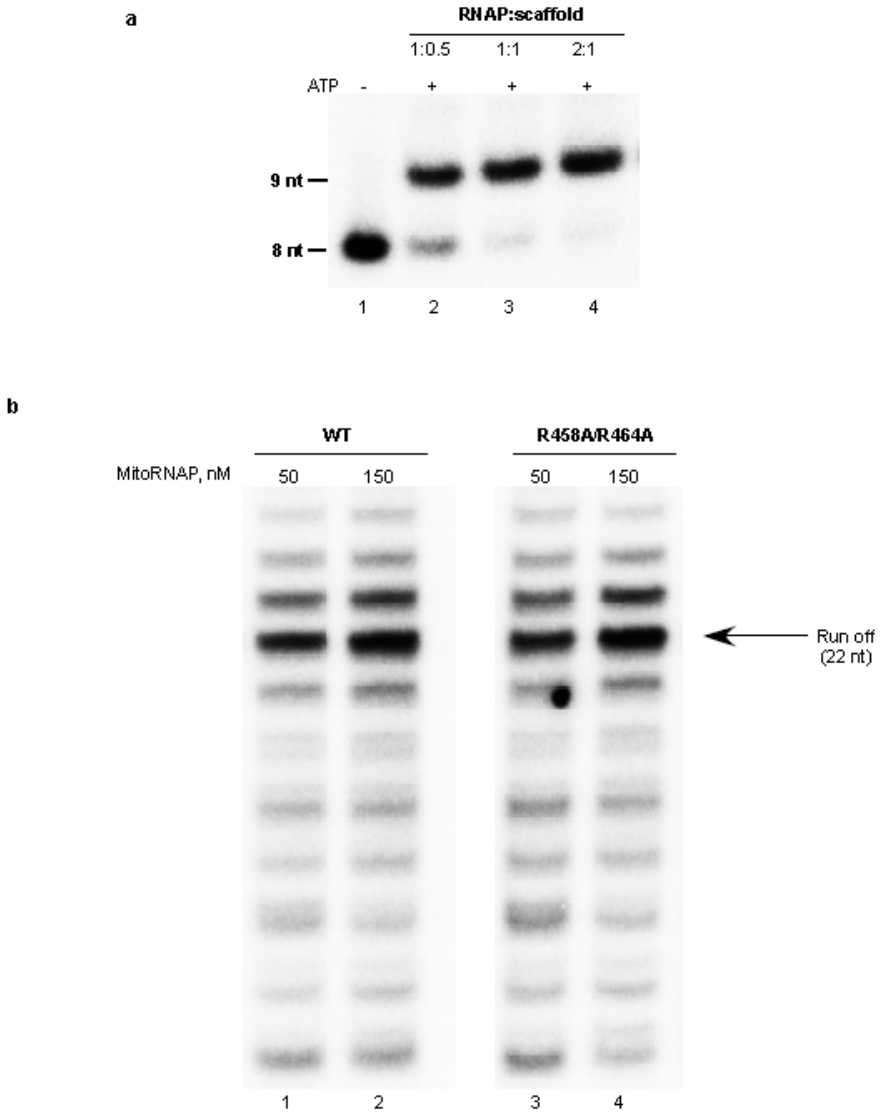

Figure 25. Substitution of residues R458 and R464 in the AT-rich recognition loop of human mitoRNAP does not change its transcription activity.
(a) R458A/R464A mutant mitoRNAP is fully catalytically active. Elongation complex formed using the mutant mitoRNAP and R8/TS1/NT1 scaffold containing P^{32}-labeled RNA (0.25 mM,(Temiakov et al., 2002)) was extended in the presence of 10 mM ATP for 2 min at 35°C. **(b)** Activity of the WT and R458A/R464A mitoRNAP on LSP promoter template. Transcription assays were performed as described in Figure 23 in the presence of TFAM (50 nM) and TFB2M (150nM) for 30 min at 35°C.

4 Alignment of full-lenght human. mitoRNAP sequence and structure with T7 RNAP (PDB 1QLN)

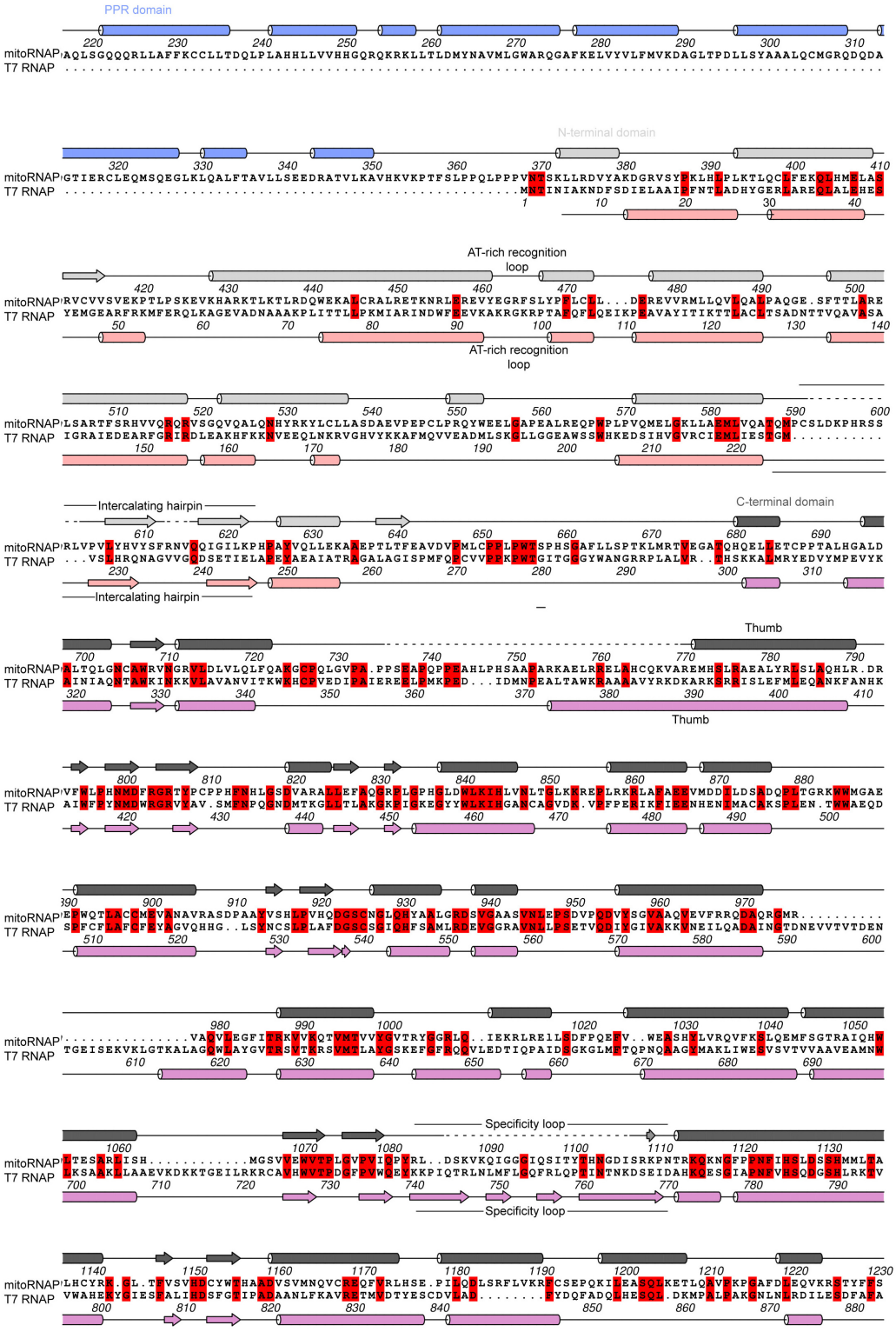

Figure 23. Alignment of human mitoRNAP with T7 RNAP.

Sequence alignment and structural conservation of human mitoRNAP and T7 RNAP (using PBD 1QLN for secondary structure allocation). Shown are mitoRNAP res. 218-1230 and full length T7 RNAP. Secondary structure elements are indicated above and under the sequences for mitoRNAP and T7 RNAP, respectively (cylinders for α-helices, arrows for β-strands, lines for loops) with colours in mitoRNAP blue for PPR domain, silver for N-terminal domain, and gray for C-terminal core and in T7 RNAP salmon for N-terminal domain, and lightpink for C-terminal core.

Reference List

Adams,K.L. and Palmer,J.D. (2003). Evolution of mitochondrial gene content: gene loss and transfer to the nucleus. Mol. Phylogenet. Evol. *29*, 380-395.

Adams,P.D., Afonine,P.V., Bunkoczi,G., Chen,V.B., Davis,I.W., Echols,N., Headd,J.J., Hung,L.W., Kapral,G.J., Grosse-Kunstleve,R.W., McCoy,A.J., Moriarty,N.W., Oeffner,R., Read,R.J., Richardson,D.C., Richardson,J.S., Terwilliger,T.C., and Zwart,P.H. (2010). PHENIX: a comprehensive Python-based system for macromolecular structure solution. Acta Crystallogr. D. Biol. Crystallogr. *66*, 213-221.

Anderson,S., Bankier,A.T., Barrell,B.G., de Bruijn,M.H., Coulson,A.R., Drouin,J., Eperon,I.C., Nierlich,D.P., Roe,B.A., Sanger,F., Schreier,P.H., Smith,A.J., Staden,R., and Young,I.G. (1981). Sequence and organization of the human mitochondrial genome. Nature *290*, 457-465.

Andersson,S.G., Karlberg,O., Canback,B., and Kurland,C.G. (2003). On the origin of mitochondria: a genomics perspective. Philos. Trans. R. Soc. Lond B Biol. Sci. *358*, 165-177.

Andrau,J.C., Sentenac,A., and Werner,M. (1999). Mutagenesis of yeast TFIIIB70 reveals C-terminal residues critical for interaction with TBP and C34. J. Mol. Biol. *288*, 511-520.

Andrecka,J., Treutlein,B., Arcusa,M.A., Muschielok,A., Lewis,R., Cheung,A.C., Cramer,P., and Michaelis,J. (2009). Nano positioning system reveals the course of upstream and nontemplate DNA within the RNA polymerase II elongation complex. Nucleic Acids Res. *37*, 5803-5809.

Antoshechkin,I. and Bogenhagen,D.F. (1995). Distinct roles for two purified factors in transcription of Xenopus mitochondrial DNA. Mol. Cell Biol. *15*, 7032-7042.

Antoshechkin,I., Bogenhagen,D.F., and Mastrangelo,I.A. (1997). The HMG-box mitochondrial transcription factor xl-mtTFA binds DNA as a tetramer to activate bidirectional transcription. EMBO J. *16*, 3198-3206.

Aphasizheva,I., Maslov,D., Wang,X., Huang,L., and Aphasizhev,R. (2011). Pentatricopeptide repeat proteins stimulate mRNA adenylation/uridylation to activate mitochondrial translation in trypanosomes. Mol. Cell *42*, 106-117.

Armache,K.J., Mitterweger,S., Meinhart,A., and Cramer,P. (2005). Structures of complete RNA polymerase II and its subcomplex, Rpb4/7. J. Biol. Chem. *280*, 7131-7134.

Bardeleben,C., Kassavetis,G.A., and Geiduschek,E.P. (1994). Encounters of Saccharomyces cerevisiae RNA polymerase III with its transcription factors during RNA chain elongation. J. Mol. Biol. *235*, 1193-1205.

Bartholomew,B., Durkovich,D., Kassavetis,G.A., and Geiduschek,E.P. (1993). Orientation and topography of RNA polymerase III in transcription complexes. Mol. Cell Biol. *13*, 942-952.

Baudin,A., Ozier-Kalogeropoulos,O., Denouel,A., Lacroute,F., and Cullin,C. (1993). A simple and efficient method for direct gene deletion in Saccharomyces cerevisiae. Nucleic Acids Res. *21*, 3329-3330.

Bernardi,G., Faures,M., Piperno,G., and Slonimski,P.P. (1970). Mitochondrial DNA's from respiratory-sufficient and cytoplasmic respiratory-deficient mutant yeast. J. Mol. Biol. *48*, 23-42.

Biegert,A., Mayer,C., Remmert,M., Soding,J., and Lupas,A.N. (2006). The MPI Bioinformatics Toolkit for protein sequence analysis. Nucleic Acids Res. *34*, W335-W339.

Birse,C.E., Lee,B.A., Hansen,K., and Proudfoot,N.J. (1997). Transcriptional termination signals for RNA polymerase II in fission yeast. EMBO J. *16*, 3633-3643.

Boguta,M., Czerska,K., and Zoladek,T. (1997). Mutation in a new gene MAF1 affects tRNA suppressor efficiency in Saccharomyces cerevisiae. Gene *185*, 291-296.

Bonawitz,N.D., Clayton,D.A., and Shadel,G.S. (2006). Initiation and beyond: multiple functions of the human mitochondrial transcription machinery. Mol. Cell *24*, 813-825.

Bond,C.S. and Schuttelkopf,A.W. (2009). ALINE: a WYSIWYG protein-sequence alignment editor for publication-quality alignments. Acta Crystallogr. D. Biol. Crystallogr. *65*, 510-512.

Boore,J.L. (1999). Animal mitochondrial genomes. Nucleic Acids Res. *27*, 1767-1780.

Brieba,L.G. and Sousa,R. (2001). T7 promoter release mediated by DNA scrunching. EMBO J. *20*, 6826-6835.

Brueckner,F., Hennecke,U., Carell,T., and Cramer,P. (2007). CPD damage recognition by transcribing RNA polymerase II. Science *315*, 859-862.

Brun,I., Sentenac,A., and Werner,M. (1997). Dual role of the C34 subunit of RNA polymerase III in transcription initiation. EMBO J. *16*, 5730-5741.

Burger,G., Gray,M.W., and Lang,B.F. (2003). Mitochondrial genomes: anything goes. Trends Genet. *19*, 709-716.

Burnol,A.F., Margottin,F., Huet,J., Almouzni,G., Prioleau,M.N., Mechali,M., and Sentenac,A. (1993). TFIIIC relieves repression of U6 snRNA transcription by chromatin. Nature *362*, 475-477.

Cabart,P., Lee,J., and Willis,I.M. (2008). Facilitated recycling protects human RNA polymerase III from repression by Maf1 in vitro. J. Biol. Chem. *283*, 36108-36117.

Carey,M.F., Peterson,C.L., and Smale,S.T. (2009). In vitro transcription using HeLa cell extracts and primer extension. Cold Spring Harb. Protoc. *2009*, db.

Carter,R. and Drouin,G. (2010). The increase in the number of subunits in eukaryotic RNA polymerase III relative to RNA polymerase II is due to the permanent recruitment of general transcription factors. Mol. Biol. Evol. *27*, 1035-1043.

Cermakian,N., Ikeda,T.M., Cedergren,R., and Gray,M.W. (1996). Sequences homologous to yeast mitochondrial and bacteriophage T3 and T7 RNA polymerases are widespread throughout the eukaryotic lineage. Nucleic Acids Res. *24*, 648-654.

Cermakian,N., Ikeda,T.M., Miramontes,P., Lang,B.F., Gray,M.W., and Cedergren,R. (1997). On the evolution of the single-subunit RNA polymerases. J. Mol. Evol. *45*, 671-681.

Chamberlin,M., Kingston,R., Gilman,M., Wiggs,J., and deVera,A. (1983). Isolation of bacterial and bacteriophage RNA polymerases and their use in synthesis of RNA in vitro. Methods Enzymol. *101*, 540-568.

Chang,D.D. and Clayton,D.A. (1985). Priming of human mitochondrial DNA replication occurs at the light-strand promoter. Proc. Natl. Acad. Sci. U. S. A *82*, 351-355.

Chedin,S., Ferri,M.L., Peyroche,G., Andrau,J.C., Jourdain,S., Lefebvre,O., Werner,M., Carles,C., and Sentenac,A. (1998a). The yeast RNA polymerase III transcription machinery: a paradigm for eukaryotic gene activation. Cold Spring Harb. Symp. Quant. Biol. *63*, 381-389.

Chedin,S., Riva,M., Schultz,P., Sentenac,A., and Carles,C. (1998b). The RNA cleavage activity of RNA polymerase III is mediated by an essential TFIIS-like subunit and is important for transcription termination. Genes Dev. *12*, 3857-3871.

Cheetham,G.M., Jeruzalmi,D., and Steitz,T.A. (1999). Structural basis for initiation of transcription from an RNA polymerase-promoter complex. Nature *399*, 80-83.

Cheetham,G.M. and Steitz,T.A. (1999). Structure of a transcribing T7 RNA polymerase initiation complex. Science *286*, 2305-2309.

Chen,H.T., Warfield,L., and Hahn,S. (2007). The positions of TFIIF and TFIIE in the RNA polymerase II transcription preinitiation complex. Nat. Struct. Mol. Biol. *14*, 696-703.

Chen,Z.A., Jawhari,A., Fischer,L., Buchen,C., Tahir,S., Kamenski,T., Rasmussen,M., Lariviere,L., Bukowski-Wills,J.C., Nilges,M., Cramer,P., and Rappsilber,J. (2010). Architecture of the RNA polymerase II-TFIIF complex revealed by cross-linking and mass spectrometry. EMBO J. *29*, 717-726.

Chiaradonna,F., Balestrieri,C., Gaglio,D., and Vanoni,M. (2008). RAS and PKA pathways in cancer: new insight from transcriptional analysis. Front Biosci. *13*, 5257-5278.

Ciesla,M. and Boguta,M. (2008). Regulation of RNA polymerase III transcription by Maf1 protein. Acta Biochim. Pol. *55*, 215-225.

Ciesla,M., Towpik,J., Graczyk,D., Oficjalska-Pham,D., Harismendy,O., Suleau,A., Balicki,K., Conesa,C., Lefebvre,O., and Boguta,M. (2007). Maf1 is involved in coupling carbon metabolism to RNA polymerase III transcription. Mol. Cell Biol. *27*, 7693-7702.

Cliften,P.F., Jang,S.H., and Jaehning,J.A. (2000). Identifying a core RNA polymerase surface critical for interactions with a sigma-like specificity factor. Mol. Cell Biol. *20*, 7013-7023.

Coffin,J.W., Dhillon,R., Ritzel,R.G., and Nargang,F.E. (1997). The Neurospora crassa cya-5 nuclear gene encodes a protein with a region of homology to the Saccharomyces cerevisiae PET309 protein and is required in a post-transcriptional step for the expression of the mitochondrially encoded COXI protein. Curr. Genet. *32*, 273-280.

Cotney,J., Wang,Z., and Shadel,G.S. (2007). Relative abundance of the human mitochondrial transcription system and distinct roles for h-mtTFB1 and h-mtTFB2 in mitochondrial biogenesis and gene expression. Nucleic Acids Res. *35*, 4042-4054.

Cramer,P. (2002). Multisubunit RNA polymerases. Curr. Opin. Struct. Biol. *12*, 89-97.

Cramer,P. (2007). Finding the right spot to start transcription. Nat. Struct. Mol. Biol. *14*, 686-687.

Cramer,P., Armache,K.J., Baumli,S., Benkert,S., Brueckner,F., Buchen,C., Damsma,G.E., Dengl,S., Geiger,S.R., Jasiak,A.J., Jawhari,A., Jennebach,S., Kamenski,T., Kettenberger,H., Kuhn,C.D., Lehmann,E., Leike,K., Sydow,J.F., and Vannini,A. (2008). Structure of eukaryotic RNA polymerases. Annu. Rev. Biophys. *37*, 337-352.

Cramer,P., Bushnell,D.A., and Kornberg,R.D. (2001). Structural basis of transcription: RNA polymerase II at 2.8 angstrom resolution. Science *292*, 1863-1876.

Dairaghi,D.J., Shadel,G.S., and Clayton,D.A. (1995a). Addition of a 29 residue carboxyl-terminal tail converts a simple HMG box-containing protein into a transcriptional activator. J. Mol. Biol. *249*, 11-28.

Dairaghi,D.J., Shadel,G.S., and Clayton,D.A. (1995b). Human mitochondrial transcription factor A and promoter spacing integrity are required for transcription initiation. Biochim. Biophys. Acta *1271*, 127-134.

Dalmay,T., Hamilton,A., Rudd,S., Angell,S., and Baulcombe,D.C. (2000). An RNA-dependent RNA polymerase gene in Arabidopsis is required for posttranscriptional gene silencing mediated by a transgene but not by a virus. Cell *101*, 543-553.

Damsma,G.E. and Cramer,P. (2009). Molecular basis of transcriptional mutagenesis at 8-oxoguanine. J. Biol. Chem. *284*, 31658-31663.

Davis,A.F. and Clayton,D.A. (1996). In situ localization of mitochondrial DNA replication in intact mammalian cells. J. Cell Biol. *135*, 883-893.

Davis,I.W., Murray,L.W., Richardson,J.S., and Richardson,D.C. (2004). MOLPROBITY: structure validation and all-atom contact analysis for nucleic acids and their complexes. Nucleic Acids Res. *32*, W615-W619.

Davis,M.W. and Hammarlund,M. (2006). Single-nucleotide polymorphism mapping. Methods Mol. Biol. *351*, 75-92.

Davydova,E.K., Santangelo,T.J., and Rothman-Denes,L.B. (2007). Bacteriophage N4 virion RNA polymerase interaction with its promoter DNA hairpin. Proc. Natl. Acad. Sci. U. S. A *104*, 7033-7038.

Delarue,M., Poch,O., Tordo,N., Moras,D., and Argos,P. (1990). An attempt to unify the structure of polymerases. Protein Eng *3*, 461-467.

Dengl,S., Mayer,A., Sun,M., and Cramer,P. (2009). Structure and in vivo requirement of the yeast Spt6 SH2 domain. J. Mol. Biol. *389*, 211-225.

Dephoure,N., Zhou,C., Villen,J., Beausoleil,S.A., Bakalarski,C.E., Elledge,S.J., and Gygi,S.P. (2008). A quantitative atlas of mitotic phosphorylation. Proc. Natl. Acad. Sci. U. S. A *105*, 10762-10767.

Desai,N., Lee,J., Upadhya,R., Chu,Y., Moir,R.D., and Willis,I.M. (2005). Two steps in Maf1-dependent repression of transcription by RNA polymerase III. J. Biol. Chem. *280*, 6455-6462.

Dieci,G., Fiorino,G., Castelnuovo,M., Teichmann,M., and Pagano,A. (2007). The expanding RNA polymerase III transcriptome. Trends Genet. *23*, 614-622.

Durieux,J., Wolff,S., and Dillin,A. (2011). The cell-non-autonomous nature of electron transport chain-mediated longevity. Cell *144*, 79-91.

Durniak,K.J., Bailey,S., and Steitz,T.A. (2008). The structure of a transcribing T7 RNA polymerase in transition from initiation to elongation. Science *322*, 553-557.

Dye,M.J. and Proudfoot,N.J. (2001). Multiple transcript cleavage precedes polymerase release in termination by RNA polymerase II. Cell *105*, 669-681.

Eichner,J., Chen,H.T., Warfield,L., and Hahn,S. (2010). Position of the general transcription factor TFIIF within the RNA polymerase II transcription preinitiation complex. EMBO J. *29*, 706-716.

Emsley,P. and Cowtan,K. (2004). Coot: model-building tools for molecular graphics. Acta Crystallogr. D. Biol. Crystallogr. *60*, 2126-2132.

Evans,P. (2006). Scaling and assessment of data quality. Acta Crystallogr. D. Biol. Crystallogr. *62*, 72-82.

Evers,R. and Grummt,I. (1995). Molecular coevolution of mammalian ribosomal gene terminator sequences and the transcription termination factor TTF-I. Proc. Natl. Acad. Sci. U. S. A *92*, 5827-5831.

Falkenberg,M., Gaspari,M., Rantanen,A., Trifunovic,A., Larsson,N.G., and Gustafsson,C.M. (2002). Mitochondrial transcription factors B1 and B2 activate transcription of human mtDNA. Nat. Genet. *31*, 289-294.

Falkenberg,M., Larsson,N.G., and Gustafsson,C.M. (2007). DNA replication and transcription in mammalian mitochondria. Annu. Rev. Biochem. *76*, 679-699.

Fernandez-Silva,P., Polosa,P.L., Roberti,M., Di,P.B., Gadaleta,M.N., Montoya,J., and Cantatore,P. (2001). Sea urchin mtDBP is a two-faced transcription termination factor with a biased polarity depending on the RNA polymerase. Nucleic Acids Res. *29*, 4736-4743.

Fernandez-Tornero,C., Bottcher,B., Rashid,U.J., Steuerwald,U., Florchinger,B., Devos,D.P., Lindner,D., and Muller,C.W. (2010). Conformational flexibility of RNA polymerase III during transcriptional elongation. EMBO J. *29*, 3762-3772.

Fernandez-Tornero,C., Bottcher,B., Riva,M., Carles,C., Steuerwald,U., Ruigrok,R.W., Sentenac,A., Muller,C.W., and Schoehn,G. (2007). Insights into transcription initiation and termination from the electron microscopy structure of yeast RNA polymerase III. Mol. Cell *25*, 813-823.

Ferri,M.L., Peyroche,G., Siaut,M., Lefebvre,O., Carles,C., Conesa,C., and Sentenac,A. (2000). A novel subunit of yeast RNA polymerase III interacts with the TFIIB-related domain of TFIIIB70. Mol. Cell Biol. *20*, 488-495.

Fisk,D.G., Walker,M.B., and Barkan,A. (1999). Molecular cloning of the maize gene crp1 reveals similarity between regulators of mitochondrial and chloroplast gene expression. EMBO J. *18*, 2621-2630.

Fraser,I.D. and Germain,R.N. (2009). Navigating the network: signaling cross-talk in hematopoietic cells. Nat. Immunol. *10*, 327-331.

Fuste,J.M., Wanrooij,S., Jemt,E., Granycome,C.E., Cluett,T.J., Shi,Y., Atanassova,N., Holt,I.J., Gustafsson,C.M., and Falkenberg,M. (2010). Mitochondrial RNA polymerase is needed for activation of the origin of light-strand DNA replication. Mol. Cell *37*, 67-78.

Gangelhoff,T.A., Mungalachetty,P.S., Nix,J.C., and Churchill,M.E. (2009). Structural analysis and DNA binding of the HMG domains of the human mitochondrial transcription factor A. Nucleic Acids Res. *37*, 3153-3164.

Gaspari,M., Falkenberg,M., Larsson,N.G., and Gustafsson,C.M. (2004a). The mitochondrial RNA polymerase contributes critically to promoter specificity in mammalian cells. EMBO J. *23*, 4606-4614.

Gaspari,M., Larsson,N.G., and Gustafsson,C.M. (2004b). The transcription machinery in mammalian mitochondria. Biochim. Biophys. Acta *1659*, 148-152.

Gavin,A.C., Aloy,P., Grandi,P., Krause,R., Boesche,M., Marzioch,M., Rau,C., Jensen,L.J., Bastuck,S., Dumpelfeld,B., Edelmann,A., Heurtier,M.A., Hoffman,V., Hoefert,C., Klein,K., Hudak,M., Michon,A.M., Schelder,M., Schirle,M., Remor,M., Rudi,T., Hooper,S., Bauer,A., Bouwmeester,T., Casari,G., Drewes,G., Neubauer,G., Rick,J.M., Kuster,B., Bork,P., Russell,R.B., and Superti-Furga,G. (2006). Proteome survey reveals modularity of the yeast cell machinery. Nature *440*, 631-636.

Geiduschek,E.P. and Kassavetis,G.A. (2001). The RNA polymerase III transcription apparatus. J. Mol. Biol. *310*, 1-26.

Geiduschek,E.P. and Kassavetis,G.A. (2006). Transcription: adjusting to adversity by regulating RNA polymerase. Curr. Biol. *16*, R849-R851.

Geiger,S.R., Lorenzen,K., Schreieck,A., Hanecker,P., Kostrewa,D., Heck,A.J., and Cramer,P. (2010). RNA polymerase I contains a TFIIF-related DNA-binding subcomplex. Mol. Cell *39*, 583-594.

Gerlach,V.L., Whitehall,S.K., Geiduschek,E.P., and Brow,D.A. (1995). TFIIIB placement on a yeast U6 RNA gene in vivo is directed primarily by TFIIIC rather than by sequence-specific DNA contacts. Mol. Cell Biol. *15*, 1455-1466.

Gleghorn,M.L., Davydova,E.K., Rothman-Denes,L.B., and Murakami,K.S. (2008). Structural basis for DNA-hairpin promoter recognition by the bacteriophage N4 virion RNA polymerase. Mol. Cell *32*, 707-717.

Goodfellow,S.J., Graham,E.L., Kantidakis,T., Marshall,L., Coppins,B.A., Oficjalska-Pham,D., Gerard,M., Lefebvre,O., and White,R.J. (2008). Regulation of RNA polymerase III transcription by Maf1 in mammalian cells. J. Mol. Biol. *378*, 481-491.

Goodrich,J.A. and Tjian,R. (2010). Unexpected roles for core promoter recognition factors in cell-type-specific transcription and gene regulation. Nat. Rev. Genet. *11*, 549-558.

Gouet,P., Courcelle,E., Stuart,D.I., and Metoz,F. (1999). ESPript: analysis of multiple sequence alignments in PostScript. Bioinformatics. *15*, 305-308.

Gray,M.W., Burger,G., and Lang,B.F. (1999). Mitochondrial evolution. Science *283*, 1476-1481.

Gray,M.W., Lang,B.F., and Burger,G. (2004). Mitochondria of protists. Annu. Rev. Genet. *38*, 477-524.

Grummt,I. (2003). Life on a planet of its own: regulation of RNA polymerase I transcription in the nucleolus. Genes Dev. *17*, 1691-1702.

Hammani,K., Colas,d.F.-S., Takenaka,M., Tanz,S.K., Okuda,K., Shikanai,T., Brennicke,A., and Small,I. (2011). The pentatricopeptide repeat protein OTP87 is essential for RNA editing of nad7 and atp1 transcripts in Arabidopsis mitochondria. J. Biol. Chem.

Herr,A.J., Jensen,M.B., Dalmay,T., and Baulcombe,D.C. (2005). RNA polymerase IV directs silencing of endogenous DNA. Science *308*, 118-120.

Hirata,A., Klein,B.J., and Murakami,K.S. (2008). The X-ray crystal structure of RNA polymerase from Archaea. Nature *451*, 851-854.

Holm,L. and Park,J. (2000). DaliLite workbench for protein structure comparison. Bioinformatics. *16*, 566-567.

Holzle,A., Jonietz,C., Torjek,O., Altmann,T., Binder,S., and Forner,J. (2011). A RESTORER OF FERTILITY-like PPR gene is required for 5'-end processing of the nad4 mRNA in mitochondria of Arabidopsis thaliana. Plant J. *65*, 737-744.

Holzmann,J. and Rossmanith,W. (2009). tRNA recognition, processing, and disease: hypotheses around an unorthodox type of RNase P in human mitochondria. Mitochondrion. *9*, 284-288.

Huang,J., Brieba,L.G., and Sousa,R. (2000). Misincorporation by wild-type and mutant T7 RNA polymerases: identification of interactions that reduce misincorporation rates by stabilizing the catalytically incompetent open conformation. Biochemistry *39*, 11571-11580.

Iyer,L.M., Koonin,E.V., and Aravind,L. (2003). Evolutionary connection between the catalytic subunits of DNA-dependent RNA polymerases and eukaryotic RNA-dependent RNA polymerases and the origin of RNA polymerases. BMC. Struct. Biol. *3*, 1.

Jang,S.H. and Jaehning,J.A. (1991). The yeast mitochondrial RNA polymerase specificity factor, MTF1, is similar to bacterial sigma factors. J. Biol. Chem. *266*, 22671-22677.

Jasiak,A.J., Armache,K.J., Martens,B., Jansen,R.P., and Cramer,P. (2006). Structural biology of RNA polymerase III: subcomplex C17/25 X-ray structure and 11 subunit enzyme model. Mol. Cell *23*, 71-81.

Jeruzalmi,D. and Steitz,T.A. (1998). Structure of T7 RNA polymerase complexed to the transcriptional inhibitor T7 lysozyme. EMBO J. *17*, 4101-4113.

Joazeiro,C.A., Kassavetis,G.A., and Geiduschek,E.P. (1994). Identical components of yeast transcription factor IIIB are required and sufficient for transcription of TATA box-containing and TATA-less genes. Mol. Cell Biol. *14*, 2798-2808.

Johnson,S.S., Zhang,C., Fromm,J., Willis,I.M., and Johnson,D.L. (2007). Mammalian Maf1 is a negative regulator of transcription by all three nuclear RNA polymerases. Mol. Cell *26*, 367-379.

Juo,Z.S., Kassavetis,G.A., Wang,J., Geiduschek,E.P., and Sigler,P.B. (2003). Crystal structure of a transcription factor IIIB core interface ternary complex. Nature *422*, 534-539.

Kassavetis,G.A., Bardeleben,C., Kumar,A., Ramirez,E., and Geiduschek,E.P. (1997). Domains of the Brf component of RNA polymerase III transcription factor IIIB (TFIIIB): functions in assembly of TFIIIB-DNA complexes and recruitment of RNA polymerase to the promoter. Mol. Cell Biol. *17*, 5299-5306.

Kassavetis,G.A., Braun,B.R., Nguyen,L.H., and Geiduschek,E.P. (1990). S. cerevisiae TFIIIB is the transcription initiation factor proper of RNA polymerase III, while TFIIIA and TFIIIC are assembly factors. Cell *60*, 235-245.

Kassavetis,G.A., Han,S., Naji,S., and Geiduschek,E.P. (2003). The role of transcription initiation factor IIIB subunits in promoter opening probed by photochemical cross-linking. J. Biol. Chem. *278*, 17912-17917.

Kassavetis,G.A., Letts,G.A., and Geiduschek,E.P. (2001). The RNA polymerase III transcription initiation factor TFIIIB participates in two steps of promoter opening. EMBO J. *20*, 2823-2834.

Kassavetis,G.A., Prakash,P., and Shim,E. (2010). The C53/C37 subcomplex of RNA polymerase III lies near the active site and participates in promoter opening. J. Biol. Chem. *285*, 2695-2706.

Kassavetis,G.A., Soragni,E., Driscoll,R., and Geiduschek,E.P. (2005). Reconfiguring the connectivity of a multiprotein complex: fusions of yeast TATA-binding protein with Brf1, and the function of transcription factor IIIB. Proc. Natl. Acad. Sci. U. S. A *102*, 15406-15411.

Khoo,B., Brophy,B., and Jackson,S.P. (1994). Conserved functional domains of the RNA polymerase III general transcription factor BRF. Genes Dev. *8*, 2879-2890.

Kim,T.K., Ebright,R.H., and Reinberg,D. (2000). Mechanism of ATP-dependent promoter melting by transcription factor IIH. Science *288*, 1418-1422.

Kostrewa,D., Zeller,M.E., Armache,K.J., Seizl,M., Leike,K., Thomm,M., and Cramer,P. (2009). RNA polymerase II-TFIIB structure and mechanism of transcription initiation. Nature *462*, 323-330.

Kravchenko,J.E., Rogozin,I.B., Koonin,E.V., and Chumakov,P.M. (2005). Transcription of mammalian messenger RNAs by a nuclear RNA polymerase of mitochondrial origin. Nature *436*, 735-739.

Krissinel,E. and Henrick,K. (2004). Secondary-structure matching (SSM), a new tool for fast protein structure alignment in three dimensions. Acta Crystallogr. D. Biol. Crystallogr. *60*, 2256-2268.

Kucej,M., Kucejova,B., Subramanian,R., Chen,X.J., and Butow,R.A. (2008). Mitochondrial nucleoids undergo remodeling in response to metabolic cues. J. Cell Sci. *121*, 1861-1868.

Kuhn,C.D., Geiger,S.R., Baumli,S., Gartmann,M., Gerber,J., Jennebach,S., Mielke,T., Tschochner,H., Beckmann,R., and Cramer,P. (2007). Functional architecture of RNA polymerase I. Cell *131*, 1260-1272.

Kwapisz,M., Beckouet,F., and Thuriaux,P. (2008). Early evolution of eukaryotic DNA-dependent RNA polymerases. Trends Genet. *24*, 211-215.

Lander,E.S., Choi,S., and Chen,Y.J. (2001). Initial sequencing and analysis of the human genome. Nature *409*, 860-921.

Landrieux,E., Alic,N., Ducrot,C., Acker,J., Riva,M., and Carles,C. (2006). A subcomplex of RNA polymerase III subunits involved in transcription termination and reinitiation. EMBO J. *25*, 118-128.

Lannutti,B.J., Persinger,J., and Bartholomew,B. (1996). Probing the protein-DNA contacts of a yeast RNA polymerase III transcription complex in a crude extract: solid phase synthesis of DNA photoaffinity probes containing a novel photoreactive deoxycytidine analog. Biochemistry *35*, 9821-9831.

Larkin,M.A., Blackshields,G., Brown,N.P., Chenna,R., McGettigan,P.A., McWilliam,H., Valentin,F., Wallace,I.M., Wilm,A., Lopez,R., Thompson,J.D., Gibson,T.J., and Higgins,D.G. (2007). Clustal W and Clustal X version 2.0. Bioinformatics. *23*, 2947-2948.

Lee,J., Moir,R.D., and Willis,I.M. (2009). Regulation of RNA polymerase III transcription involves SCH9-dependent and SCH9-independent branches of the target of rapamycin (TOR) pathway. J. Biol. Chem. *284*, 12604-12608.

Lefevre,S., Dumay-Odelot,H., El-Ayoubi,L., Budd,A., Legrand,P., Pinaud,N., Teichmann,M., and Fribourg,S. (2011). Structure-function analysis of hRPC62 provides insights into RNA polymerase III transcription initiation. Nat. Struct. Mol. Biol. *18*, 352-358.

Legros,F., Malka,F., Frachon,P., Lombes,A., and Rojo,M. (2004). Organization and dynamics of human mitochondrial DNA. J. Cell Sci. *117*, 2653-2662.

Leslie,A.G., Liddell,J.M., and Shaw,W.V. (1986). Crystallization of a type III chloramphenicol acetyl transferase. J. Mol. Biol. *188*, 283-285.

Levine,M. and Tjian,R. (2003). Transcription regulation and animal diversity. Nature *424*, 147-151.

Lightowlers,R.N. and Chrzanowska-Lightowlers,Z.M. (2008). PPR (pentatricopeptide repeat) proteins in mammals: important aids to mitochondrial gene expression. Biochem. J. *416*, e5-e6.

Linder,T., Park,C.B., sin-Cayuela,J., Pellegrini,M., Larsson,N.G., Falkenberg,M., Samuelsson,T., and Gustafsson,C.M. (2005). A family of putative transcription termination factors shared amongst metazoans and plants. Curr. Genet. *48*, 265-269.

Litonin,D., Sologub,M., Shi,Y., Savkina,M., Anikin,M., Falkenberg,M., Gustafsson,C.M., and Temiakov,D. (2010). Human mitochondrial transcription revisited: only TFAM and TFB2M are required for transcription of the mitochondrial genes in vitro. J. Biol. Chem. *285*, 18129-18133.

Loguercio,P.P., Roberti,M., Musicco,C., Gadaleta,M.N., Quagliariello,E., and Cantatore,P. (1999). Cloning and characterisation of mtDBP, a DNA-binding protein which binds two distinct regions of sea urchin mitochondrial DNA. Nucleic Acids Res. *27*, 1890-1899.

Lorenzen,K., Vannini,A., Cramer,P., and Heck,A.J. (2007). Structural biology of RNA polymerase III: mass spectrometry elucidates subcomplex architecture. Structure. *15*, 1237-1245.

Lurin,C., Andres,C., Aubourg,S., Bellaoui,M., Bitton,F., Bruyere,C., Caboche,M., Debast,C., Gualberto,J., Hoffmann,B., Lecharny,A., Le,R.M., Martin-Magniette,M.L., Mireau,H., Peeters,N., Renou,J.P., Szurek,B., Taconnat,L., and Small,I. (2004). Genome-wide analysis of Arabidopsis pentatricopeptide repeat proteins reveals their essential role in organelle biogenesis. Plant Cell *16*, 2089-2103.

Manam,S. and Van Tuyle,G.C. (1987). Separation and characterization of 5'- and 3'-tRNA processing nucleases from rat liver mitochondria. J. Biol. Chem. *262*, 10272-10279.

Mangus,D.A., Jang,S.H., and Jaehning,J.A. (1994). Release of the yeast mitochondrial RNA polymerase specificity factor from transcription complexes. J. Biol. Chem. *269*, 26568-26574.

Manthey,G.M., Przybyla-Zawislak,B.D., and McEwen,J.E. (1998). The Saccharomyces cerevisiae Pet309 protein is embedded in the mitochondrial inner membrane. Eur. J. Biochem. *255*, 156-161.

Marshall,L. (2008). Elevated RNA polymerase III transcription drives proliferation and oncogenic transformation. Cell Cycle *7*, 3327-3329.

Martinez-Rucobo,F.W., Sainsbury,S., Cheung,A.C., and Cramer,P. (2011). Architecture of the RNA polymerase-Spt4/5 complex and basis of universal transcription processivity. EMBO J. *30*, 1302-1310.

Mayer,C. and Grummt,I. (2006). Ribosome biogenesis and cell growth: mTOR coordinates transcription by all three classes of nuclear RNA polymerases. Oncogene *25*, 6384-6391.

McCoy,A.J., Grosse-Kunstleve,R.W., Adams,P.D., Winn,M.D., Storoni,L.C., and Read,R.J. (2007). Phaser crystallographic software. J. Appl. Crystallogr. *40*, 658-674.

McCulloch,V. and Shadel,G.S. (2003). Human mitochondrial transcription factor B1 interacts with the C-terminal activation region of h-mtTFA and stimulates transcription independently of its RNA methyltransferase activity. Mol. Cell Biol. *23*, 5816-5824.

Mili,S. and Pinol-Roma,S. (2003). LRP130, a pentatricopeptide motif protein with a noncanonical RNA-binding domain, is bound in vivo to mitochondrial and nuclear RNAs. Mol. Cell Biol. *23*, 4972-4982.

Moir,R.D., Lee,J., Haeusler,R.A., Desai,N., Engelke,D.R., and Willis,I.M. (2006). Protein kinase A regulates RNA polymerase III transcription through the nuclear localization of Maf1. Proc. Natl. Acad. Sci. U. S. A *103*, 15044-15049.

Mootha,V.K., Lepage,P., Miller,K., Bunkenborg,J., Reich,M., Hjerrild,M., Delmonte,T., Villeneuve,A., Sladek,R., Xu,F., Mitchell,G.A., Morin,C., Mann,M., Hudson,T.J., Robinson,B., Rioux,J.D., and Lander,E.S. (2003). Identification of a gene causing human cytochrome c oxidase deficiency by integrative genomics. Proc. Natl. Acad. Sci. U. S. A *100*, 605-610.

Murakami,K.S., Davydova,E.K., and Rothman-Denes,L.B. (2008). X-ray crystal structure of the polymerase domain of the bacteriophage N4 virion RNA polymerase. Proc. Natl. Acad. Sci. U. S. A *105*, 5046-5051.

Murshudov,G.N., Vagin,A.A., and Dodson,E.J. (1997). Refinement of macromolecular structures by the maximum-likelihood method. Acta Crystallogr. D. Biol. Crystallogr. *53*, 240-255.

Narendra,D.P. and Youle,R.J. (2011). Targeting Mitochondrial Dysfunction: Role for PINK1 and Parkin in Mitochondrial Quality Control. Antioxid. Redox. Signal.

Nayak,D., Guo,Q., and Sousa,R. (2009). A promoter recognition mechanism common to yeast mitochondrial and phage t7 RNA polymerases. J. Biol. Chem. *284*, 13641-13647.

Oficjalska-Pham,D., Harismendy,O., Smagowicz,W.J., Gonzalez de,P.A., Boguta,M., Sentenac,A., and Lefebvre,O. (2006). General repression of RNA polymerase III transcription is triggered by protein phosphatase type 2A-mediated dephosphorylation of Maf1. Mol. Cell *22*, 623-632.

Ojala,D., Montoya,J., and Attardi,G. (1981). tRNA punctuation model of RNA processing in human mitochondria. Nature *290*, 470-474.

Ono,T., Isobe,K., Nakada,K., and Hayashi,J.I. (2001). Human cells are protected from mitochondrial dysfunction by complementation of DNA products in fused mitochondria. Nat. Genet. *28*, 272-275.

Painter,J. and Merritt,E.A. (2006). Optimal description of a protein structure in terms of multiple groups undergoing TLS motion. Acta Crystallogr. D. Biol. Crystallogr. *62*, 439-450.

Paratkar,S., Deshpande,A.P., Tang,G.Q., and Patel,S.S. (2011). The N-terminal domain of the yeast mitochondrial RNA polymerase regulates multiple steps of transcription. J. Biol. Chem.

Paule,M.R. and White,R.J. (2000). Survey and summary: transcription by RNA polymerases I and III. Nucleic Acids Res. *28*, 1283-1298.

Pham,X.H., Farge,G., Shi,Y., Gaspari,M., Gustafsson,C.M., and Falkenberg,M. (2006). Conserved sequence box II directs transcription termination and primer formation in mitochondria. J. Biol. Chem. *281*, 24647-24652.

Pluta,K., Lefebvre,O., Martin,N.C., Smagowicz,W.J., Stanford,D.R., Ellis,S.R., Hopper,A.K., Sentenac,A., and Boguta,M. (2001). Maf1p, a negative effector of RNA polymerase III in Saccharomyces cerevisiae. Mol. Cell Biol. *21*, 5031-5040.

Pontier,D., Yahubyan,G., Vega,D., Bulski,A., Saez-Vasquez,J., Hakimi,M.A., Lerbs-Mache,S., Colot,V., and Lagrange,T. (2005). Reinforcement of silencing at transposons and highly repeated sequences requires the concerted action of two distinct RNA polymerases IV in Arabidopsis. Genes Dev. *19*, 2030-2040.

Ranish,J.A. and Hahn,S. (1991). The yeast general transcription factor TFIIA is composed of two polypeptide subunits. J. Biol. Chem. *266*, 19320-19327.

Reina,J.H., Azzouz,T.N., and Hernandez,N. (2006). Maf1, a new player in the regulation of human RNA polymerase III transcription. PLoS. One. *1*, e134.

Roberts,D.N., Wilson,B., Huff,J.T., Stewart,A.J., and Cairns,B.R. (2006). Dephosphorylation and genome-wide association of Maf1 with Pol III-transcribed genes during repression. Mol. Cell *22*, 633-644.

Rodeheffer,M.S., Boone,B.E., Bryan,A.C., and Shadel,G.S. (2001). Nam1p, a protein involved in RNA processing and translation, is coupled to transcription through an interaction with yeast mitochondrial RNA polymerase. J. Biol. Chem. *276*, 8616-8622.

Rohde,J., Heitman,J., and Cardenas,M.E. (2001). The TOR kinases link nutrient sensing to cell growth. J. Biol. Chem. *276*, 9583-9586.

Rollins,J., Veras,I., Cabarcas,S., Willis,I., and Schramm,L. (2007). Human Maf1 negatively regulates RNA polymerase III transcription via the TFIIB family members Brf1 and Brf2. Int. J. Biol. Sci. *3*, 292-302.

Ruvkun,G. and Hobert,O. (1998). The taxonomy of developmental control in Caenorhabditis elegans. Science *282*, 2033-2041.

Sadhale,P.P. and Woychik,N.A. (1994). C25, an essential RNA polymerase III subunit related to the RNA polymerase II subunit RPB7. Mol. Cell Biol. *14*, 6164-6170.

Savkina,M., Temiakov,D., McAllister,W.T., and Anikin,M. (2010). Multiple functions of yeast mitochondrial transcription factor Mtf1p during initiation. J. Biol. Chem. *285*, 3957-3964.

Scheffler,I.E. (2001). Mitochondria make a come back. Adv. Drug Deliv. Rev. *49*, 3-26.

Schinkel,A.H., Groot Koerkamp,M.J., and Tabak,H.F. (1988). Mitochondrial RNA polymerase of Saccharomyces cerevisiae: composition and mechanism of promoter recognition. EMBO J. *7*, 3255-3262.

Schramm,L. and Hernandez,N. (2002). Recruitment of RNA polymerase III to its target promoters. Genes Dev. *16*, 2593-2620.

Schubot,F.D., Chen,C.J., Rose,J.P., Dailey,T.A., Dailey,H.A., and Wang,B.C. (2001). Crystal structure of the transcription factor sc-mtTFB offers insights into mitochondrial transcription. Protein Sci. *10*, 1980-1988.

Shadel,G.S. and Clayton,D.A. (1995). A Saccharomyces cerevisiae mitochondrial transcription factor, sc-mtTFB, shares features with sigma factors but is functionally distinct. Mol. Cell Biol. *15*, 2101-2108.

Shadel,G.S. and Clayton,D.A. (1996). Isolation and characterization of vertebrate mitochondrial transcription factor A homologs. Methods Enzymol. *264*, 149-158.

Shadel,G.S. and Clayton,D.A. (1997). Mitochondrial DNA maintenance in vertebrates. Annu. Rev. Biochem. *66*, 409-435.

Shor,B., Wu,J., Shakey,Q., Toral-Barza,L., Shi,C., Follettie,M., and Yu,K. (2010). Requirement of the mTOR kinase for the regulation of Maf1 phosphorylation and control of RNA polymerase III-dependent transcription in cancer cells. J. Biol. Chem.

Shutt,T.E., Bestwick,M., and Shadel,G.S. (2011). The core human mitochondrial transcription initiation complex: It only takes two to tango. Transcription. *2*, 55-59.

Shutt,T.E. and Gray,M.W. (2006). Bacteriophage origins of mitochondrial replication and transcription proteins. Trends Genet. *22*, 90-95.

Shutt,T.E., Lodeiro,M.F., Cotney,J., Cameron,C.E., and Shadel,G.S. (2010). Core human mitochondrial transcription apparatus is a regulated two-component system in vitro. Proc. Natl. Acad. Sci. U. S. A *107*, 12133-12138.

sin-Cayuela,J. and Gustafsson,C.M. (2007). Mitochondrial transcription and its regulation in mammalian cells. Trends Biochem. Sci. *32*, 111-117.

Small,I.D. and Peeters,N. (2000). The PPR motif - a TPR-related motif prevalent in plant organellar proteins. Trends Biochem. Sci. *25*, 46-47.

Soeding,P.E., Sha,S., Royse,C.E., Marks,P., Hoy,G., and Royse,A.G. (2005). A randomized trial of ultrasound-guided brachial plexus anaesthesia in upper limb surgery. Anaesth. Intensive Care *33*, 719-725.

Sologub,M., Litonin,D., Anikin,M., Mustaev,A., and Temiakov,D. (2009). TFB2 is a transient component of the catalytic site of the human mitochondrial RNA polymerase. Cell *139*, 934-944.

Sousa,R. (1996). Structural and mechanistic relationships between nucleic acid polymerases. Trends Biochem. Sci. *21*, 186-190.

Sousa,R., Chung,Y.J., Rose,J.P., and Wang,B.C. (1993). Crystal structure of bacteriophage T7 RNA polymerase at 3.3 A resolution. Nature *364*, 593-599.

Steitz,T.A. (2004). The structural basis of the transition from initiation to elongation phases of transcription, as well as translocation and strand separation, by T7 RNA polymerase. Curr. Opin. Struct. Biol. *14*, 4-9.

Steitz,T.A. (2009). The structural changes of T7 RNA polymerase from transcription initiation to elongation. Curr. Opin. Struct. Biol. *19*, 683-690.

Steitz,T.A. and Steitz,J.A. (1993). A general two-metal-ion mechanism for catalytic RNA. Proc. Natl. Acad. Sci. U. S. A *90*, 6498-6502.

Steitz,T.A. and Yin,Y.W. (2004). Accuracy, lesion bypass, strand displacement and translocation by DNA polymerases. Philos. Trans. R. Soc. Lond B Biol. Sci. *359*, 17-23.

Taanman,J.W. (1999). The mitochondrial genome: structure, transcription, translation and replication. Biochim. Biophys. Acta *1410*, 103-123.

Tahirov,T.H., Temiakov,D., Anikin,M., Patlan,V., McAllister,W.T., Vassylyev,D.G., and Yokoyama,S. (2002). Structure of a T7 RNA polymerase elongation complex at 2.9 A resolution. Nature *420*, 43-50.

Temiakov,D., Anikin,M., and McAllister,W.T. (2002). Characterization of T7 RNA polymerase transcription complexes assembled on nucleic acid scaffolds. J. Biol. Chem. *277*, 47035-47043.

Temiakov,D., Mentesana,P.E., Ma,K., Mustaev,A., Borukhov,S., and McAllister,W.T. (2000). The specificity loop of T7 RNA polymerase interacts first with the promoter and then with the elongating transcript, suggesting a mechanism for promoter clearance. Proc. Natl. Acad. Sci. U. S. A *97*, 14109-14114.

Temiakov,D., Patlan,V., Anikin,M., McAllister,W.T., Yokoyama,S., and Vassylyev,D.G. (2004). Structural basis for substrate selection by t7 RNA polymerase. Cell *116*, 381-391.

Temperley,R.J., Seneca,S.H., Tonska,K., Bartnik,E., Bindoff,L.A., Lightowlers,R.N., and Chrzanowska-Lightowlers,Z.M. (2003). Investigation of a pathogenic mtDNA microdeletion reveals a translation-dependent deadenylation decay pathway in human mitochondria. Hum. Mol. Genet. *12*, 2341-2348.

Terwilliger,T.C. (2003). SOLVE and RESOLVE: automated structure solution and density modification. Methods Enzymol. *374*, 22-37.

Terwilliger,T.C. and Berendzen,J. (1999). Automated MAD and MIR structure solution. Acta Crystallogr. D. Biol. Crystallogr. *55*, 849-861.

Thuillier,V., Stettler,S., Sentenac,A., Thuriaux,P., and Werner,M. (1995). A mutation in the C31 subunit of Saccharomyces cerevisiae RNA polymerase III affects transcription initiation. EMBO J. *14*, 351-359.

Tiranti,V., Savoia,A., Forti,F., D'Apolito,M.F., Centra,M., Rocchi,M., and Zeviani,M. (1997). Identification of the gene encoding the human mitochondrial RNA polymerase (h-mtRPOL) by cyberscreening of the Expressed Sequence Tags database. Hum. Mol. Genet. *6*, 615-625.

Tjian,R. (1996). The biochemistry of transcription in eukaryotes: a paradigm for multisubunit regulatory complexes. Philos. Trans. R. Soc. Lond B Biol. Sci. *351*, 491-499.

Tomecki,R., Dmochowska,A., Gewartowski,K., Dziembowski,A., and Stepien,P.P. (2004). Identification of a novel human nuclear-encoded mitochondrial poly(A) polymerase. Nucleic Acids Res. *32*, 6001-6014.

Towpik,J., Graczyk,D., Gajda,A., Lefebvre,O., and Boguta,M. (2008). Derepression of RNA polymerase III transcription by phosphorylation and nuclear export of its negative regulator, Maf1. J. Biol. Chem. *283*, 17168-17174.

Upadhya,R., Lee,J., and Willis,I.M. (2002). Maf1 is an essential mediator of diverse signals that repress RNA polymerase III transcription. Mol. Cell *10*, 1489-1494.

Urban,J., Soulard,A., Huber,A., Lippman,S., Mukhopadhyay,D., Deloche,O., Wanke,V., Anrather,D., Ammerer,G., Riezman,H., Broach,J.R., De,V.C., Hall,M.N., and Loewith,R. (2007). Sch9 is a major target of TORC1 in Saccharomyces cerevisiae. Mol. Cell *26*, 663-674.

Vannini,A., Ringel,R., Kusser,A.G., Berninghausen,O., Kassavetis,G.A., and Cramer,P. (2010). Molecular basis of RNA polymerase III transcription repression by Maf1. Cell *143*, 59-70.

Wallace,D.C. (2001). Mitochondrial defects in neurodegenerative disease. Ment. Retard. Dev. Disabil. Res. Rev. *7*, 158-166.

Wallace,D.C. (2005). A mitochondrial paradigm of metabolic and degenerative diseases, aging, and cancer: a dawn for evolutionary medicine. Annu. Rev. Genet. *39*, 359-407.

Wang,Y. and Shadel,G.S. (1999). Stability of the mitochondrial genome requires an amino-terminal domain of yeast mitochondrial RNA polymerase. Proc. Natl. Acad. Sci. U. S. A *96*, 8046-8051.

Wang,Z. and Roeder,R.G. (1997). Three human RNA polymerase III-specific subunits form a subcomplex with a selective function in specific transcription initiation. Genes Dev. *11*, 1315-1326.

Warner,J.R. (1999). The economics of ribosome biosynthesis in yeast. Trends Biochem. Sci. *24*, 437-440.

Wei,Y., Tsang,C.K., and Zheng,X.F. (2009). Mechanisms of regulation of RNA polymerase III-dependent transcription by TORC1. EMBO J. *28*, 2220-2230.

Wei,Y. and Zheng,X.S. (2010). Maf1 regulation: A model of signal transduction inside the nucleus. Nucleus. *1*, 162-165.

Werner,F. and Grohmann,D. (2011). Evolution of multisubunit RNA polymerases in the three domains of life. Nat. Rev. Microbiol. *9*, 85-98.

Werner,M., Chaussivert,N., Willis,I.M., and Sentenac,A. (1993). Interaction between a complex of RNA polymerase III subunits and the 70-kDa component of transcription factor IIIB. J. Biol. Chem. *268*, 20721-20724.

Westermann,B. (2010). Mitochondrial fusion and fission in cell life and death. Nat. Rev. Mol. Cell Biol. *11*, 872-884.

White,R.J. (2008). RNA polymerases I and III, non-coding RNAs and cancer. Trends Genet. *24*, 622-629.

White,R.J. (2005). RNA polymerases I and III, growth control and cancer. Nat. Rev. Mol. Cell Biol. *6*, 69-78.

White,R.J. and Sharrocks,A.D. (2010). Coordinated control of the gene expression machinery. Trends Genet. *26*, 214-220.

Willis,I.M., Desai,N., and Upadhya,R. (2004). Signaling repression of transcription by RNA polymerase III in yeast. Prog. Nucleic Acid Res. Mol. Biol. *77*, 323-353.

Woiwode,A., Johnson,S.A., Zhong,S., Zhang,C., Roeder,R.G., Teichmann,M., and Johnson,D.L. (2008). PTEN represses RNA polymerase III-dependent transcription by targeting the TFIIIB complex. Mol. Cell Biol. *28*, 4204-4214.

Woo,D.K. and Shadel,G.S. (2011). Mitochondrial stress signals revise an old aging theory. Cell *144*, 11-12.

Wyrick,J.J. and Young,R.A. (2002). Deciphering gene expression regulatory networks. Curr. Opin. Genet. Dev. *12*, 130-136.

Yin,Y.W. and Steitz,T.A. (2004). The structural mechanism of translocation and helicase activity in T7 RNA polymerase. Cell *116*, 393-404.

Yin,Y.W. and Steitz,T.A. (2002). Structural basis for the transition from initiation to elongation transcription in T7 RNA polymerase. Science *298*, 1387-1395.

Zhang,G., Campbell,E.A., Minakhin,L., Richter,C., Severinov,K., and Darst,S.A. (1999). Crystal structure of Thermus aquaticus core RNA polymerase at 3.3 A resolution. Cell *98*, 811-824.

Zhong,S., Zhang,C., and Johnson,D.L. (2004). Epidermal growth factor enhances cellular TATA binding protein levels and induces RNA polymerase I- and III-dependent gene activity. Mol. Cell Biol. *24*, 5119-5129.

Abbreviations

AA	aminoacids
ABC	subunit prefix for RNAP I (A), II (B) and III (C)
AC	subunit prefixes for RNAP I (A) and III (C)
BdpI	B double prime I
Brf1	B-related factor 1
C	subunit prefix for RNAP III (C)
C. elegans	*Caenorhabditis elegans*
Cryo-EM	cryo-electron microscopy
CTD	carboxy-terminal domain
C-terminus	carboxy-terminus
Ct-NLS	C-terminal NLS
cv	column volume
D.melanogaster	*Drosophila melanogaster*
DNA	deoxyribonucleic acid
DNAP	DNA dependent DNA poylmerase
dsDNA	double strand DNA
DTT	dithiothreitol
E.coli	*Escherichia coli*
EDTA	ethylene diamine tetraacetic acid
EM	electron microscopy
ESRF	European Synchrotron Radiation Facility (Genoble, France)
ETC	electron transport chain
fl	full lenght
FSC	Fourier shell correlation
G	earth´s gravity
GTF	general transcription factor
h	hour
Hepes	4-(2-hydroxyethyl)-1-piperazineethanesulfonic acid
H.sapiens	Homo sapiens
H-strand	heavy strand of mtDNA
kbp	kilo basepairs
kDa	kilo Dalton
LB	lysogeny broth
L-strand	light strand of mtDNA
MAD	multiple-wavelenghts anormalous diffraction
MES	2-(N-morpholino)ethanesulfonic acid
mitoRNAP	mitochondrial RNAP
MOPS	3-(N-morpholino)propanesulfonic acid
mRNA	messenger RNA
mtDNA	mitochondrial DNA
mTERF	mitochondrial transcription termination factor
NCBI	National Center for Biotechnology Information
Ni-NTA	Nickel-nitrilotriacetic acid
NLS	nuclear localization signal
N-site	NTP binding site
nt	nucleotides
NTD	N-terminal domain
N-terminus	amino-terminus
Nt-NLS	N-terminal NLS

NTP	nucleotide triphosphate
o.n.	over night
OD	optical density
PBD	promoter binding domain
PCR	polymerase chain reaction
PDB	Protein Data Bank
PI	protease inhibitor
PIC	pre-initiation complex
PKA	protein kinase A
PMSF	phenylmethylsulfonyl fluoride
PP_i	pyrophosphate
PPR	pentatricopeptide
P-site	priming site
PVDF	polyvinylidene fluoride
R-factor	normalized linear residual between observed and calculated structure factor amplitudes
RNA	ribonucleic acid
RNAP	DNA dependent RNA polymerase
ROS	reactive oxygen species
Rpb	prefix of RNAP II subunits
rpm	rounds per minute
r.m.s.d.	root mean sqare deviation
rRNA	ribosomal RNA
RT	room temperature
RTZ	rotation function Z-score
S.cerevisiae	*Saccharomyces cerevisiae*
SDG	Saccharomyces genome database
SDS-PAGE	sodium dodecylsulfate polyacrylamide gel electrophoresis
SLS	Swiss Light Source
snRNA	small nuclear RNA
snoRNA	small nucleolar RNA
S.pombe	*Schizosaccharomyces cerevisiae*
ss	single subunit
TBE	Tris/Borate/EDTA
TBP	TATA-box binding protein
TCEP	tris(2-carboxyethyl)phosphine
TF	transcription factor
TFZ	translation function Z-score
TORC	target of rapamycin complex
TPR	tetratricopeptide
Tris	trishydroxymethylaminomethane
tRNA	transfer RNA
TSS	transcription start site
UTP	uridine triphosphate
v/v	volume per volume
WH	winged helix
Wt	wild type
w/v	weight per volume
YPD	yeast peptone dextrose
YPGly	yeast peptone glycerol

Curriculum Vitae

Eva Rieke Ringel (M.Sc. Biochemistry)

Personal data

Date of birth	23.10.1982
Place of birth	Essen, Germany

Research

Genecenter Ludwig-Maximilians University – Munich 11. 2007-07.2011
Dissertation "Molecular basis of RNA polymerase III transcription repression by Maf1 & Structure of the human mitochondrial RNA polymerase"
(group of Prof. P. Cramer)

Education

Max-Planck Institute of Molecular Physiology – Dortmund 10.2006 – 08.2007
Master´s thesis "Characterization of the SOS_PH/ Ras-interaction"
(group of Prof. A. Wittinghofer)

Ruhr-University Bochum 10.2005 – 08.2007
Master's course of study in biochemistry
Major field of study: protein-biochemistry; structural biology

Ruhr-University Bochum 10.2002 – 09.2005
Bachelor's course of study in biochemistry
Major field of study: protein-biochemistry; structural biology; neuronal biochemistry

Helmholtz-Gymnasium – Essen 09.1993 – 07.2002
Abitur

Further Education

IWW of the distance teaching university Hagen
Course of studies „Betriebswirtin (IWW)" 08.2009 – 03.2011
Intensive course in business studies and business management 03.2009 – 08.2009

Scholarships and Prizes

Roemer prize of the Ludwig Maximilians University Munich 12.2010

Graduate Student Award for the best podium presentation at the 7th International Biennial RNA Polymerases I und III Conference 2010 06.2010

International Max-Planck-Research School for Molecular and Cellular Life Sciences (IMPRS) – MPI of Biochemistry in Martinsried, Germany 11.2008-07.2011

Publications

Ringel,R., Sologub, M., Morozov, Y.I., Litonin D., Cramer, P. and Temiakov, D. (2011). **Structure of the human mitochondrial RNA polymerase**. *Nature (accepted)*

Vannini,A.*, Ringel,R.*, Kusser,A.G.*, Berninghausen,O., Kassavetis,G.A., and Cramer,P. (2010). **Molecular basis of RNA polymerase III transcription repression by Maf1.** Cell *143*, 59-70.

Pechlivanis M, Ringel R, Popkirova B, Kuhlmann J. (2007). **Prenylation of Ras Facilitates hSOS1-Promoted Nucleotide Exchange, upon Ras Binding to the Regulatory Site.** Biochemistry *46(18)*;5341-8.